UNIVERSIDAD AUTÓNOMA DE NUEVO LEÓN

FACULTAD DE INGENIERÍA MECÁNICA Y ELÉCTRICA

SUBDIRECCIÓN DE ESTUDIOS DE POSGRADO

"SPENT COFFEE GROUND INCORPORATED NATURAL POZZOLANS FOR DEVELOPING CEMENT PASTES"

Por:

SOORYA PUSHPAN

COMO REQUISITO PARCIAL PARA OBTENER EL GRADO DE

DOCTOR EN INGENIERÍA DE MATERIALES

SAN NICOLÁS DE LOS GARZA, NUEVO LEÓN **FEBRERO 2023**

UNIVERSIDAD AUTONOMA DE NUEVO LEON

FACULTAD DE INGENIERÍA MECÁNICA Y ELÉCTRICA

SUBDIRECCIÓN DE ESTUDIOS DE POSGRADO

“SPENT COFFEE GROUND INCORPORATED NATURAL POZZOLANS FOR DEVELOPING CEMENT PASTES”

Por:

SOORYA PUSHPAN

COMO REQUISITO PARCIAL PARA OBTENER EL GRADO DE

DOCTOR EN INGENIERÍA DE MATERIALES

SAN NICOLÁS DE LOS GARZA, NUEVO LEÓN **FEBRERO 2023**

UNIVERSIDAD AUTÓNOMA DE NUEVO LEÓN
Facultad de Ingeniería Mecánica y Eléctrica
Posgrado

Los miembros del Comité de Evaluación de Tesis recomendamos que la Tesis "Spent coffee grounds incorporated natural pozzolans for devoloping cement pastes", realizada por la estudiante SOORYA PUSHPAN, con número de matrícula 1983190, sea aceptada para su defensa como requisito parcial para obtener el grado de Doctor en Ingeniería de Materiales.

El Comité de Evaluación de Tesis

LAUREN YOLANDA GÓMEZ ZAMORANO
Director

ANA MARIA GUZMAN HERNANDEZ
Revisor

EDÉN AMARAL RODRÍGUEZ CASTELLANOS
Revisor

JUAN JACOBO RUÍZ VALDÉS
Revisor

JORGE LEOBARDO ACEVEDO DÁVILA
Revisor

ALDO RUBEN CAMPOS SILVA
Revisor

Vo.Bo.

Dr. Simón Martínez Martínez
Subdirector de Estudios de Posgrado

Institución 190001

Programa 122608

Acta Núm. 323

Ciudad Universitaria, a 24 de Julio de 2023.

ACKNOWLEDGMENTS

In this section, I want to express my gratitude to all the people and institutions that have supported me to achieve this professional have supported me to reach this professional achievement.

I am most grateful to god for opening my path and giving me the necessary strength not to give up, for allowing me to get to where I am, and for always counting on him in good and bad times.

To my mother and my father for being my most important pillar, for always giving me their unconditional love and support, for always bearing this distance with a smile and for always being there for me.

To my brother Sooraj, for supporting me in my decisions and for being present whenever I have needed him because I know it will always be that way.

To my husband Dr Sanal, for having been a part of my life and for completing my family, for all the steps we have taken together and for those to come. Since I met him, I knew she was the person I wanted to be with me in my life, the person I wanted to accompany me to take the steps through life together and she has made it much more pleasant and for all his love and support.

I have no words to thank my daughters, Naomi and Naylah, for the time I took from them, in the conquest of this personal achievement. I hope to repay them someday.

To Mexico for opening its doors to me and giving me the opportunity to experience its culture.

To Dra. Lauren Y. Gómez Zamorano, for all the support and knowledge that she has given me for the completion of this thesis, and I thank her for her quality as a

person because more than an advisor-student relationship, she always offered me her friendship and support.

To my friends and my colleagues in the cement and concrete laboratory: Loth, Erika, Adriagni, Luis, Lucio, Javier and Mauricio and with whom I have had the opportunity to work and with whom I have received all their support during this time.

I would like to thank all the doctors in the postgraduate program that I had the opportunity to meet and who gave me their knowledge and experience in the subjects taught. Dr. Moises Hinojosa, Dr. Shaji, Dr. Domingo, Dr. Alberto Pérez, Dr. Josue, Dra. Selene, Dra. Sofía, Dra. Bindu, Dra. Ana María Arato, Dra. Ana María Guzmán, Dr. Edgar Reyes Melo, Dr. Edgar García, Dra. Dora Irma, Dra. Beatriz, Dr. Arturo Juárez for their support in the use of laboratory equipment and tools, without them it would not have been possible to perform some characterization tests for finishing the research work successfully.

To all my Indian friends with whom I share good times in Mexico and for all their love and support, Vineetha, Jacob, Anjali, Sreed, Aiswarya, Akshana, Tijin, Sebin, Paulosutty, Albert, Varshika, Pooja, Ashley, Karan and Ramsha.

To all my colleagues in the graduate program at FIME and especially to those in my semester, with whom I shared good times and helped each other. Diego Andres, Carlos Cuao, Jose Carlos, Martin Miranda, Andres Salamon, and Alan Ricardo

To the Universidad Autónoma de Nuevo León and the Faculty of Mechanical and Electrical Engineering for giving me the opportunity to study this doctoral degree in their facilities.

To the National Council of Science and Technology (CONACYT), for financing this research.

To the doctors and facilities of COMIMSA and CIIIA, who allowed me to use their equipment to carry out the characterization of my samples, especially Dr. Josué Aguilar and Dr. Jorge Acevedo, who I felt more strongly their support.

DEDICATION

To my mother Vanaja Pushpan and my father Pushpan Puthenvely Ramakrishnan, I know how proud they are, because their daughter has known how to grow up and I owe that to the love, dedication, and teaching that they have given me and have encouraged me to be a better person every day. Distance has been a hard obstacle in these times, but soon we will be able to celebrate this achievement together.

To my husband Sanal, I know how happy he is that I have dedicated my effort and time to the world of research.

To my two little princesses Naomi Janaki and Naylah Padmini, you are the best thing that has happened to me in my life.

TABLE OF CONTENTS

LIST OF TABLES

LIST OF FIGURES

NOMENCLATURE AND ABBREVIATIONS

Materials

OPC	Ordinary Portland Cement
CSA	Calcium Sulfoaluminate Cement
SCM	Supplementary Cementitious Materials
FA	Fly ash
VA	Volcanic ash
SCG	Spent coffee grounds

Oxides

CO_2	Carbon dioxide
CaO	Calcium oxide
SiO_2	Silicon dioxide
Al_2O_3	Aluminum oxide (alumina)
Na_2O	Sodium oxide
SO_3	Sulfur oxide
MgO	Magnesium oxide

Mineralogical Phases

C_3S	Tricalcium silicate	Alite	Ca_3SiO_5
C_2S	Dicalcium Silicate	Belite	Ca_2SiO_4
C_3A	Tricalcium Aluminate	Aluminate	$Ca_3Al_2O_6$
C_4AF	Tetracalcic aluminoferrite	Ferrite	$Ca_2(Al,Fe)O_5$
$C_4A_3\hat{S}$	Calcium Sulfoaluminate	Ye'elimite	$Ca_4Al_6O_{12}SO_4$

Hydration Products

C-S-H	Calcium silicate hydrate	$CaO.SiO_2.H_2O$
CH	Calcium hydroxide -Portlandite	$Ca(OH)_2$
AF_t	Calcium sulfoaluminate hydrate – Ettringite	$3CaO.Al_2O_3.3CaSO_4.32H_2O$
AH3	Aluminum hydroxide	$Al(OH)_3$
AFm	Mono sulfate	$3CaO.Al_2O_3.CaSO_4.12H_2O$
C-A-S-H	Calcium Aluminosilicate Hydrate	$CaO.Al_2O_3.SiO_2.H_2O$

Characterization techniques

CS	Compressive strength
XRD	X-Ray Diffraction
SEM	Scanning Electron Microscopy
EDS	Energy Dispersive Spectroscopy
EIS	Electrochemical Impedance Spectroscopy
IR-ATR	Attenuated Total Reflectance Infrared Spectroscopy

RESUMEN

Los materiales cementantes suplementarios pueden utilizarse para sustituir parcial o totalmente al cemento portland ordinario (OPC), lo que se considera una de las formas eficaces de reducir las emisiones de CO_2 de las industrias cementeras. Las puzolanas más utilizadas son la ceniza volante, la ceniza volcánica, el metacaolín, la escoria de alto horno, etc. En este trabajo se realizó un estudio comparativo del efecto de la incorporación de residuos de café, ceniza volante y ceniza volcánica en dos cementos diferentes (OPC y cemento sulfoaluminato (CSA)). La caracterización de las muestras de cemento se llevó a cabo mediante el análisis de la resistencia a la compresión hasta 210 días, la microscopía electrónica de barrido con espectroscopia de rayos X de energía dispersiva, la reflexión total atenuada, la difracción de rayos X y la espectroscopia de impedancia electroquímica. Los resultados mostraron que la resistencia a la compresión del cemento mezclado se vio afectada por la presencia de café gastado junto con la ceniza volcánica sin ninguna activación alcalina. Tanto los compuestos de cemento con un 3.5% de café usados con 30% de ceniza volante y un 30% de ceniza volcánica cumplían el requisito mínimo de resistencia a la compresión (20.2 MPa) para aplicaciones no estructurales, según la norma ASTM C109/C109M. La formación del gel cementante C-S-H para los compuestos de cemento Portland ordinario; la C-A-S-H y ettringita fueron responsables de la resistencia del cemento compuesto preparado con cemento sulfoaluminato. La adición de ceniza volcánica mejora la durabilidad de las pastas de cemento tanto en OPC como en CSA. Los datos EIS son una técnica indirecta para probar la durabilidad de las pastas de cemento; los resultados mostraron que las pastas de cemento compuestas incorporadas con ceniza volcánica serían más duraderas que otras pastas de cemento compuestas.

ABSTRACT

Ordinary portland cement (OPC), regarded as one of the efficient strategies to minimize CO_2 emission from the cement industry, can be partially or entirely replaced with supplementary cementitious materials. Fly ash, volcanic ash, metakaolin, blast furnace slag, etc., are among the most common pozzolans. The effects of adding spent coffee grounds, fly ash, and volcanic ash to two types of cement (OPC and Calcium Sulfoaluminate Cement (CSA)) were compared in this reasearch. Compressive strength studies up to 210 days, scanning electron microscopy with energy-dispersive X-ray spectroscopy, attenuated total reflection, X-ray diffraction, and electrochemical impedance spectroscopy were used to characterize the cement samples. The results demonstrated that the inclusion of spent coffee grounds coupled with fly ash and volcanic ash impacted the compressive strength of blended cement. According to ASTM C109/C109M, the cement composites with 3.5 per cent spent coffee grounds, 30 per cent fly ash, and 30 per cent volcanic ash achieved the minimum compressive strength requirement of 20.2 MPa for nonstructural applications. The strength of the composite cement made using sulfoaluminate cement was due to the production of the cementitious gel C-A-S-H and ettringite; and for ordinary portland cement and composite cements it was due to C-S-H. The addition of volcanic ash enhances the durability of the cement paste in both OPC and CSA. As per EIS data, an indirect technique for testing cement paste durability supports that volcanic ash incorporated composite cement pastes would be more durable than other composite cement pastes.

CHAPTER 1

INTRODUCTION

The most common artificial substance on earth is cement. Because of the increase in world population, cement consumption is set to soar to unpredicted proportions [1]. Due to the CO_2 emissions throughout its manufacturing process, cement production is inextricably tied to the continuing phenomena of climate change, global warming, ocean acidification, etc. [2–4]. Alternative actions must be implemented to lower CO_2 emissions. Supplementary Cementitious Materials(SCMs) are one of the most excellent solutions to the issue. SCM may possess pozzolanic or cementitious characteristics [5,6]. SCM (volcanic ash, kaolin, fly ash, blast furnace slag, etc.) helps concrete function better when it is raw and hardened. The primary justifications for adding pozzolans to the cement matrix are, improved workability, durability, and strength. SCM assists the manufacturer of concrete in designing and modifying the concrete mixture to accommodate the specified application [7]. Alumina-rich SCM enhances the absorption of aluminate in C-S-H. In contrast, silica-rich SCM aids in producing additional hydrates and affects the porosity and durability of the cement pastes [8].

Comparing OPC (Ordinary Portland Cement) with CSA (Calcium Sulfoaluminate Cement), CSA has better grindability, can be made at lower temperatures, and contains less lime. CSA is manufactured at a temperature of 1250 ℃ while comparing the production of OPC; it is about 200 ℃ less and 25 to 30% less in net

CO_2 emission [9,10]. Benefits extend beyond reduced energy use and carbon emissions [11]. Ye'elimite (C_4A_3S), which was first included into cement as a phase by Klein and utilized as an expanding or shrinkage-compensating additive to cement binders, makes up 30–70% of CSA. Ettringite (Af_t), the primary hydration product, enhances the strength of sulfate cement, is formed quickly by the hydration processes of calcium sulfates in addition to the reduction of CO_2. [12]. The introduction of calcium sulfate, its amount and reactivity, as well as the type and quantity of minor phases, all play major roles in determining how hydrated CSA becomes. Ettringite is the principal hydration product formed, coupled with amorphous aluminum hydroxide. Ye'elimite reacts with water during the hydration reaction to form aluminium hydroxide and monosulfate, which is usually amorphous. In addition to aluminium hydroxide, non-expansive ettringite particles develop in the form of large prismatic crystals responsible for high mechanical strength. The essential characteristics of the hydration process are high reaction rate and stability, a considerable consumption of free water, and a reduction of capillary porosity [12]; other hydration products like C-S-H, monoCarb aluminate, and gibbsite may be produced based on the minor phases present in CSA.

Naturally occurring volcanic ash (VA) has a substantially lower embodied energy than other materials; embodied energy refers to the total energy needed for all direct and indirect activities associated with the material. This includes excavation, transportation, fabrication, etc., until the product or material is ready. Since VA is a natural pozzolan, energy consumption is very low, reducing the carbon footprint [13]. Introducing VA into concrete improves mechanical strength and minimizes the cost of concrete production [14,15]. VA is rich in alumina and helps resist sulfate attacks. Binding gel known as calcium-alumino-silicate-hydrate (C-A-S-H) gel is formed as a result of high alumina content in the composition of VA [16,17].

The residual waste of the coal-fired electricity industry is fly ash (FA). By adding FA, the compressive strength of cement paste is enhanced. When FA combines with calcium hydroxide, the reaction product of OPC, additional calcium silicate

hydrate products (C-S-H) are created [18,19]. FA increases how easily cement and concrete can be worked. Also, factors such as segregation, bleeding, heat evolution, and permeability are reduced, inhibit the alkali-aggregate reaction, and enhance sulfate resistance [20,21]. FA in OPC can function as a micro filler and as a pozzolan. The filler effect results from the existence of extra nucleation sites connected to the areas the SCM provides. The granulometry of the ashes allows a better accommodation of the mixture. The FA can dissolve (very slowly) because of the high pH in the pore solution of cement. C-S-H is produced more frequently when FA reacts with portlandite [22].

Tons of municipal waste are produced daily, and altering these waste materials from landfills has become a defined goal for the public and the community. Coffee is considered the most consumed refreshment drink all over the world. In 2018–2019, the total production of green coffee beans reached 10256 million tons [23]. Spent coffee grounds (SCG) are considered a significant municipal waste from households and cafes to be landfilled which is the focus of this research. The residue obtained during hot water or steam passes through coffee powder to prepare instant coffee is SCG [24]. SCG, the waste product has been utilized as dump bioleaching absorbent or household agro manure [25]. Teck-Ang Kua reported in his studies that they developed a derivative construction material with SCG to keep this insoluble trash out of landfills. From the studies of [26], 15 wt.% SCG mixed with clay have the capability of producing premium lightweight clay aggregates for drainage reasons. A study on SCG and tea waste was carried out by L. L. P. Chung [27] to prepare alkali-activated bricks. The results demonstrated that SCG and tea dust may be included as a component to create environmentally friendly unfired clay bricks. As per ASTM C62, In samples containing 1-2.5 wt% of SCG and 1–10 wt% of tea waste, the minimum compressive strength requirement of 8.6 MPa for structural applications was met with negligible weathering. However, the use of SCG in amounts greater than 5% wt% results in the growth of fungus, which has an impact on the durability and strength development of structure.

Geopolymer prepared using SCG with blast furnace slag at a temperature of 50 ℃ can be used as pavement filling material [28]. On the strength performance and microstructure analysis based on the composite cement manufactured using SCG and other pozzolans, very few investigations have been done.

J. I. Escalante-Garcia and Sharp conducted several investigations on blended cement containing OPC, Ground Granulated Blast Furnace Slag (GGBS), FA, and VA between 1996 and 2004 [29–33]. In combination with OPC, they employed 60 percent blast furnace slag, 30 percent FA, and 22 percent VA. Curing temperatures ranged from 10 ℃ to 60 ℃. The investigations found that the porosity also increased as the curing temperature rose. [29]. The lower curing temperature of 10 ℃ decreased the porosity and elevates the rate of hydration. The C-S-H produced for the VA composite showed a change in greater Si and Al concentration and a decrease in Ca content. In 2017, S. Al-Fadala and his team used OPC and VA to research the mechanical characteristics of blended cement [34]. As the replacement amount grew from 10 to 40%, they discovered that it aids in low release of heat during the process of hydration. In the first several days of curing, a 40% substitution of OPC with VA reduced compressive strength by around 40%. The reactivity to the composite cement was more important in later ages; nevertheless, it steadily increased in the latter curing phase.

Suksiripattanapong created geopolymer pastes by combining SCG, rice husk ash (RHA), and blast furnace slag (S) to develop materials for pavements. According to the investigation, the mix that produced 2 MPa was the greatest compressive strength after 90 days of curing for SCG:RHA:S was 70:20:10 at a curing temperature of 50 ℃ [35]. An investigation was done on the strength of a geopolymer mixture made from SCG, S, and FA [25]. According to their analysis, the ideal blend was SCG 70 percent:S 30 percent with a 55 percent liquid-to-solid ratio; FA did not help in the reaction process to attain the advised unconfined compressive strength. Slag activation enabled the geopolymer mix to reach its maximum compressive strength in the initial curing process without needing heat

treatment. They utilized 70% Na_2SiO_3 and 30% NaOH as the liquid activator. To understand the geopolymer stabilization of highly organic materials for embankment structural fill material, Arulrajah presented a study on alkali-activated SCG with FA geopolymer mix. The results showed that when cured at 50 ℃, 30 percent FA with 70 percent SCG demonstrated superior mechanical strength. In this instance, a 50:50 ratio of the liquid activator Na_2SiO_3:NaOH was utilized, and the FA to liquid ratio was 1.8 [36].

Several researchers have studied the performance of cement pastes, mortars, and concretes that partially replace OPC with VA. and found that 20% replacement of OPC improved tensile and compressive strengths for the composite mix [37,38]. The alkaline activation of Peruvian VA for generating new geopolymer materials with the NaOH solution has been conducted to analyze mechanical properties (compressive strength and porosity), and the improved performance was due to the formation of the reaction product N-A-S-H gel. This gel is responsible for the wear resistance in the geopolymer mix [39]. Numerous investigations employing OPC and FA on composite cement have been done. At ten to twenty replacement percentages, partial FA replacement with OPC increases mechanical strength. C-S-H gel, the reaction product, helps to improve the strength of composite cement. Average pore size is similarly impacted by FA fineness, which likewise boosts mechanical strength and reduces porosity [40–49]. The impact of FA addition on the hydration processes of calcium sulfoaluminate cement was studied by L.H.J. Martin in 2017. As the FA% rose, the filler effect of FA owed the hydration reaction of CSA cement to accelerate [50]. The mortar formulated with 7.5 percent FA showed higher compressive strength. The most extensive range documented for FA that can be used without losing strength is 15 percent by mass [50]. Additionally, CSA with FA mortars at various ages of hydration was carried out. These findings support the partial replacement of calcium sulfoaluminate with FA positively affects the environment and the economy [51]. As an alternative to OPC, calcium sulfoaluminate cement and FA-based geopolymer mortar were made to

evaluate the hydration behavior and the physicomechanical characteristics [52]. According to the study, sodium silicate and potassium hydroxide were used for the alkali activation of FA. Ettringite quickly forms when composite cement is made using CSA and FA; it exhibits superior mechanical strength. Lower water capillary adsorption was seen in geopolymer mortars due to the reduced porosity of the mixture.

Considering the above discussion, in this work, the mechanical strength and microstructural characteristics of two types of cement (OPC, and CSA) were the main topics of our comparison. These cements were partially replaced with SCG, FA, and VA, to reduce the use of OPC and, therefore, CO_2 emission.

CHAPTER 2

LITERATURE REVIEW

2.1 Ordinary Portland Cement

Ordinary Portland cement is a critical component of global infrastructure. A "cementing agent" can be considered an adhesive substance capable of bonding fragments or masses of materials together into a "whole." It is a finely ground powdered material, which, when in contact with water, has the property of setting and hardening, which makes it a hydraulic binder [53]. The versatility, economy, and ease of construction make cement an indispensable material in the construction industry. The massive production of Portland cement leads to high energy consumption, severe environmental concerns during mining, manufacturing, and transporting of the cement, and related air pollution, including the release of the greenhouse gas CO_2, NO_x, SO_2, and particulates. It was estimated that 10% of world carbon dioxide emission is due to the production of Portland cement [54]. To meet the needs of the growing population, The International Energy Agency has estimated that cement production will increase by between 12 and 23% by 2050.

2.1.1 Manufacturing process

When limestone and clays or other components with a comparable composition and enough reactivity are combined, they are heated to a temperature of 1450 °C to create clinker, which is then used to make Ordinary Portland Cement (OPC). Once the clinker is obtained, it is mixed with small quantities (5%) of calcium sulfate dihydrate (gypsum) and then ground to produce ordinary Portland cement (OPC). The gypsum can be partially or fully replaced by other forms of calcium sulfate, such as hemihydrate or anhydrite because gypsum can be dehydrated by the temperatures present in the mixing process. The setting and strength development rates are both influenced and controlled by gypsum. The average composition of clinker is around 67% CaO, 22% SiO_2, 5% Al_2O_3, 3% Fe_2O_3, and 3% other components. Alite, belite, aluminate, and ferrite are the typically present four major phases. Alkali sulfates and calcium oxide are two more phases that could be present in lower quantities. The hardening of cement occurs through the reaction of its main phases with water. Thus, the main property of cement is its hydraulic activity. For a material to be considered a hydraulic binder, it must meet two fundamental requirements: (a) it must react with water to a sufficient extent and at a good rate, and (b) the reaction produces newly formed solids with extremely little solubility and a microstructure that can give rise to a capacity of high mechanical strength, volumetric stability, and durability.

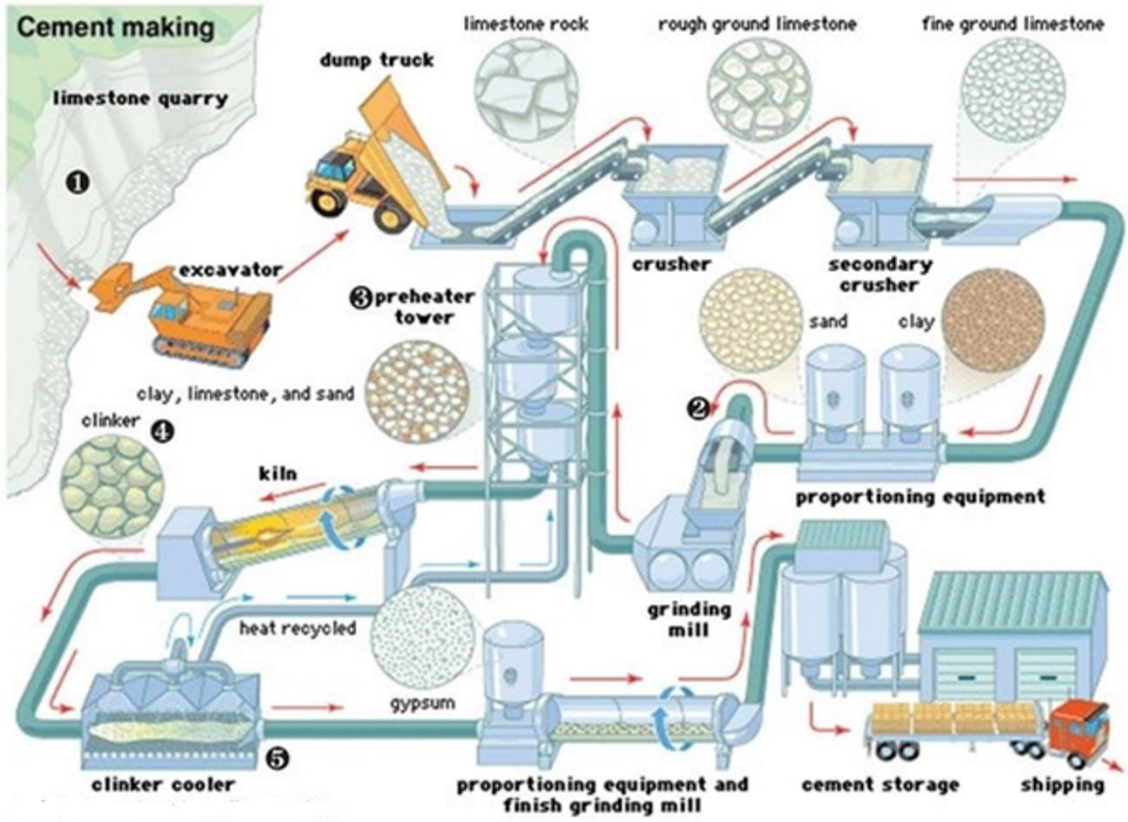

Figure 1. Schematic diagram of the manufacturing process of Ordinary Portland Cement [55]

2.1.2 Principal phases of Portland cement clinker

The ASTM-C-219 19 standard defines Portland cement as the hydraulic material product of clinker milling [56].

2.1.2.1 Tricalcium silicate

The most crucial element in all typical Portland cement clinkers is alite. Portland cement clinkers constitute 50 to 70%. Ionic substitutions alter the composition and crystalline structure of tricalcium silicate (Ca_3SiO_5) [57].

2.1.2.2 Dicalcium silicate

In the clinkers of OPC, belite makes up 15 to 30 percent. Ionic substitutions modify the compound dicalcium silicate (Ca_2SiO_4), which can be present whole or in part as a polymorphic β-phase [57].

2.1.2.3 Tricalcium aluminate

In most typical OPC clinkers, aluminate makes about 5 to 10%. Ionic substitutions significantly alter the composition and occasionally the structure of tricalcium aluminate ($Ca_3Al_2O_6$) [57].

2.1.2.4 Calcium Ferroaluminate

A typical OPC clinker contains 5 to 15% ferrite. Its composition has been significantly altered by changes in the Al/Fe ratio and ionic replacements, making it tetracalcic aluminoferrite (Ca_2AlFeO_5) [57].

Table 1. Mineralogical composition of clinker in Ordinary Portland Cement

Nomenclature	Mineral	Composition in oxides	Percentage of clinker in OPC (%)
C_3S	Tricalcium silicate (Alite)	$3CaO.SiO_2$	50-70
C_2S	Dicalcium silicate (Belite)	$2CaO.SiO_2$	15-30
C_3A	Tricalcium aluminate (Celite)	$3CaO.Al_2O_3$	5-15
C_4AF	Tetracalcium ferroaluminate (Ferrite)	$4CaO.Al_nFe_{2-n}O_3$	5-10

2.1.3 Hydration reaction of Portland cement

Cement hydration is the reaction of unhydrated cement or any of its elements with water, which causes physical and chemical changes in the system, as well as changes in its mechanical behavior. An exothermic chemical reaction between the clinker components causes OPC to hydrate, which, together with the setting regulator (gypsum) and water, will cause the cement paste to set and harden. The following factors have the greatest influence on the rate of hydration and its kinetics:

- The cement phase composition and the presence of dopant ions within the clinker phase crystal lattices.
- Cement fineness, particularly particle size dispersion and specific surface area.
- Water/cement ratio.
- Use of chemical additives.
- Curing temperature.
- The presence of addition (FA, metakaolin, blast furnace slag, VA, etc.)

The main hydration reaction products of Portland cement are C-S-H gel and Portlandite ($Ca(OH)_2$) [58]. The role played by each of the phases that compose both alite and belite favor the kinetics of hydration and the formation of new phases, in addition to contributing essentially to the setting and hardening of the cement paste. The aluminate favors resistance to chemical attack and must behave in small quantities because it is the phase responsible for producing ettringite. The ferrite phase is the one that acts as a flux and is the one that causes hydration to be slower.

The chemical reactions involved in cement hydration are very complex. Understanding these processes is ideal for studying the hydration of each mineral in the clinker separately. In this scenario, it is assumed that the hydration of each compound is considered an independent process.

2.1.3.1 Tricalcium silicate (C_3S)

Tricalcium silicate ($3CaO\text{-}SiO_2$), also known as C_3S, is the crucial component of Portland cement and so plays an important role in the setting and hardening processes. C_3S hydrated to form an amorphous hydrated silicate commonly called the calcium silicate hydrate (C-S-H) phase, and calcium hydroxide [$Ca(OH)_2$], or CH [58]. Since it is challenging to pinpoint exactly how C-S-H and CH are formed, the following equation is approximative.

$$2[3CaO.SiO2] + 7H2O \rightarrow 3CaO.SiO2.4H2O + 3Ca\,(OH)2 \qquad \Delta H= \text{-114kJ/mol}$$

Equation 1

2.1.3.2 Dicalcium silicate (C_2S)

The products of C_2S hydration are practically the same as those obtained during C_3S hydration, varying only in the amount of $Ca(OH)_2$ formed and the heat of hydration released. This hydration reaction is slower than that of C_3S.

$$2[2CaO.SiO2] + 5H2O \rightarrow 3CaO.SiO2.4H2O + Ca\,(OH)2 \qquad \Delta H= \text{-43kJ/mol}$$

Equation 2

2.1.3.3 Tricalcium aluminate (C_3A)

Hydration of C_3A in the absence of gypsum: the hydration reaction of C_3A is very fast and with a great generation of heat since, in contact with water, calcium aluminate hydrates are rapidly formed on contact with water:

$$2[3CaO.Al2O3] + 21H2O \rightarrow 4CaO.Al2O3.19H2O + 2CaO.Al2O3.8H2O$$

Equation 3

These hydrates belong to the family of AF_m phases, and they are unstable, so they quickly convert to their stable form.

$$2[4CaO.Al2O3.13H2O] + 2CaO.Al2O3.8H2O \rightarrow 2[3CaO.Al2O3.6H2O] + 9H2O$$ Equation 4

$3CaO.Al_2O_3.6H_2O$ (C_3AH_6) hydrate is the only thermodynamically stable C_3A hydrate at room temperature. The conversion of the initial hydrate to its stable form, C_3AH_6, occurs at a high rate and involves a high heat release. It is influenced by the water/cement ratio, the grain size of the C_3A, and the presence or absence of CO_2.

Hydration of C_3A in the presence of gypsum: here, compared to hydration in the absence of gypsum, a much lower percentage of C_3A is hydrated at the beginning of the hydration process. In the presence of gypsum, the main hydration product is ettringite or $C_6AS_3H_{32}$ trisulfate, according to the following equation:

$$3CaO.Al2O3 + 2[Ca.SO4.2H2O] + 26H2O \rightarrow 6[Ca.Al2O3.3SO4.32H2O]$$
Equation 5

A significant release of heat accompanies this process. Once all the gypsum has been consumed in the reaction to form ettringite, the excess C_3A can react with the ettringite to form a hydrated sulfoaluminate, also known as monosulfate.

$$C6AS3H32 + 2C3A + 4H \rightarrow 3C4ASH12$$ Equation 6

When monosulfate is in the presence of a new source of sulfate ions, ettringite can form again.

2.1.3.4 Tetracalcium aluminoferrite (C_4AF)

Calcium ferroaluminate can range in composition from C_2 ($A_{0.7}F_{0.3}$) to C_2 ($A_{0.3}F_{0.7}$). The hydration products of C_4AF are substantially similar to those produced in the hydration reactions of C_3A when equivalent environments are present. However, the reaction rates differ, with C_4AF being much slower than C_3A. The Al/Fe ratio can affect the reactivity of ferrite phase, which typically declines as the Fe concentration rises. It performs better than C3A for cement with good workability and has less of an impact on the amount of water in the normal consistency of the cement paste. Its contribution to compressive strength is minimal. In the presence of water, the hydration reactions are:

$$\mathrm{C4AF} + 16H \rightarrow 2C2(A,F)H8 \qquad \text{Equation 7}$$

$$\mathrm{C4AF} + 16H \rightarrow C4(A,F)H13 + (A,F)H3 \qquad \text{Equation 8}$$

2.1.4 Stages in hydration of Portland cement

As we have already discussed, cement hydration is an exothermic process. Chemical interactions involving the various clinker minerals, calcium sulfate, and water take place concurrently and at various rates throughout the hydration process of Portland cement. The following factors determine how the process develops:

- The pace at which the various phases dissolve.
- The speed at which the hydrate crystals will form and the nucleation.
- The rate of water diffusion and ions dissolution through the already formed hydrated components.

The hydration mechanism of a cement paste at room temperature is characterized by different stages:

2.1.4.1 Stage I: Pre-induction period (first few minutes)

The ionic species in the liquid phase rapidly dissolve as soon as the cement comes into contact with water, and the hydrated phases start to develop.The alkaline sulfates present in the cement dissolve completely in seconds, contributing K^+, $Na^{+,}$ and SO_4^{2-} ions. When the calcium sulfate is fully dissolved, extra Ca^{2+} and SO_4^{2-} ions are produced. The C-S-H layer precipitates on the surface of the cement particles as the tricalcium silicate dissolves congruently. In this phase, the concentration of Ca^{2+} and OH^- ions increases. Simultaneously, though in insufficient quantities, silicate ions move into the liquid phase. The fraction of hydrated C_3S in the pre-induction phase remains at 2 and 10%. C_3A dissolves and reacts with the Ca^{2+} and SO_4^{2-} ions present in the liquid phase forming ettringite (AF_t) which also precipitates on the surface of the cement particle. The content of C_3A that hydrates in the pre-induction period can vary between 5% and 25%. Only a small fraction of C_2S reacts in this phase.

2.1.4.2 Stage II: Induction period (within a few hours)

Just after the initial period of accelerated hydration, the rate of hydration reactions of all the minerals in the clinker develops at a very low rate. During this period, water consumption and the amount of hydrates formed are minimal, which explains why the cement acquires plasticity and is workable for a certain period. When the pH approaches 12.5, the amount of calcium hydroxide (CH) in the liquid phase reaches its maximum and starts to decline. According to some evidence, the second step of C-S-H synthesis from the liquid phase was primarily responsible for the end of the induction period and the start of the major reaction.

2.1.4.3 Stage III: Acceleration period (3-12 hours after mixing)

After 1-3 hours, i.e., at the end of the induction period, the initial solidification or initial setting begins. The nucleation and development of the hydration products at this time regulate the hydration reaction, which is again accelerated. The C_3S

velocity accelerates, and the C-S-H of the second phase begins to form. Hydration of C_2S also starts during this period. Once a critical value of Ca^{+} ions and Ca^{2+} and hydroxyl ions are reached, precipitation of C-S-H and CH begins. The final set reached the end of this stage.

2.1.4.4 Stage IV: Deceleration period

As the quantity of unreacted materials declines, the rate of hydration gradually slows down, and diffusion regulates this process. During this period, hydration of C3S and C2S causes the C-S-H gel to continue to develop. With time, this mechanism results in a greater contribution of C2S to the reaction products, while producing less CH at a faster pace. The amount of SO_4^{2-} in the liquid phase diminishes when the calcium sulfate is used up. Consequently, the AF_t formed in the initial hydration stages begins to react with the remaining C_3A and C_4AF to form AF_m.

2.1.4.5 Stage V: Diffusion limit

At this stage, the cement grains have been covered by a layer of hydrates (rings around the anhydrous grains), known as internal products, and further reaction through this layer is difficult, especially when it is very dense. Thus, the reaction rate decreases as it depends on the diffusion of water molecules and aqueous solution through the hydrate layer. Depending on the processing variables, such as casting, setting, and curing, this layer can have a variable porosity.

Figure 2 shows the five stages of Portland cement hydration as determined by conduction calorimetry.

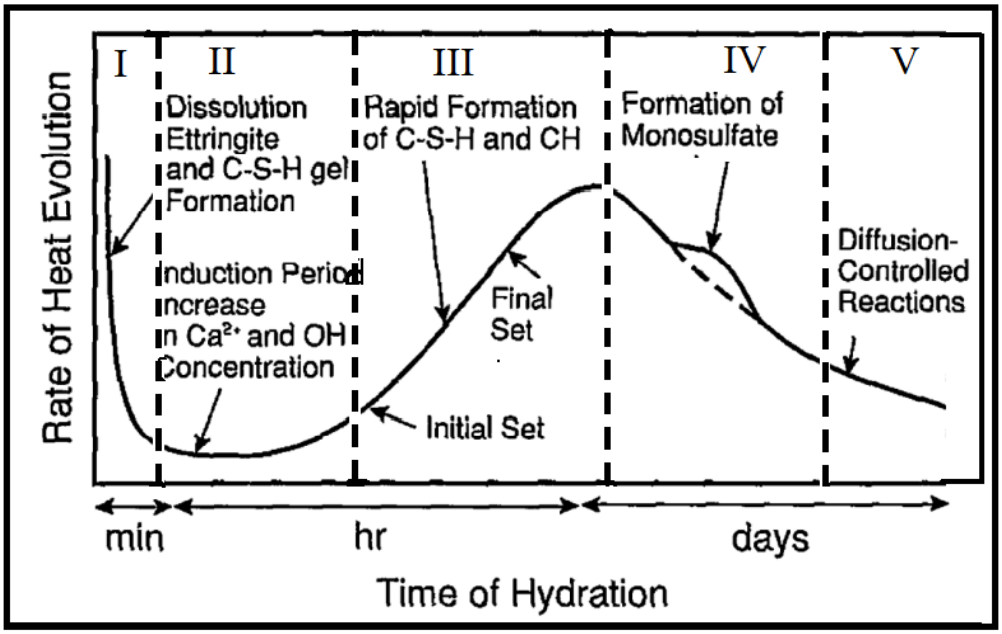

Figure 2. Schematic representation of hydration of cement, (I) Pre induction period, (II) Induction period, (III) Acceleration period, (IV) Deceleration period, (V) Diffusion- controlled reactions [57]

2.1.5 Hydration products of Portland cement

The formation of so-called hydration products is caused by the kinetics and reaction processes that take place during the hydration process of the portland cement phases.The main four major compounds are presented below.

2.1.5.1 Calcium Silicate Hydrate (C-S-H)

Calcium silicate hydrate (C-S-H) gel is the main product of hydration reactions, as it is responsible for strength and durability properties of cement. It occupies 50-60% of the volume of the cement paste. It is essential to mention that it is a compound with an undefined stoichiometry, which presents a ratio of C/S ratio that ranges between 1.5 and 2.01 [58]. The morphology it generally gives is of fibers, although some authors have found it in more rounded and less dense forms.

According to the literature [59–61], the structure of the C-S-H gel has not been fully defined, and several models have been proposed to describe it., although there are still many discrepancies among authors continue to exist. However, it is generally assumed to have a structure similar to a natural mineral called tobermorite, sometimes called tobermorite gel. In addition, some researchers have found a significant difference in composition between internal and external hydration products. The internal products (rings around anhydrous cement grains) are pure C-S-H gels with an average range of C/S ratio range of 1.5 [59], 1.7 [60,62], 2.1 [60], and 1.75 [61]. In the external products, other elements such as Al, K, and S have been reported to have a C/S ratio range between 1.60 [59] and 2.70 [60]. In addition, the C/S ratio can increase with the reduction in the water/cement ratio.

Thus, the variability in the composition of the C-S-H gel depends on

- Incomplete chemical equilibrium
- Substitution of Ca and Si by other ions in the structure of the hydrated C-S-H gel.
- A mixture of the C-S-H gel with other hydration products.
- Variation in the water/cement ratio and curing and setting temperature.
- Use of admixtures and replacement materials

2.1.5.2 Calcium hydroxide (CH)

The CH component of hydrated cement pastes is the second-most prevalent product with defined stoichiometry $Ca(OH)_2$, which can react with the pozzolanic additions to become C-S-H, as described below.

Calcium hydroxide crystals (also called portlandite) make up 20 to 25 percent of the volume of solids in the hydrated paste. This compound tends to form elongated crystals with a hexagonal prism morphology. The morphology is usually affected by the space available for its formation, the hydration temperature, and the impurities present in the system [58].

According to Taylor, the morphology of C-S-H and CH can be observed by employing backscattered electron imaging analysis (BSEI) of cement pastes, mortars, and concretes at different curing ages. Karen L. Scrivener [63] published the microstructure of a portland cement mortar, which is presented in Figure 3. Appreciating the appearance of the external and internal products of C-S-H and CH is possible.

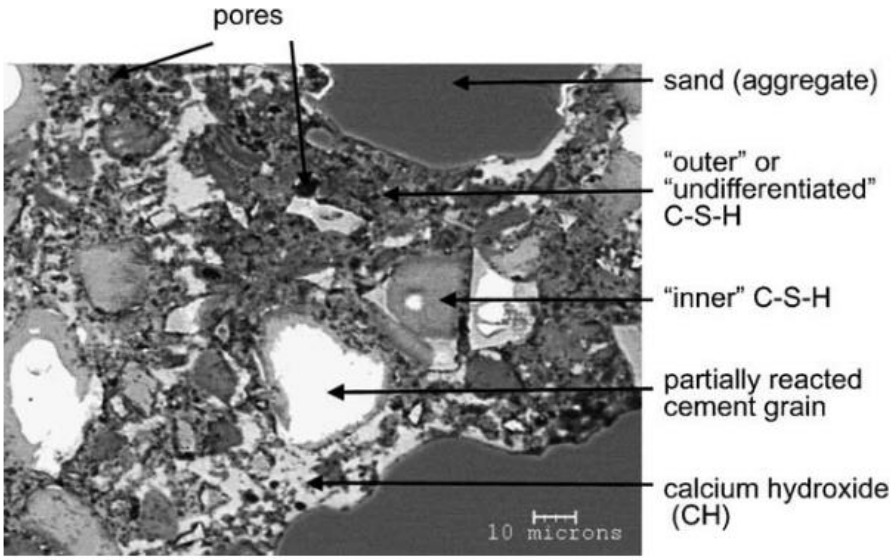

Figure 3. Back-scattered electron microscopy of a portland cement mortar at 200 days of curing [63]

2.1.5.3 Ettringite (AF_t) and Monosulfate (AF_m)

The ettringite, $C_6AS_3H_{32}$, initially formed during cement hydration, can occupy a volume fraction of about 0.15 to 0.2 of the total hydrated cement paste and is commonly referred to as AF_t. The formation of ettringite during the initial hydration stage is important in controlling the setting time of the highly reactive calcium aluminates [64].

After initial hydration, ettringite is partially converted to monosulfate, C_4ASH_{12}; this monosulfate is very susceptible to carbonation, forming ettringite and a Hemi-

carbonate. The late formation of ettringite in hardened cement can be harmful, causing significant expansion and cracking in structures [65].

According to Taylor4, ettringite is characterized by a hexagonal needle-like morphology, and monosulfate has a layered structure derived from CH by the replacement of a Ca^{2+} ion by Al^{3+} or Fe^{3+}. Backscattered electron image analysis, which is used to observe the morphology of C-S-H and CH, is also used for ettringite and monosulfate.

Paul Stutzman [66] published microstructures of hydrated cement pastes, one of the images is shown in Figure 4, where it is possible to appreciate the type of morphology of monosulfate. On the other hand, Zhidong [67] reported the microstructure of concrete, in which the ettringite can be observed (see Figure 5).

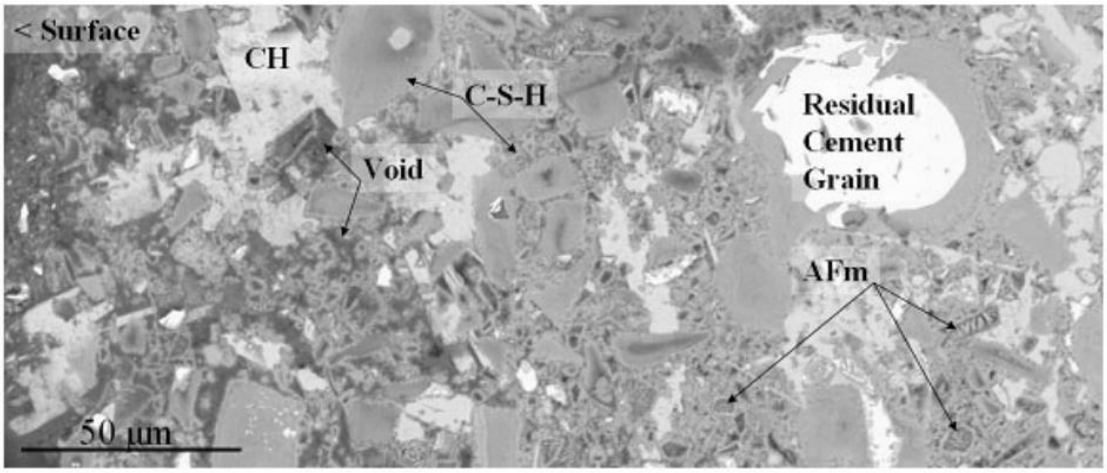

Figure 4. Cross-section of hardened cement paste, showing residual cement grain, calcium silicate hydrate (C-S-H), calcium hydroxide (CH), monosulfate (AF_m), and voids [66]

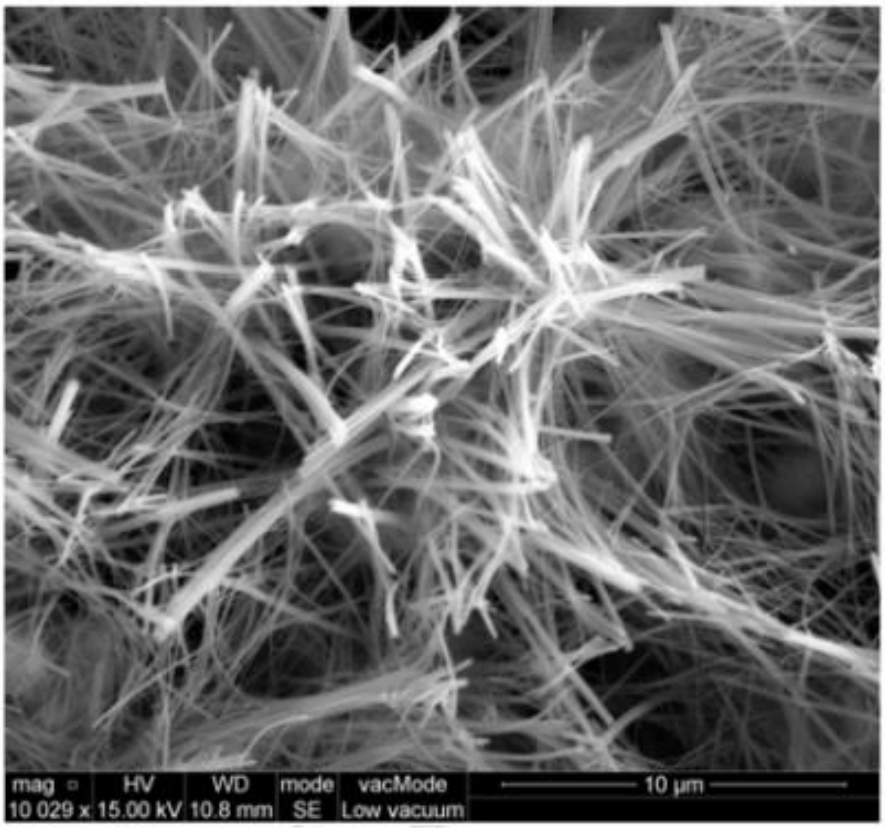

Figure 5. Ettringite fibers are seen in hydrated OPC paste cured for 24 hours [67]

In summary, hydration reactions between silicates, aluminates, calcium sulfate, and water produce C-S-H, CH, ettringite, and monosulfate and determine the mechanical properties, chemical composition, and microstructure of cement paste. However, the hydration process changes when another material of a similar chemical nature is added to portland cement. The mixture of portland cement and other materials is known as composite cement.

2.2 Sulfoaluminate cement

Research on alternative cement has increased in recent years in search of new, less polluting binder options. In the present work, the behavior of sulfoaluminate cement (CSA) was also studied, and the importance of this type of material will acquire over time. It is worth mentioning that cement manufacturing produces large amounts of CO_2 due to the use of energy and the calcination of $CaCO_3$. The percentage of CO_2 produced per ton of cement varies depending on the cement composition and efficiency, among other factors, and is, therefore, difficult to quantify. However, recent data on global CO_2 emissions from the cement industry estimate an average of 0.88 tons of CO_2 per ton of cement produced.

The Portland cement industry produces CO_2 in two ways: by converting calcium carbonate to calcium oxide inside the kiln. It needs to calcine a large amount of fossil fuels to heat the kilns to almost 1500ºC to form the clinker components [57,58]. Since the production of traditional Portland cement produces enormous emissions of CO_2 and is expected to increase in both production and consumption, great efforts are being made to replace it. ASCs have been known since the patent of Alexander Klein in 1963. However, they are not widely used in Europe and the U.S.; they have been produced, used, and standardized in China for approximately 30 years as a binder for concrete in bridges, leak and seepage prevention projects, concrete pipelines, precast (e.g., beams and columns), prestressed concrete elements, waterproof coatings, fiberglass reinforced concrete products, low-temperature construction and shotcrete [12].

These cements are drawing more interest because they promise to offer a substitute for Portland cement that emits less CO_2. Compared to alite (hydrated calcium silicate in cement clinkers), which releases 0.578 g of CO_2 per g produced, sulfoaluminate clinker releases only 0.216 g of CO_2 per g.

CSA cement contains ye'elimite ($C_4A_3\hat{S}$) as the main constituent (30-70%), which was introduced as a phase of the cement by Klein, who used it as an expansive or

shrinkage compensating addition to cement binders so that in addition to the CO_2 reduction, the hydration reactions of C4A3Ŝ with calcium sulfates initiate rapidly to form ettringite (AF_t), the main hydrate, which contributes to the accelerated strength of sulfoaluminate cement [12][68]. The manufacturing temperature used to produce CSA clinker is generally 1250°C, approximately 200°C lower than that used for Portland cement clinker. It should be noted that CSA clinker requires less energy for grinding, which reduces energy consumption.

2.2.1 Manufacturing process

CSA clinker can be produced from limestone, bauxite, and calcium sulfate (anhydrite or gypsum). Generally, the same production process can be applied for Portland cement clinker, either in the kiln or furnaces.

These cement were produced by adding gypsum to the two types of CSA cement clinker: the first with belite sulfoaluminates: ye'elimite (C4A3Ŝ and belite (C2S) and the second with ferroaluminates consisting mainly of ye'elimite (C4A3Ŝ), belite (C2S), calcium sulfate (CŜ) and smaller quantities of aluminoferrite (C4AF). The different types of calcium sulfate that can be present in these clinkers are gypsum (CŜH2), basanite (CŜH0.5), anhydrite (CŜ), or mixtures of them [68], which results in rapid hardening, high mechanical strength, and at the same time undesirable expansions.

CSA can be produced at temperatures around 1250°C, which is 200°C less than the production temperatures of Portland cement [69][70]. The amount of limestone required to produce CSA is considerably less than that needed for Portland cement, and, in addition, the high porosity of CSA clinkers facilitates their grinding [69]. These advantages represent a 25-35% reduction in net CO_2 emissions compared to portland cement [71] [72], thus contributing to reducing energy demand and carbon footprint [73] [74]. However, SO_2 emissions are significantly higher [69]. Generally, the production process is very similar to that of Portland cement clinker based on rotary kilns.

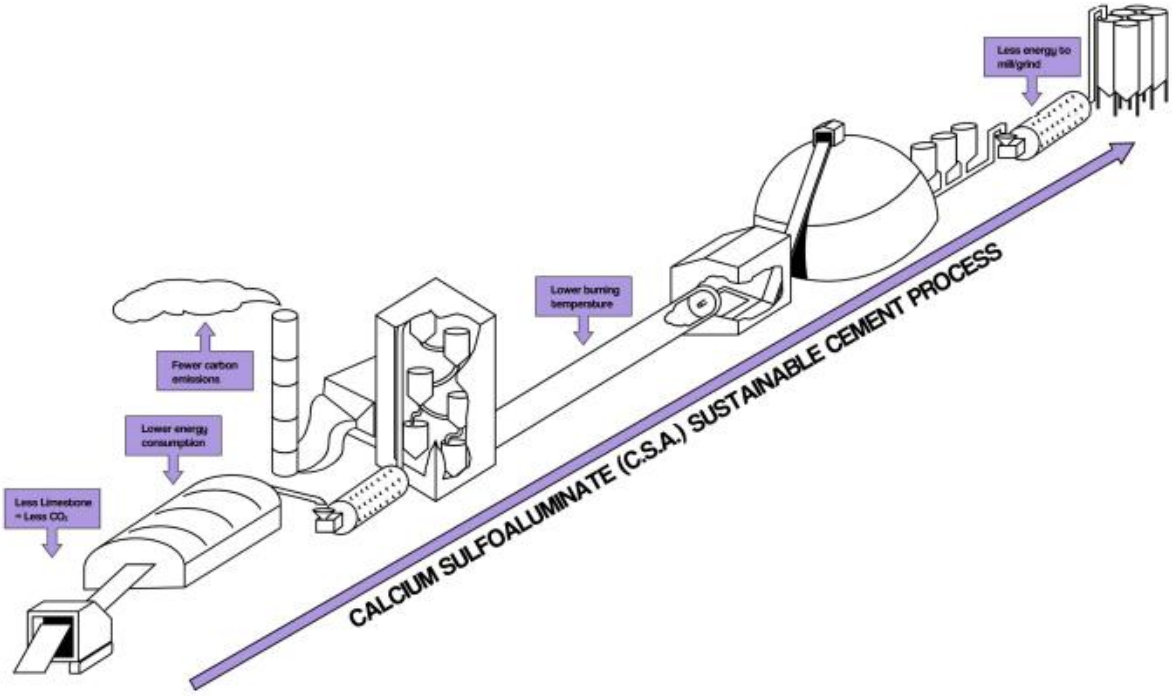

Figure 6. Schematic diagram of the manufacturing process of Sulfoaluminate cement [74]

Depending on the composition of the raw material, CSA clinkers may contain various hydraulic phases, such as belite, calcium aluminoferrite, excess anhydrite or free lime, and calcium aluminates. To increase the reactivity of the belite phase, which is responsible for developing the late strengths of sulfoaluminate cement, secondary ingredients can be added to the raw material. Typically, 15 to 25% of the weight of gypsum is ground with the clinker to achieve the optimum volumes for setting time, strength, and stability [69].

2.2.2 Raw materials

The primary raw materials for CSA are limestone (calcite), clay, bauxite, and calcium sulfate or gypsum as sources of calcium, silica or aluminium, and sulfur, respectively [73] [75], and the main chemical reactions occurring in the CaO-SiO_2-Al_2O_3-SO_3 system from these raw materials, during the formation of CSA clinker are summarized in the following equations (1 to 7) [71]. It is essential to point out that the high cost of bauxite makes cement more expensive, which allows a limited application compared to low-cost Portland cement [73].

$$CaCO3 \rightarrow CaO + CO2 \quad \text{equation 9}$$

$$2CaO + Al2O3 + SiO2 \rightarrow C2AS \quad \text{equation 10}$$

$$3CaO + Al2O3 + CaSO4 \rightarrow C4A3S \quad \text{equation 11}$$

$$3CaO + 3C2AS + CaSO4 \rightarrow C4A3S + 3C2S \quad \text{equation 12}$$

$$2CaO + SiO2 \rightarrow C2S \quad \text{equation 13}$$

$$2CaO + CaSO4 \rightarrow 2C2S.CS \quad \text{equation 14}$$

$$2C2S.CS \rightarrow 2C2S + CS \quad \text{equation 15}$$

2.2.3 Hydration of Sulfoaluminate cement

Hydration of ye'elimite in the presence of calcium sulfate and water forms ettringite ($C_3A.3C\hat{S}.32H$ or also written as $C_6A\hat{S}_3H_{32}$) and aluminium hydroxide (AH_3), which contributes to the expansion and development of the properties of CSA cement at early ages [72].

The main ingredient of the CSA cement is ye'elimite ($C4A3\hat{S}$), which, when reacting with gypsum, basanite, or calcium sulfate in the presence of water, forms ettringite [71] [76]. The phase is fundamental to the properties of concrete, such

as high early strengths, dense matrix, and durability. When ye'elimite reacts with insufficient amounts of calcium sulfate, monosulfoaluminate is formed, and when the reaction contains excess calcium sulfate, the system is likely to be dimensionally unstable. Therefore, one of the important factors underpinning the performance and durability of CSA/anhydrite cement combinations is the ratio between the ye'elimite and calcium sulfate content [71].

2.2.4 Reactions and hydration products

During the first 24 hours of hydration, the majority of the heat is released [69]. During the hydration process, three main problems occur 1) the dissolution of anhydrous crystalline phases, 2) the appearance of new phases such as crystalline ettringite (AF_t) and amorphous gels such as aluminium hydroxide (AH_3), and 3) water consumption. The precipitation can be summarized as follows: ye'elimite in the presence of a sulfate source (gypsum, basanite, or anhydrite) and the aqueous media will form ettringite and gibbsite (AH_3), according to equations 8-10, respectively. AH3 precipitates as an amorphous phase or poorly crystallized phase.

$$C4A3S + 2CSH2 + 34H \rightarrow C6AS3H32 + 2AH3\ gel$$ equation 16

(formation of ettringite)

$$C4A3S + 2CSH0.5 + 37H \rightarrow C6AS3H32 + 2AH3\ gel$$ equation 17

$$C4A3S + 2CS + 38H \rightarrow C6AS3H32 + 2AH3\ gel$$ equation 18

The formation of ettringite crystals achieves the necessary expansion caused by compressive stress, so the main cause of expansion in the CSA cement is the formation of late ettringite [76].

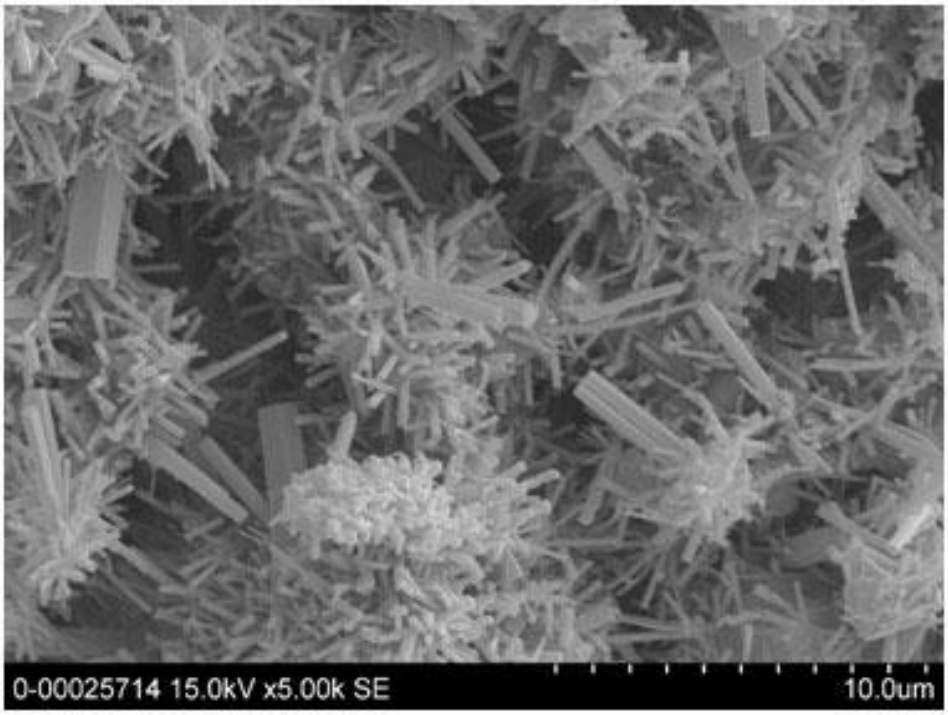

Figure 7. SEM micrograph showing ettringite after 1 day of hydration of sulfoaluminate belite cement [77]

The primary crystalline hydration product is ettringite, which is formed along with amorphous aluminum hydroxide. Once the source of sulfate (gypsum, basanite, or anhydrite) is depleted and sufficient free water is available, the monosulfate, also known as AF_m ($C_4A\hat{S}H_{12}$), is formed according to equation 19 [68]

$$C4A3S + 18H \rightarrow C4ASH12 + 2AH2 \qquad \text{equation 19}$$

(formation of monosulfate)

In the presence of belite, stratlingite is formed as an additional hydration product.

$$C2S + AH3 + 5H \rightarrow C2ASH8 \qquad \text{equation 20}$$

(formation of stratlingite)

A commercial CSA clinker was mixed with different amounts of gypsum in the experiments by Glasser and Zhang [78]. Gypsum addition of 30% or more is required for the specific CSA clinker, it has been demonstrated, in order to create just the AF_t phase. There is evidence that CSA cement expands more when calcium sulfate is added [79–81]. Because of this, selecting the source of sulfate is very important to achieve the desired properties [68].

The microstructure of the cement is quite dense even after 16 h of hydration, with little pore space available at the age of 28 days [82] (Figure 8).

Other hydration products may occur depending on the minor phases present in CSA cement, such as C-S-H phases, monocarboaluminate, gibbsite, or hydrogarnet.

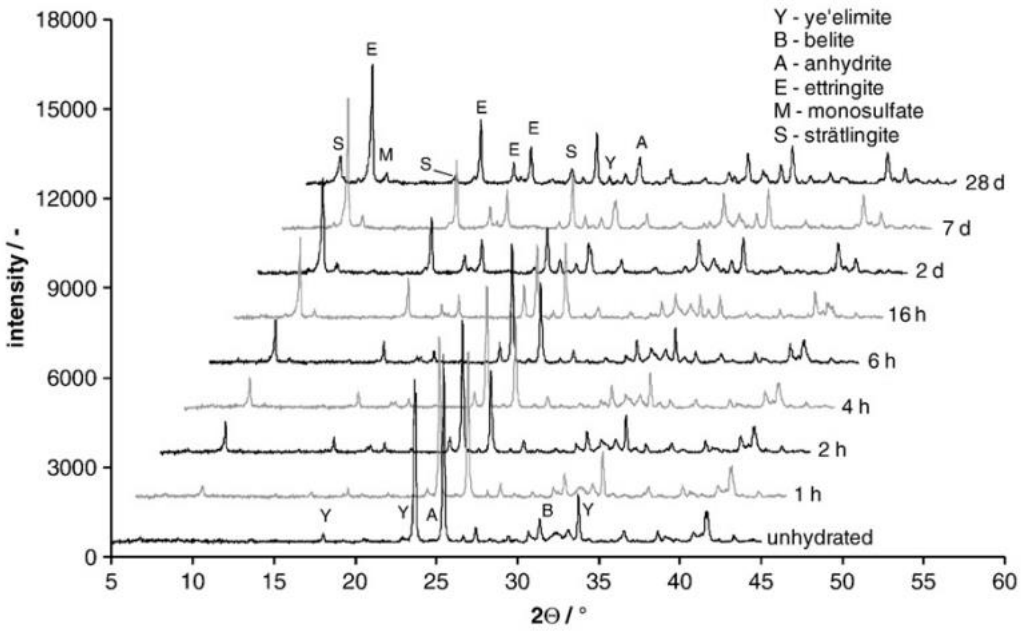

Figure 8. X-ray diffraction analysis of CSA; unhydrated sample and after 1, 2, 4, 6, 16 h, 2, 7, 28 days of hydration at w/c=0.80 [82].

2.2.5 Water/ cement ratio

For complete hydration with CSA, a higher water/cement (w/c) ratio is needed than with OPC. The particular amount of water required for full hydration is largely dependent on the contents of ye'elimite and belite [83]. It has been found that the water-cement ratio (w/c) significantly alters the expansion behavior and durability of cement. It has been shown that a reduction in the w/c ratio increases the expansion [80]. Additionally, a low w/c ratio causes ye'elimite to hydrate insufficiently, delaying its expansion in the humid environment. It has also been found that slow hydration of ye'elimite at a low w/c ratio affects the expansion rate [76,84]. Due to a decline in supersaturation and an elevation in porosity, Bizzozero [80] reported that the expansion at higher w/c ratios is reduced (which can be accommodated in crystals without developing can be accommodated in crystals without generating much crystallization stress).

According to M. Garca-Maté [51,83], a w/c ratio of 0.78 is necessary for the purest ye'elimite to react stoichiometrically with anhydrite to generate ettringite. This implies that a w/c ratio of 0.5 is required for a CSA containing roughly 50% by weight of ye'elimite, which can result in pastes with wider pore diameters than OPC pastes. Furthermore, they assert that high w/c ratios could indicate significant expansion, which also contributes to poor end strengths; nevertheless, lower initial particle sizes or additives could lessen some unfavorable qualities.

According to Sanchez Herrero [85], they stated that concerning the formation due to the amount of added water is reported by many researchers who have seen monosulfoaluminate as the main reaction product in the hydration of C4A3Š with water; others have argued that ettringite and monosulfoaluminate precipitate from the beginning in C4A3Š pastes [86]. These differences are associated with variations in the water/cement ratio used in the studies [87]. It has been observed that an increase in the amount of water required for the hydration of C4A3Š favors the precipitation of ettringite, calcium monosulfoaluminate, cubic hydrate, and gibbsite [87].

2.3 Supplementary cementitious materials

Today, to enhance the physical and mechanical characteristics of cement paste, whether in the fresh or hardened stage, supplementary cementitious materials (SCM) have been added to cement [8]. While Portland cement clinker continues to be the primary component of various forms of cement, cement containing SCMs has taken the role of Portland cement [4]. The difference that can be found in the chemical composition of SCM with respect to an OPC is in its lower calcium content which can be seen in the ternary diagram shown in Figure 9A and 9B [8,88]. Figure 9B shows the main hydration phases for Portland cement and SCM [8,89], the latter having a higher content of silica and alumina and less calcium; this is the difference in obtaining different phases [35].

The high cost of bauxite presents an economic challenge for CSA cement, making them more expensive than OPC. They can be used with supplementary cementitious materials (SCMs), including industrial by-products, to lower prices and the quantity of CO_2 related to CSA production (e.g., slag or FA).

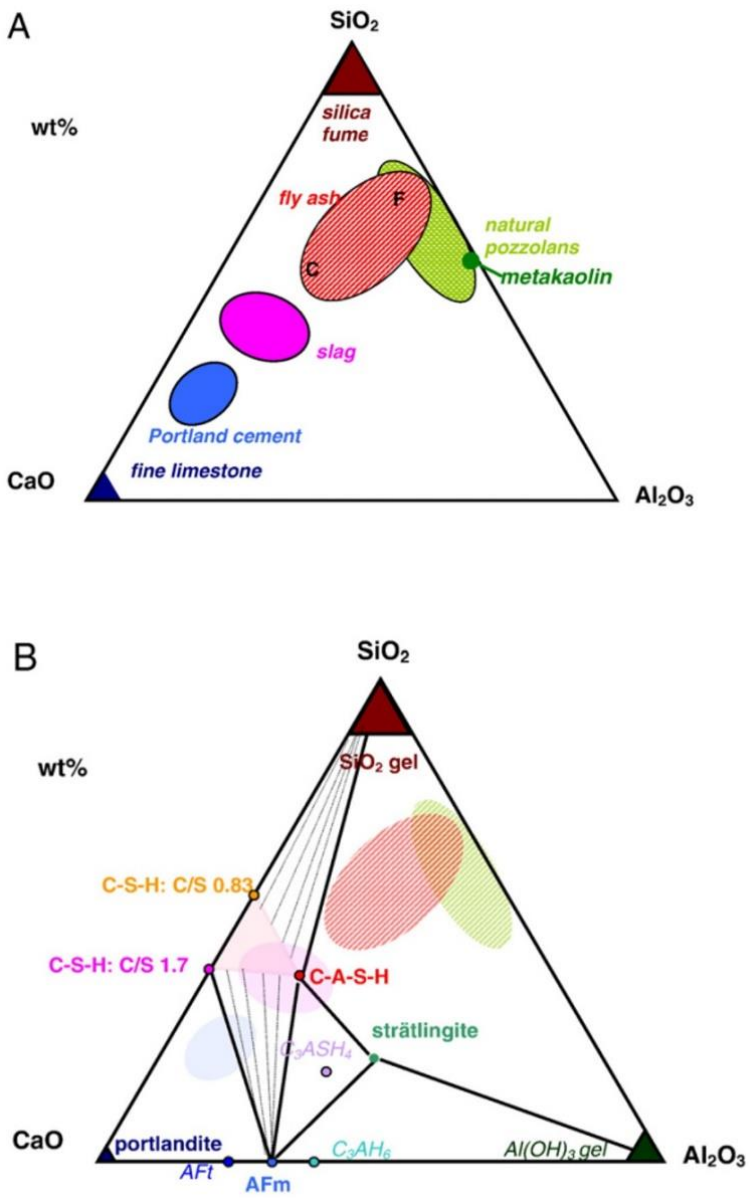

Figure 9. A) $CaO–Al_2O_3–SiO_2$ ternary diagram of cementitious materials, B) hydrate phases in the $CaO–Al_2O_3–SiO_2$ system. Without carbonate or sulfate, C_3AH_6 will be more stable than the AF_m phases [8].

2.3.1 Fly ash

Fly ash (FA) is a pozzolanic material that is a by-product of kilns that uses coal for power generation. The FA consists of fine particles of spherical morphology, which can be solid or hollow. Amorphous, carbonaceous material in FA is composed of angular particles [90]. When coal is burned at a temperature between 1250 °C and 1600 °C, the non-combustible materials collide to form small glassy spheres of silica (SiO_2), alumina (Al_2O_3), iron oxide (Fe_2O_3), and other minor constituents [91]. The physical and chemical properties of FA depend on the composition of the inorganic fraction of the coal, the degree of pulverization, history, and oxidation conditions.

The FA can be composed of mineral phases such as quartz, lignite, siderite, and mullite, and an amorphous fraction consisting of SiO_2-Al_2O_3-(CaO)-(MgO). Based on the chemical composition, two classes of FA are distinguished and defined by ASTM C618-8924 [93]: the low calcium content class, called Class F, and the high calcium content class, called Class C. Class F FA is generally produced by calcination of anthracite or bituminous coal with a minimum of 70% silica, alumina, and ferric oxide, it also requires that the SO_3 content be less than 5% and that its loss by ignition is not greater than 6%.; Class C from sub-bituminous coal, or lignite, contains less SiO_2 and Al_2O_3 than Class F but high amounts of CaO. In Mexico, the production of FA is of class F, which has a low CaO content and little or no cementitious properties.

In cement pastes, fine and spherical FA particles increase compressive strength at later ages due to the packing effect of fine FA, as the small, spherical particles fill the pores and increase density [41,43,91]. In addition, the presence of very fine particles with a large surface area favors pozzolanic reactivity. The filling effect is important, as FA shows little reaction for up to 7 days. Compared to cement mixtures, FA additions show a better contribution to strength after 13 days due to the influence exerted by the FA on tricalcium aluminate(C_3A) and tetra-calcium

ferroaluminate (C_4AF) phases present in the clinker, reducing the heat released and stimulating the formation of hydrated silicates [88]. The pore solutions of cementitious materials are also very sensitive to the heat released from the clinker.

The factors involved in the behavior of FA are size and spherical morphology, chemical composition, pH of the medium, the surface area of the particles, CH availability, and the amorphous fraction of the FA. These factors have been found to modify the development of the mechanical, chemical and microstructural properties of Portland cement pastes, concretes and mortars [89]. Also other important factors are the curing temperature and the level of FA replacement, as they affect the hydration process, hydration products, and microstructure development of Portland cement pastes [46].

At temperatures below 35°C, during the initial hydration of cement pastes with FA, the amorphous fraction of FA did not react with the CH; rather, the reaction occurred until the FA had generated nucleation sites and the hydration of C_3S was accelerated. Due to CH consumption by the pozzolanic reaction of FA, the hydration of C_2S and C_4AF of Portland cement was delayed [44]. Based on the analysis of the heat of hydration performed by Durán et al [90], the addition of FA does not delay the hydration acceleration period of C_2S; however, it reduces the heat of hydration.

The use of FA as a replacement for cement has been associated with increased workability of the fresh mix, decreased permeability, and increased mechanical strength. In addition, in the hydration process, FA decreases the heat of hydration, reducing the risk of thermal cracking [38,42]. The properties of FA have been used mainly to improve mechanical strength and develop durability (by reducing the possibility of alkali-aggregate reaction) in concrete. However, its use has been reported to delay the setting time of cement [42].

The hydration products formed by the pozzolanic reaction of the FA in cement pastes fill the interstitial pores, reducing the permeability of the C-S-H matrix and

producing C-S-H gel with a different C/S ratio than the C-S-H from the hydration of portland cement [92].

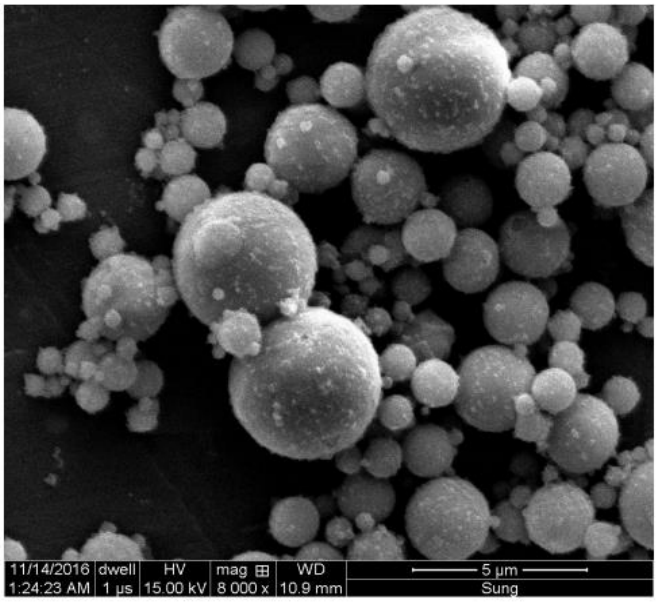

Figure 10. SEM micrograph of fly ash [93]

2.3.2 Volcanic ash

Volcanic ash comes under natural pozzolan as per ASTM C618-93 [94], which contains raw or calcined material which shows pozzolanic properties. This natural silicoaluminous material is produced by volcanic eruptions. Its structure comprises vitreous silicoaluminous particles with more than 50% silica content. When combined with Portland cement or lime in water, it produces compounds of low solubility and cementitious properties. These materials do not require additional treatment other than grinding to react with the lime.

The physical characteristics of natural pozzolans are very diverse. The characteristics of new concrete as well as the development of strength are influenced by the fineness, density, specific surface area and particle shape, of natural pozzolans [95].

Natural pozzolans have a wide range of chemical compositions that rely on their origins. In incoherent volcanic pozzolans, usually, there are high amounts of silica and alumina. Iron, calcium, and magnesium oxides are the other oxidized elements. Alkali concentration ranges from 3 to 10%. Loss on ignition is typically minimal, although in some pozzolans it can reach 9% [96,97].

The pozzolanic reaction is the reaction between the active phases of pozzolan and lime. The amount of amorphous material often affects how reactive natural pozzolans are. It can be difficult to determine which parts of natural pozzolans are reactive, but generally speaking, the consumption of lime estimates the pozzolanic reaction in a lime-pozzolan mixture or by measuring the acid-soluble silica and acid-soluble alumina [95].

The pozzolanic activity of naturally occurring pozzolans depends on a variety of factors. The particle fineness and surface area, the amount of water used for mixing and the lime pozzolan mixture, the curing technique, and the temperature all have a significant impact on the active phase character and concentration in the pozzolan [95,98].

The hydration of Portland cement is comparable to the reaction products of the lime-pozzolan system. The silicate and aluminate hydrates produced by natural pozzolans are identical to those produced by Portland cement. Their slight discrepancies typically manifest in the quantity of reaction byproducts. Calcium silicate hydrate and calcium aluminate are the main reaction products of the natural pozzolans in a saturated lime solution [99].

The water-to-cement ratio of the blended cement mix and the length of wet curing are related to the porosity of cement paste with and without pozzolans. The volume of big pores also grows with elevated temperature. The amount of substitution and the reactivity of the natural pozzolan influences the porosity of the cement paste. Using the mercury intrusion method, the total porosity of the pozzolanic cement paste was found to be higher than that of the reference cement paste with Portland

cement [100]. Like Portland cement paste, the overall porosity of pozzolanic cement paste diminishes over time.

Permeability, when compared to parent cement paste, cement pastes containing pozzolan have a higher rate of fluid intrusion when pressure is applied early on. The permeability of pozzolanic cement paste is reduced significantly more by moist curing it for longer ages than normal cement paste. Although it has been around longer, pozzolanic cement paste still has a higher porosity than regular cement paste [100,101]. When well cured in humid conditions at later ages, the water infiltration of the concrete containing natural pozzolans was greater than that of the control concretes.

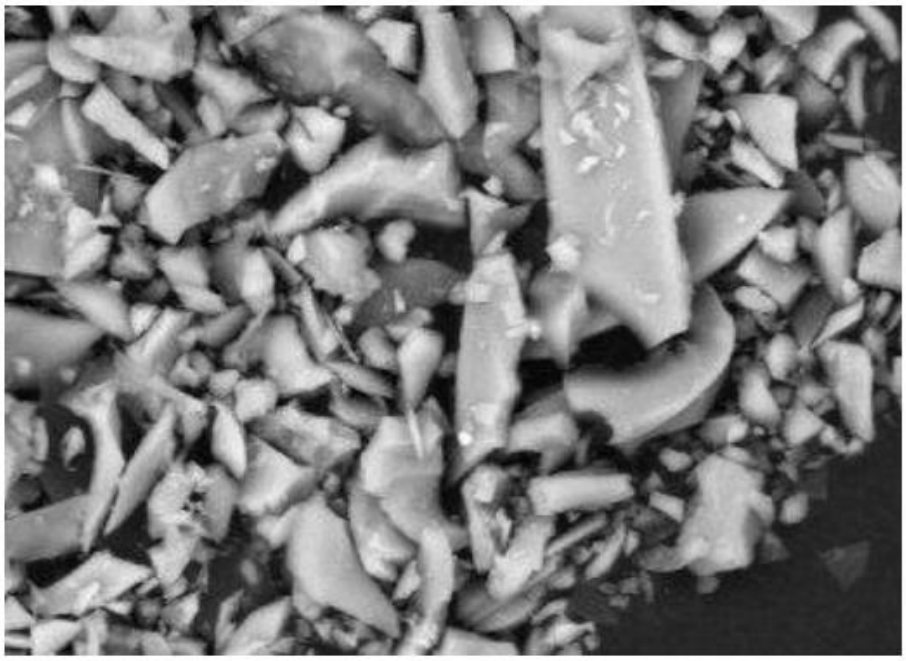

Figure 11. SEM micrograph of Volcanic ash [102]

The principal benefit of adding natural pozzolans to bulk concrete is that it controls thermal cracking by lowering the temperature at which natural pozzolanic cement hydrates. Calcium alumino silicate hydrate (C-A-S-H) gel forms when the amount of alumina in VA is high. in the blended cement paste as the hydration reaction

product; this positively affects sulfate attack. The strength of the cement paste samples was directly correlated with the hydration products in the system, C-S-H and C-A-S-H specifically, play a vital role in the strength of the cement paste samples [106]. They are also commonly employed in dam construction as mass concrete structures due to the increase in sulfate resistance and the reaction time of the alkaline aggregates in concrete containing suitable amounts of natural pozzolans [95,103].

Kunal Kupwade-Patil [104] reported in his research that varying the percentage of OPC with VA from 10%-50% results in forming C-S-H, C-A-S-H, and M-S-H along with the other crystalline products detected as the main hydration products. Increasing the replacement percentage of OPC from 30% leads to increased porosity and vesicularity in the cementitious matrix.

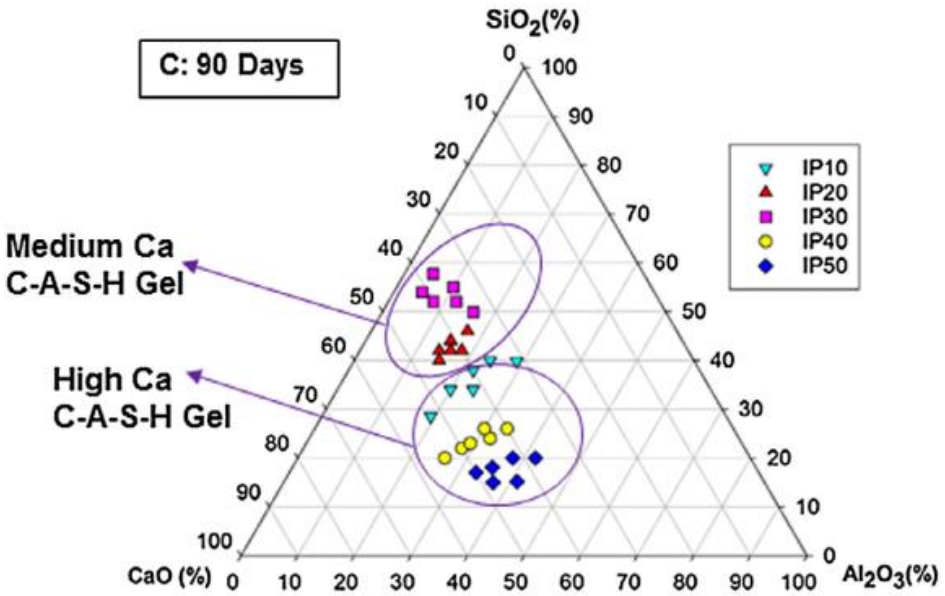

Figure 12. Ternary phase diagram of OPC-VA combinations after 90 days of curing

2.3.3 Spent coffee grounds

One of the most consumed beverages and yet popular trading products globally is coffee. This is accountable for many environmental hazards in the form of SCG. Due to the fact that SCG is a solid by-product specifically linked to coffee consumption, substantial amounts of SCG from coffee shops are landfilled [105]. SCGs require a tremendous amount of oxygen to more effectively break down the organic structure because there are more organic chemicals present in them [105,106]. SCG contains environmentally hazardous substances including caffeine, tannins, and polyphenols that need a lot of oxygen to break down the organic shell. Proper composting or vermiculture can decompose SCGs, in a highly nitrogen-rich compost; however, the disposal process is not as direct as most other waste materials [107–110]. Due to its high organic content, SCG has a higher risk of self-combustion, which could result in the production of significant volumes of methane and carbon dioxide as well as the emission of bad smells associated with fermentation processes when it is disposed of in large quantities and left untreated [111,112].

In a variety of civil engineering applications, SCGs are a great match. For example, SCGs may be used in road subgrades because of their physical characteristics, which are similar to those of sand [25,113,114]. Embedding SCG in clay bricks also leads to improved thermal properties of these bricks and reduces heat loss by up to 50% [115]. It is an efficient complement to acoustic walls due to its microscopic composition and high compressibility [115].

Agro-industrial biowaste volumes and SCG will multiply as the demand for coffee-based beverages continues to climb internationally. These produce harmful effects on the environment; therefore, the physical characteristics and chemical composition of SCGs must be understood. It can provide some clues to handle these SCG for recycling purposes and application to construction industries [116].

SCG always contains high moisture content due to its brewing process. Due to the fact that SCGs are created by reacting with water, their total volume of pores and specific surface area are smaller than those of fresh coffee. This means that according to Brunauer-Emmett-Teller (BET) analysis, SCGs can be categorized as non-porous materials. The total pore volume for SCG was determined to be 0.02-0.07 cm^3/g, while the specific surface area was reported to be in the range of 0.305- 0.88 m^2/g [110,117] and also had high adsorption capacity [118]. The specific gravity was found to be in the range of 0.6-1.4, and the density of 917-1367 kg/m^3 [111]. By contrasting the densities of SCG with lightweight aggregates, it can be suggested that SGC can be used to produce lightweight structural concrete with a unit weight less than1900 kg/m^3 [119].

The composition of SCG contains considerable amounts of potassium oxide, calcium oxide, titanium oxide, and iron oxide, according to X-ray fluorescence (XRF) analysis [35,120]; the Loss on Ignition (LOI) was also very high due to the high amounts of organic compounds [26].

The SCG particles are granular and are similar to sand; that is why they were used as a recycled construction material; due to their high friction angle and shear strength, SCG was used to form the majority of embankment fills [113].

SCGs were additionally utilized for generating lightweight clay aggregates. Also, this can be used to prepare clay with a 15% mass of SCG, which can yield future applications because of its porosity and bulk density. Other than SCG, the coffee husk is also used in ceramic production. As discussed for SCG, a 15% additional coffee husk in ceramics also shows better mechanical strength. Coffee husks were also used for applying roof tiles and industrial clay products as a replacement for cement in mortars and concrete; reports suggest the addition of 10% coffee husk can be used for all the above applications. It was claimed that the lasting revitalized binder could be utilized to manufacture asphalt for web visitor traffic and for fixing damaged asphalt or even reclaimed mature asphalt.

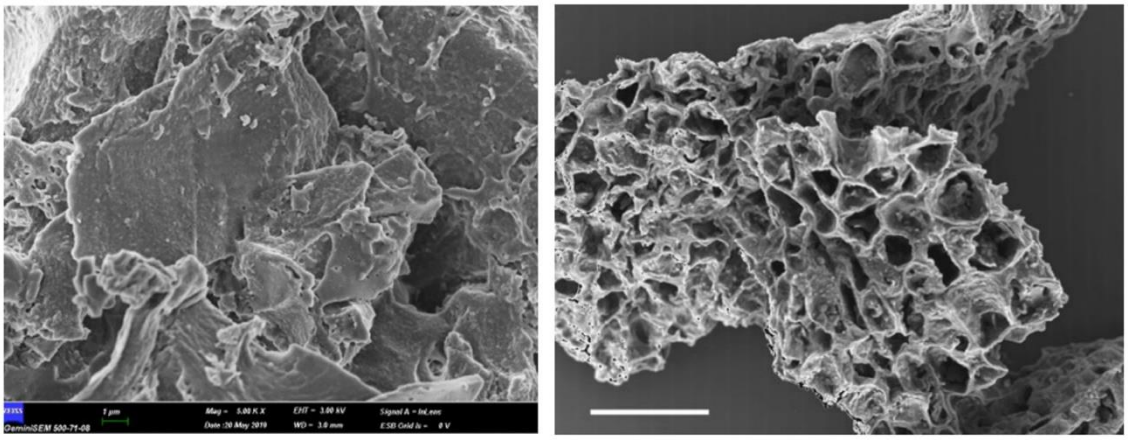

Figure 13. SEM micrograph of spent coffee grounds [118,121]

2.4 Effect of supplementary cementitious materials on OPC

The use of SCM, in combination with cement, is affected by considerations such as chemical composition, particle size, pozzolanic or hydraulic activity, replacement level, and morphology of the cement. These characteristics affect various properties of the concrete. The complexity of understanding composite cement increases when cement substitutions are of more than one material. This creates the ideal environment for analyzing these systems as a synthesis of chemical and physical effects. SCMs have been discovered to have a yet unclear impact on the hydration kinetics of concrete.

Partial substitution of Portland cement with FA has been studied and observed to have favorable effects on the properties of blended cement, such as reduced heat of hydration, reduced permeability, and higher subsequent strengths due to the pozzolanic reaction between the portlandite and glassy phases present in the FA. However, it must be considered that the percentage of replacement of the Portland cement clinker with FA is limited to only 30% due to the poor development of initial strength [45,47,122] since the pozzolanic reaction between the FA and portlandite is slow at room temperature [123]. The fineness of FA also affects the mechanical strength of cement mix, mortar, and concrete [41–43].

The mixture of Portland cement with FA causes a decrease in the amount of portlandite in the hydrated mixture because: (i) FA has very low reactivity and (ii) the CaO in the FA serves as an additional source of calcium. Class F FA contains between 15 and 35% alumina, so mixing OPC with this material results in high amounts of Al-rich phases and low amounts of CaO [8].

For ≥60% replacement of portland cement by FA, complete depletion of portlandite has been observed after hydration periods of 1 year or more. After this time, when a significant amount of FA has reacted, there is a decrease in the amount of ettringite, which is due to the high Al_2O_3 and low SO_3 content of this material. At the same time, an increase in the amount of AF_m as monosulfate or monocarbonate, and the presence of strätlingite has also been reported. The formation of C-S-H observed in OPC - FA blends have a lower Ca/Si ratio and contain more Al. However, in contrast to the thermodynamic modeling results, the presence of strätlingite has been observed, which increases with increasing % FA in the mixture [8].

FA affects the hydration of the cement paste. The effect depends on the percentage replacement of FA and the curing temperature; when the replacement percentage is higher and the curing temperature also higher, it improves the pozzolanic reaction and formation of hydration reaction products in the early ages [46]. The early age strength of FA blended mix can be enhanced using alkaline activators such as sodium sulfate or using C-S-H seeds [40].

In 2003 Hossain [124] studied the consistency and setting times of blended cement using VA as a partial replacement for OPC. Chemical analysis results showed that VA had very similar compositions to that of OPC.

As the percentage replacement of cement increased, it affected the normal consistency of the paste. The normal consistency decreased to 13 % up to 50% replacement of cement. The specific gravity of VA was lower than that of OPC. This implies more volume for VA than OPC resulting in more water to get the exact

consistency for the cement paste. Replacing OPC with VA increases setting time due to the decrease in the heat of hydration during the hydration process [124].

The high silica content in VA and the formation of calcium hydroxide due to the reaction of cement with water results in the formation of calcium silicates and other stable compounds; this pozzolanic action helps in the durability and strength gain for blended cement with VA and OPC. Early ages of the cement paste showed lower compressive strength findings compared to the reference cement paste. The capillary porosity of the mortar is reduced by adding a secondary C-S-H, and as a result, a higher level of hydration is reached, leading to higher strength in later ages [125]. The formation of gels C-S-H and C-A-S-H was attributed to a dense matrix in the hardened cement paste [104]. Also, as the particle size decreases, the reactivity of the VA with OPC increases [13,100,126,127].

The electrical resistance was more excellent for blended cement with OPC and VA. As the percentage replacement of OPC with VA increased, the pozzolanic action also improved, leading to increased electrical resistance. Electrical resistivity measurements can be used to predict diffusivity and porosity. The electrical resistivity of the cement mortars affects the rate of corrosion. Since the replacement of cement with VA increases, this also aids in less corrosion [128,129].

Studies on composite cement with OPC, VA, and blast furnace slag pulverized fuel ash was carried out by Escalante Garcia from 1998 to 2004. He used 60% of blast furnace slag, 30% FA, and 22% VA with OPC and cured at various temperatures ranging from 10 ℃ to 60 ℃. The studies observed that as the curing temperature increased, the porosity also increased [29]. The hydration rate was more significant for lower curing temperature at 10 ℃ and observed lower porosity. The C-S-H formed for the composite with VA showed a shift in higher Si and Al; also a lowered Ca content [30–33].

2.5 Effect of supplementary cementitious materials on CSA

The physical qualities and pore solution chemistry of the expansive cement system are altered by the effect of mineral additions on the expansion characteristics of CSA [75]. Alkali binding during the creation of the C-(A)-S-H gel is known to reduce the alkalinity of the pore solution when mineral admixtures are used [75,130]. A study by Folliard et al. reported that mixing CSA cement with FA reduces the degree of expansion [75].

In the early phases of hydration, CSA cement pore solutions often have a lower pH than OPC, which implies that it is anticipated that FA would dissolve even more slowly than in OPC systems. Additionally, portlandite, the primary component with which the FA interacts, gives way to the pozzolanic reaction to create new C-S-H gels, resulting in concrete with better physical and mechanical properties [92], is often not generated when CSA is hydrated. Since $Al(OH)_3$ is formed and not $Ca(OH)_2$ is formed, which is known as portlandite. But if C-S-H is found in hydrated CSA cement, it can give calcium ions to C-S-H with a lesser Ca/Si ratio, as was the case with blended Portland cement with FA.

In CSA cement, FA encourages early ettringite generation. Strätlingite, on the other hand, is discovered only after 180 days at a high water/cement ratio, and this is thought to indicate that FA has only a very limited reaction [50].

According to García-Maté [51], P. Chaunsali, and P. Mondal [75], there are very limited studies on using mineral admixtures with CSA cement. CSA cement, thus justifying detailed investigations in this direction, the beneficial effect of the addition of mineral admixtures on the properties of concrete.

2.6 Effect of spent coffee grounds

Waste material obtained after the preparation of instant coffee, SCG, have been employed as a home fertilizer or landfill [25]. From the studies of Teck-Ang Kua, these wastes can be successfully converted into construction material that can be used as an embankment fill instead of land fill which is a non-soluble material in soil [36,113,131,132]. The chemical composition of SCG, which is extremely polysaccharidal and has a high burning capability, is toxic to the environment, making them unsuitable for compost and landfills. SCG were used for the preparation of alkali-activated bricks with 2.5% of SCG and showed a decrease of compressive strength for structural applications but can be used for nonstructural applications since it meets the compressive strength 8.6 MPa for construction applications as per ASTM C62. Geopolymer prepared using SCG with blast furnace slag at 50 ℃ can be used as subgrade filling material [28]. Formation of gels C-S-H, C-A-S-H, N-A-S-H attributed to the strength of geopolymer mix [114].

CHAPTER 3

HYPOTHESIS AND OBJECTIVES

3.1 HYPOTHESIS

Varying, the amount of pozzolans and SCG to OPC & CSA cement will improve the compressive strength, durability, electrical resistance and will modify the microstructure by producing a dense matrix of hydration products of the cement.

3.2 OBJECTIVES

3.2.1 General Objectives

To study the physical, chemical, electrical, and mechanical properties of blended cement with SCG and pozzolans.

3.2.2 Specific Objectives

- To characterize the structure and chemical composition of the raw materials using SEM, EDS, and XRD
- To replace the cement (OPC and CSA) in various percentages with pozzolans.
- To find the hydration temperature of the composite cement.

- To find the optimum strength of blended cement by partially replacing OPC and CSA cement from 10% to 33.5 % with SCG, FA, and VA and then characterize the cement.
- To find the electrical resistance of the blended cement cubes using electrochemical impedance spectra.
- Finally, to investigate the characterization of cement paste cubes using compressive strength tests up to 210 days, SEM, EDS, ATR, and XRD.

3.3 SCIENTIFIC-TECHNOLOGICAL CONTRIBUTION

The use of FA and VA in recent years has made it possible to effectively reduce cement consumption in different ways of inclusion in certain types of mixes, providing a solution for recycling these industrial by-products. An ecological and economical alternative with the combination of two pozzolans and spent coffee grounds with cement: FA, VA, SCG, giving us the possibility of less pollution and helping in producing less expensive concretes.

CHAPTER 4

EXPERIMENTATION

This section presents the methodology used in the research. The whole work was divided into four stages. First, the preparation and characterization of the raw material, followed by the design and synthesis of preliminary pastes to find the most suitable water/cement ratio for the mix to reach adequate mechanical strength, according to the reviewed literature. Following the identification of the best formulations, the design and final synthesis were completed in order to carry out the characterization on the designated days. An explanation of each characterisation approach is provided before examining the impact of the various materials utilized on the characteristics, microstructure, and production of hydration products.

4.1 Experimental methodology

The variables involved in the experimentation were:

- OPC and CSA partially replaced with FA and VA individually up to 30%.
- Percentage of SCG used (from 1.5 to 3.5% by weight).
- Curing times (3,7,28,90 and 210 days).

In general terms, Figure 14 shows a diagram that summarizes the experimental methodology used for the development of this research work.

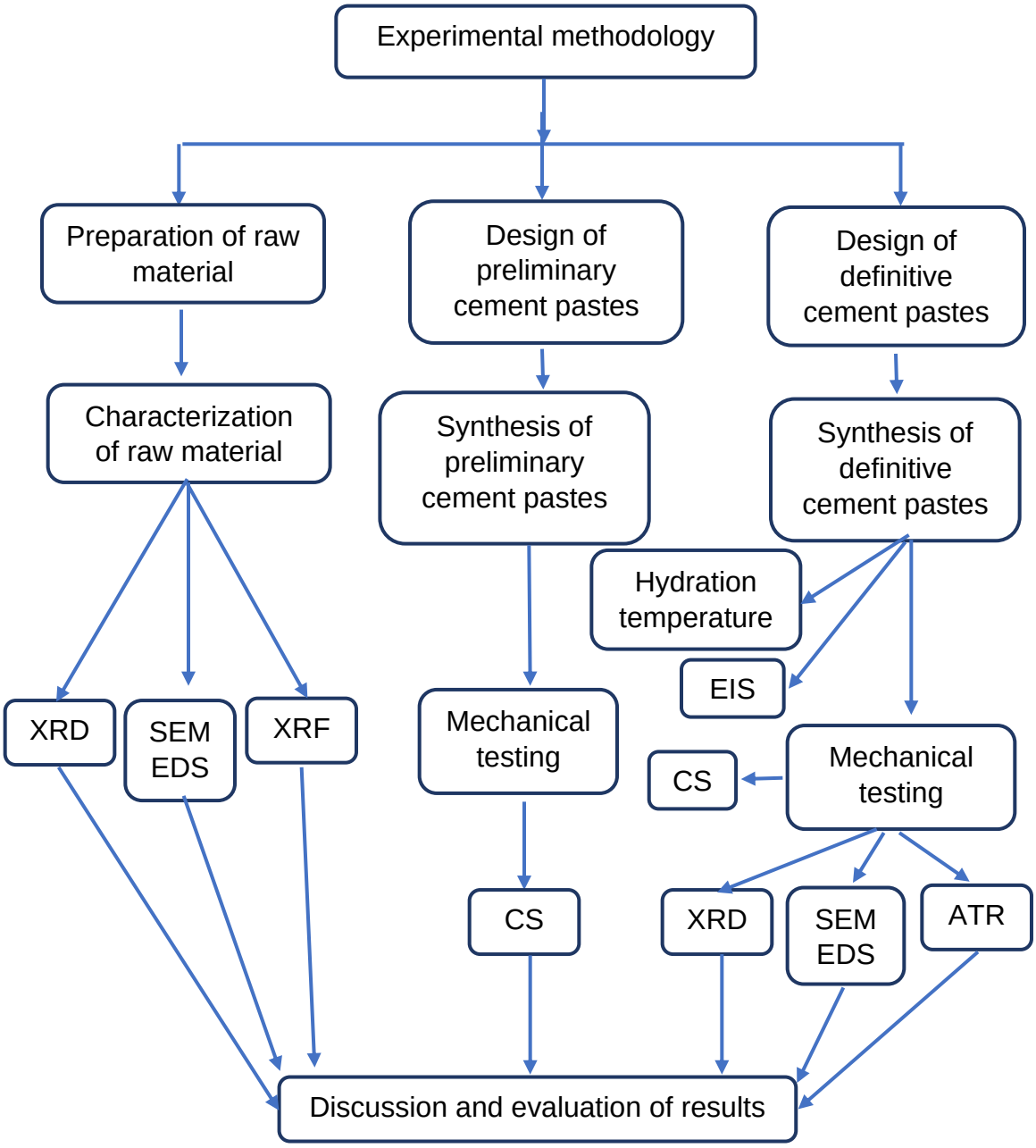

Figure 14. Experimental methodology used in the investigation

4.1.1 Stage 1: Preparation and characterization of the raw material

The conditioning of the raw material focused on the treatment of the materials to comply mainly with regulatory requirements or to improve their properties. The materials used in this research were two types of cement, (OPC, CSA), FA, VA, and SCG. The characteristics of each material and the processes carried out to condition the materials for preparing composite cement systems are described below.

- OPC: donated by the laboratory of the Faculty of Civil Engineering, Universidad Autónoma de Nuevo León from CEMEX Monterrey.
- Calcium Sulfoaluminate Cement: from Cemento Fraguamax of Cementos Chihuahua.
- FA: provided by CEMEX Monterrey.
- VA: from Vulkano Block Termico, Monterrey, Nuevo Leon.
- SCG: collected from houses and offices.
- Double-distilled water: For the preparation of the samples, double-distilled water was used to avoid the interference of other ions in the pore solution of the paste.

4.1.1.1 Ordinary Portland Cement

XRF, XRD and SEM characterization techniques were used to determine the chemical composition of the oxides present, crystalline phases and morphology of the material, respectively. The OPC cement used in the investigation was OPC40, which has a compressive strength of 40 MPa at 28 days. Before preparing the samples, the cement was kiln dried at 60 °C to eliminate hydrated particles, sieving with a 200 mesh was to control the particle size (see Figure 15).

Figure 15. Dried at 60 °C, OPC sieved through mesh No.200

4.1.1.2 Calcium sulfoaluminate cement

Sulfoaluminate cement was sieved through 200 mesh after being dried for 24 hours at a temperature of 60 °C to standardize the particle size and ensure that the particles were below 75µm, see Figure 16. X-ray fluorescence (XRF), the characterization technique that helps to determine the chemical composition of the oxides present, X-ray diffraction (XRD) to determine the crystalline phases present in the material. Using secondary electrons, scanning electron microscopy (SEM) was used to examine the morphology.

Figure 16. Dried at 60 °C, CSA sieved through mesh No.200

4.1.1.3 Fly Ash

FA was first dried in an oven at 60 °C to eliminate the moisture present in the material. Afterward, they were sieved with mesh No. 200 to adequately adjust the particle size distribution for the synthesis of pastes and to eliminate all the impurities in the material, see figure 17. The sieved FA has then characterized as similar to the cement; its chemical composition was analyzed by XRF and XRD to identify the crystalline and amorphous phases. SEM was used through secondary electrons to observe their morphology.

Figure 17. Dried at 60 °C, FA sieved through mesh No.200

4.1.1.4 Volcanic ash

The purchased volcanic sand was dried at 60 °C to eliminate moisture from the material. Subsequently, the volcanic sand was then subjected to a grinding process in a vibrating ball mill with a capacity of 5 kg per charge. The material obtained was ground at different grinding times to determine the required milling time to allow the VA to enable 100% of the material to be under 75 microns; that is, it could pass through no. 200 mesh, and it was found that the optimum time for grinding was one and a half hours, see figure 18. VA was characterized by XRF to obtain its chemical composition. To know the phases present in the material, and to know the content of amorphous and crystalline phases XRD was used. SEM was used to observe their morphology.

Figure 18. Dried at 60 °C, Volcanic sand was ground in a ball mill, VA sieved through mesh No.200

4.1.1.5 Spent coffee grounds

SCG was collected from offices and houses. The collected SCG was mixed with filter papers; these were separated before drying. The coffee grounds were dried in an oven at 100°C. Then they were sieved with mesh No. 200 to adequately adjust the particle size distribution for use in the synthesis of pastes (see figure 19). The sieved coffee grounds were then characterized the same as the cement; its chemical composition was analyzed by XRF and XRD to identify the crystalline and amorphous phases, and to observe their morphology, SEM was used using secondary electrons.

Figure 19. Spent coffee grounds dried at 100 °C, sieved through mesh No.200

4.1.2 Stage 2: Design and synthesis of preliminary pastes

Before synthesizing the final systems, preliminary tests were performed (see Tables 2 and 3) to analyze the behavior of the supplementary cementitious materials with the OPC and CSA. Based on these results, the final design of the pastes was carried out. This way, the percentages of the pozzolans used FA and VA were varied at various water-to-cement ratios (0.40, 0.42, 0.45). Another aspect considered was the temperature variation (values of 60 and 80 °C) in the curing process to observe if there were improvements in mechanical strength due to the acceleration of the reactions. Their characteristics were then analyzed to determine the best mixtures, observing the workability, fluidity, compressive strength, and porosity of the samples.

Table 2. Preliminary mix design with OPC

Sample name	OPC %	FA %	VA %	SCG %	W/C	Temperature 60 °C and 80 °C for 24h
O1	100	-	-	-		-
O2	90	10	-	-		-
O3	80	20	-	-		-
O4	70	30	-	-		-
O5	60	40	-	-		-
O6	50	50	-	-		-
O7	90	-	10	-	(0.4,	-
O8	80	-	20	-	0.42,	-
O9	70	-	30	-	0.45)	-
O10	60	-	40	-		-
O11	50	-	50	-		-
O12	98.5	-	-	1.5		✓
O13	97.5	-	-	2.5		✓
O14	96.5	-	-	3.5		✓
O15	95.5	-	-	4.5		✓
O16	66.5	30	-	3.5		✓
O17	66.5	-	30	3.5		✓

Table 3. Preliminary mix design with CSA

Sample name	CSA %	FA %	VA %	SCG %	W/C	Temperature 60°C and 80 °C for 24h
S1	100	-	-	-		-
S2	90	10	-	-		-
S3	80	20	-	-		-
S4	70	30	-	-		-
S5	60	40	-	-		-
S6	50	50	-	-		-
S7	90	-	10	-	(0.4,	-
S8	80	-	20	-	0.42,	-
S9	70	-	30	-	0.45)	-
S10	60	-	40	-		-
S11	50	-	50	-		-
S12	98.5	-	-	1.5		✓
S13	97.5	-	-	2.5		✓
S14	96.5	-	-	3.5		✓
S15	95.5	-	-	4.5		✓
S16	66.5	30	-	3.5		✓
S17	66.5	-	30	3.5		✓

4.1.3 Stage 3: Design and synthesis of definitive cement pastes

With the information from the preliminary results, it was possible to synthesize definitive pastes (see Table 5) using the methodology described below:

a) The precursor powders were weighed and added to bidistilled water, according to ASTM C305-06 [133]. The mixing was carried out in a mechanical stirrer, where the mixing time of composite cement mix was 2.5-3 minutes, according to the workability and setting time of the mixtures. This time was distributed as follows, 30 seconds for water absorption when the powders were added to the mixing water; 30 seconds for the mixer at medium speed; 15 seconds to clean the material from the sides, and the final 1 minute that completes the mixing at high speed (see figure 20).

b) The mixtures were poured in two layers into the molds of 2.5 cm, previously greased, to prevent the material from adhering during demolding and thus damaging the samples, according to ASTM C31/C31M-09 standards [134].

c) After all the cubes were filled, the molds were covered with a plastic film to prevent water loss by evaporation. They were left to rest for 24 hours using two methodologies: the first at room temperature, which was applied to the majority of the systems created, and the second was with temperature assistance, when the mixture was placed in the molds, they were protected with more plastic film and wrapped in a damp before being placed in an oven set to 80 °C.

d) After 24 hours, the samples were demolded according to ASTM C31/C31M-09 [134], OPC incorporated composite cement mix was then immersed in bidistilled water, which is mixed with calcium hydroxide. In the case of sulfoaluminate composite cement, calcium hydroxide was not added to the curing water in order to protect the hydration products.

e) Electrochemical Impedance Spectroscopy (EIS) studies were carried out at 7, 28 90 days of curing, and subsequently compressive strength tests at each of the indicated dates 3, 7, 28, 90, and 210 days of water curing according to ASTM C109/C109M-08 [135].

f) Once the samples were tested, they were placed in isopropyl alcohol to stop the hydration process for 72 hours and were then placed in an oven at 40 °C for 72 hours to dry them; when they were taken out of the oven, they were put in plastic bags, leaving them ready for the characterization techniques.

g) The exact mixing procedure was used to analyze hydration temperature; according to ASTM C305-06 and ASTM C186, [136] the hydration temperature of the composite cement was carried out for 24 hours

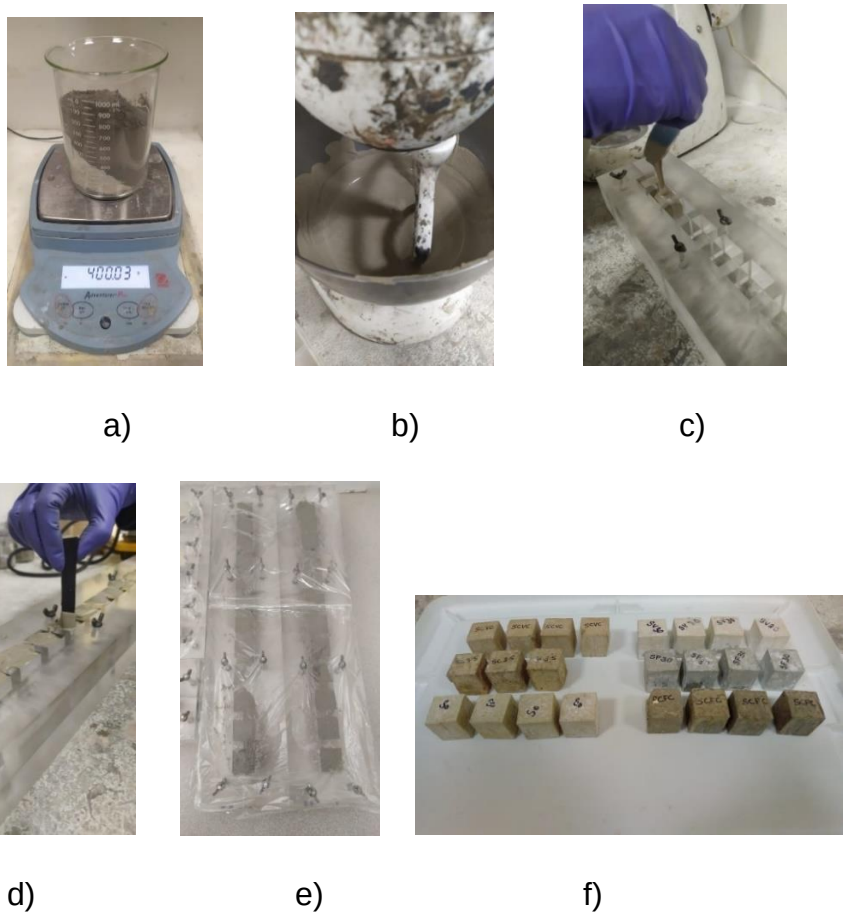

a) b) c)

d) e) f)

Figure 20. The procedure of mixing. a) weighed powders b) composite cement mix mixed with water in mixer c) pouring the mix into 25 mm x 25 mm cube molds d) compaction e) prepared cubes covered with plastic films f) demolded cubes

4.1.4 Stage 4: Characterization of composite cement samples

4.1.4.1 Compressive strength

When complying with the curing times described earlier (3, 7, 28, 90, and 210 days), the samples were taken from the water, letting them dry for 5 min to measure the faces of the cubes; several measurements of each face were taken using a digital vernier, then the average was calculated to obtain the actual area. This trial was used to conduct compressive strength using a hydraulic press ELE International compression machine, model 1913B0001 (Figure 21), with a maximum testing capacity of 200 kN; the speed of application of the load used was 500 N/s for cubes of size 25 x 25 mm, and the failure limit of 20%. For each type of mixture, 4 specimens were taken at each date, the average of their strength obtained was taken as the final compressive strength. The whole process followed the procedure set out in ASTM C109/C109M-08 [135].

The tested samples were crushed and immersed in isopropyl alcohol to stop hydration reactions. After 3 days, they were dried at 40 °C to remove the remaining moisture, and thus proceeded with them to the rest of the characterization.

Table 4. Definitive mixing systems with OPC

Sample name	OPC %	FA %	VA %	SCG %	W/C	Curing Temperature 80 °C for 24h
OC0	100	-	-	-		-
OCV10	90	-	10	-		-
OCV20	80	-	20	-		-
OCV30	70	-	30	-		-
OCF10	90	10	-	-		-
OCF20	80	20	-	-		-
OCF30	70	30	-	-	0.45	-
OCC1.5	98.5	-	-	1.5		-
OCC2.5	97.5	-	-	2.5		-
OCC3.5	96.5	-	-	3.5		-
OCFC	66.5	30	-	3.5		-
OCVC	66.5	-	30	3.5		-
OCC1.5 (W/T)	98.5	-	-	1.5		✓
OCC2.5 (W/T)	97.5	-	-	2.5		✓
OCC3.5 (W/T)	96.5	-	-	3.5		✓
OCFC (W/T)	66.5	30	-	3.5		✓
OCVC (W/T)	66.5	-	30	3.5		✓

Table 5. Definitive mixing systems with CSA

Sample name	CSA %	FA %	VA %	SCG %	W/C	Curing Temperature (80 °C for 24h)
SC0	100	-	-	-		-
SCV10	90	-	10	-		-
SCV20	80	-	20	-		-
SCV30	70	-	30	-		-
SCF10	90	10	-	-		-
SCF20	80	20	-	-		-
SCF30	70	30	-	-		-
SCC1.5	98.5	-	-	1.5	0.45	-
SCC2.5	97.5	-	-	2.5		-
SCC3.5	96.5	-	-	3.5		-
SCFC	66.5	30	-	3.5		-
SCVC	66.5	-	30	3.5		-
SCC1.5 (W/T)	98.5	-	-	1.5		✓
SCC2.5 (W/T)	97.5	-	-	2.5		✓
SCC3.5 (W/T)	96.5	-	-	3.5		✓
SCFC (W/T)	66.5	30	-	3.5		✓
SCVC (W/T)	66.5	-	30	3.5		✓

Figure 21. Compression testing machine ELE International

4.1.4.2 X-Ray Diffraction (XRD)

Mineralogical characterization of raw materials and paste systems was developed from qualitative analyses of the powder samples by the XRD technique to analyze the crystalline phases present in the raw material and the different mixtures synthesized. In the case of raw materials, a diffractometer with the copper tube was used, with monochromatic radiation and Cu kα detector (λ=1.5406 Å), and the run was set from 5-90 degrees for 10 minutes. In the case of mixtures synthesized were analyzed after being tested to compressive strength to meet 28 and 90 days of curing. Figure 22 represents the agate mortar used to prepare the samples for XRD and other characteristics. The finely grounded powdered samples with less than 75 microns were used for the XRD analysis. They were added as a powder directly on the diffractometer sample holder to run the analysis. A Bruker-D8 Advance diffractometer with a Cu-Kα radiation (λ= 1.54) set at 5-90 degrees for 8 minutes, with a voltage of 40kV and a current of 40mA, was used to analyze the mineralogical phases and the crystalline structure present in the powdered sample.

Figure 22. Agate mortar

Figure 23. Empyrean Panalytical X-Ray Diffractometer

4.1.4.3 Scanning electron microscopy and Energy dispersive electron spectroscopy

The selected composite cement systems were cold-mounted using epoxy resin and then polished for SEM and EDS analysis. With the EDS technique, it is possible to obtain the compositional analysis of the material, and the method consists of the characterization of x-ray photons according to the energies that affect using a semiconductor detector. Using SEM, the information obtained is focused on the development of the microstructural and chemical composition of the material. The point of view of morphology is based on the interaction of a high-energy electron beam with the sample analyzed using specific physical processes.

For the analysis by SEM, two microscopic equipment were used; the first HITACHI brand, model SU8020, see figure 24 a). The second brand JEOL, model JSM-6510LV, figure 24 b) using which micrographs of the samples could be obtained, using secondary electrons or backscattered, and energy dispersive spectroscopy (EDS) for the chemical composition and hydration products formed according to the sample. In this case, the first (Hitachi, model SU8020) was used to obtain images with both secondary electrons of the raw material and the fractures of the synthesized samples, with an acceleration voltage of 1, 2, or 5 kV (depending on the image quality) and a specific magnification (x500, x1000 and x1500). With the second SEM (JEOL, model JSM-6510LV), electron imaging was obtained backscattered at 20 kV acceleration voltage, applying energy dispersive spectroscopy (EDS) analysis for composite cement systems after 90 days of curing.

Figure 24**.** Field emission scanning electron microscopy a) Hitachi, model SU8020. b) JEOL, model JSM- 6510LV

Composite cement systems tested after 90 days of curing were selected to analyze EDS. At first, residues were taken from the compression tests of each system developed. To better understand what happens during hydration, the parts in the center of the specimen were selected because these areas give a more accurate study of hydration reactions. The samples were then mounted using epoxy resin and EpoFix hardener. After 24 hours, they were unmolded and underwent polishing with isopropyl alcohol and polishing paper (sandpaper) of 80, 180, 240, 320, 400, 600, 800, 1200, and 2400. Finally, cloth with a diamond paste of 0.5 microns was used to obtain the resin as a polished mirror surface, subsection a), showing that the specimens were in the same condition, see figure 25. They were then placed in a container with alcohol to the Aquasonic ultrasound model 75T for 1 minute, see figure 25 subsection (b) to remove any impurities acquired in the previous process. Finally, the samples were coated with two layers of gold using the Quorum equipment model Q150R ES (see figure 25 subsection c) to increase the conductivity by being in the SEM.

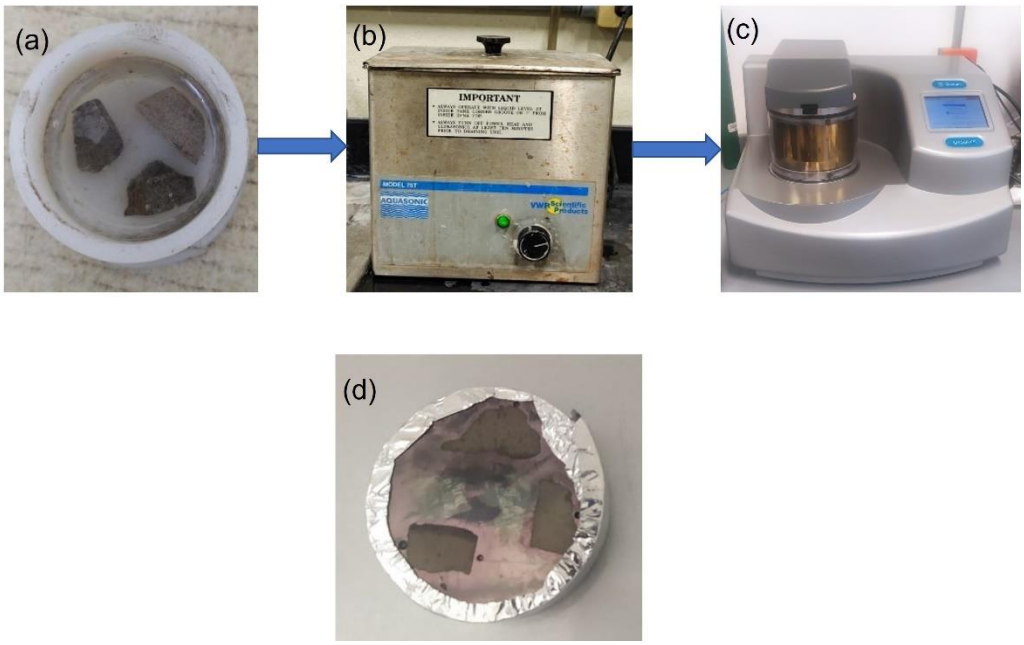

Figure 25. a) Samples mounted in resin b) Aquasonic ultrasound model 75T c) Quorum gold coater model Q150R ES (d) gold coated sample

4.1.4.4 Density

This characterization method was performed according to ASTM C 188 [137] standard, for which a graduated Le Chatelier flask was used, which was then filled with kerosene upto the mark. To that, 64 g of cement is added, and the volume difference is measured. The temperature was maintained at 23±2 °C (see figure 26). The same procedure was used for all the supplementary cementitious materials used in work.

Figure 26. The density of Portland cement using the Le Chatlier apparatus

4.1.4.5 Attuenataed total reflectance Infrared spectroscopy (ATR)

For the analysis of this technique, a BRUKER Alpha II FT-IR (Bruker, Ettlingen, Germany) brand equipment was used (see Figure 27). IR spectra were analyzed for the composite cement systems created and strength tested at 90 days.

First, fine grinding of the material was carried out in a mortar of agate, to be then introduced this powder in a trapezoidal block of an infrared transparent material (diamond was used) on which it was made impinge a beam of photons at one end with an angle less than the critical angle so that it undergoes internal reflection until it emerges from the other end. Despite the internal reflection, part of the radiation penetrates something beyond the surface of the prism. The immobilized material is found on the surface, absorbing part of the radiation, and the internal reflection will remain attenuated. The extent of radiation penetration into the sample depends on the frequency of radiation, the relationship between the indices of refraction of the sample, the material of the accessory, and the angle of incidence.

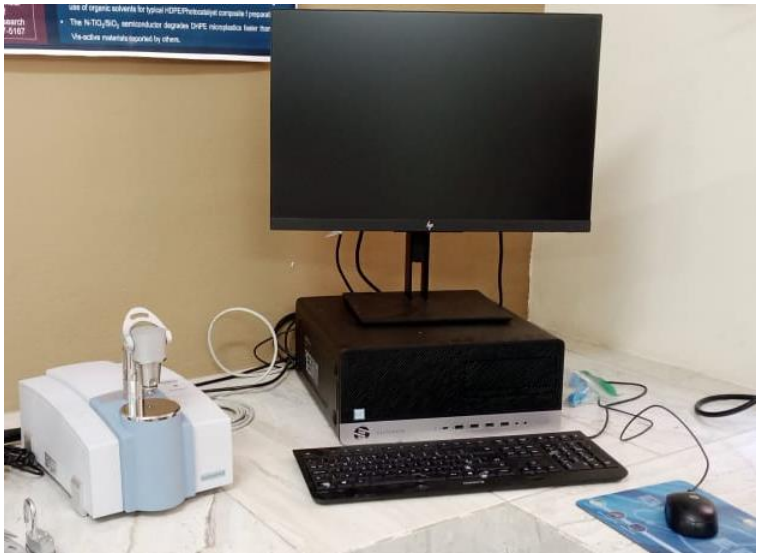

Figure 27. Equipment of infrared spectroscopy, BRUKER Alpha II

4.1.4.6 Electrochemical impedance spectroscopy (EIS)

The set of blended cement cubes that gave better mechanical strength was chosen to carry out Electrochemical Impedance Spectroscopy. When complying with the curing times described earlier (7,28, and 90 days), the samples were taken from the water, letting them dry for 5 min to perform the measurement. The experimental procedure is to apply a small potential signal to an electrode and determine the corresponding response. However, under certain circumstances, it is possible to apply a small current signal and measurements of potential - time and current - time, resulting in a series of impedance values corresponding to each frequency studied. This relationship between impedance and frequency is called the impedance spectrum. The impedance spectra obtained are usually analyzed by Nyquist plots. The spectra obtained are usually analyzed utilizing Nyquist diagrams and equivalent electrical circuit diagrams composed of components such as Resistances (R), Capacitances (C), and Inductances (L). SOLARTRON SI 1287 ELECTROCHEMICAL INTERFACE was used to analyze the EIS of the cement

cube samples in a three-electrode setup with a frequency of $3x10^6$ Hz and an amplitude of 10 mV. The cement cube was placed between two parallel stainless-steel electrodes. A polyester sheet dipped in 3% NaCl solution was placed between the cement cube and the stainless-steel electrodes. The reference electrode (KCl) was placed over the cement cube, as shown in the figure. A small potential signal is applied to an electrode, and the response is measured at different frequencies. The spectra obtained are analyzed and adjusted with commercial software Zview® from Scribner Associates Inc. to obtain values such as electrical resistivity and equivalent electrical circuit models of the treated and reference specimens. For each type of mixture, 4 specimens were taken at each date, from which the average of their electrical resistances was taken as the final measurement.

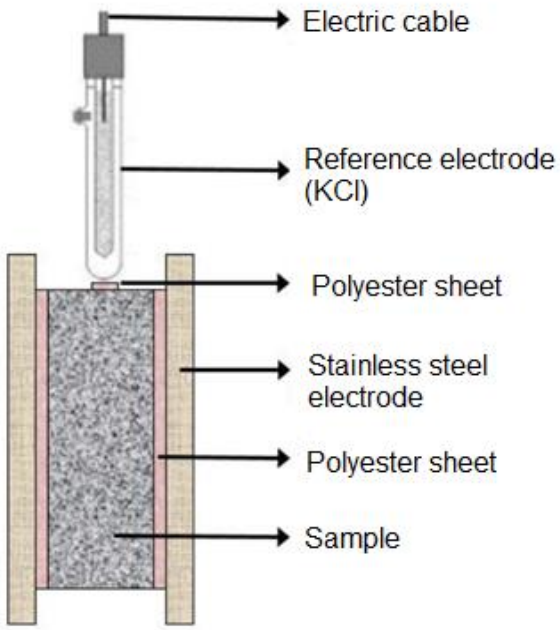

Figure 28. Experimental setup for Electrochemical Impedance Spectra

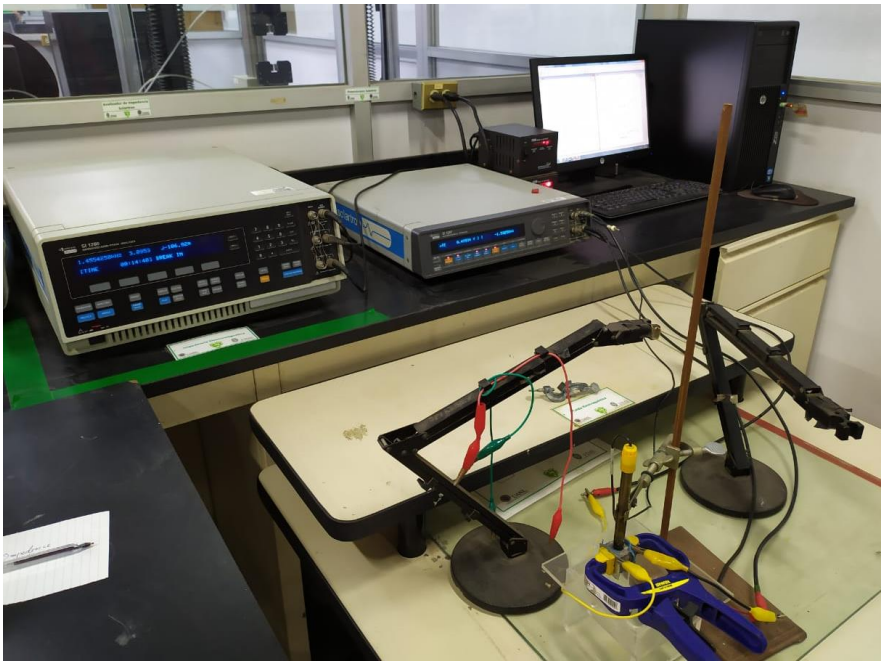

Figure 29. Solartron SI 1287 electrochemical interface for EIS

4.1.4.7 Hydration temperature

The blended cement was fully combined with water in accordance with ASTM C305 [133] in order to evaluate the hydration temperature of the cement paste, and the mix was poured into a thermal disposable glass. The copper constantan thermocouples were inserted into the cement paste, and the whole arrangement was placed in a double-walled box, which was then tightly sealed. The thermocouples were connected to a potentiometer that recorded the temperature of the cement paste every second for 24 hours. Lab view 2011 program was used to plot the hydration temperature vs. time graph of the cement paste [136,138]. Four samples of each composite cement mix were studied, and the average of the measurement was taken as the final result.

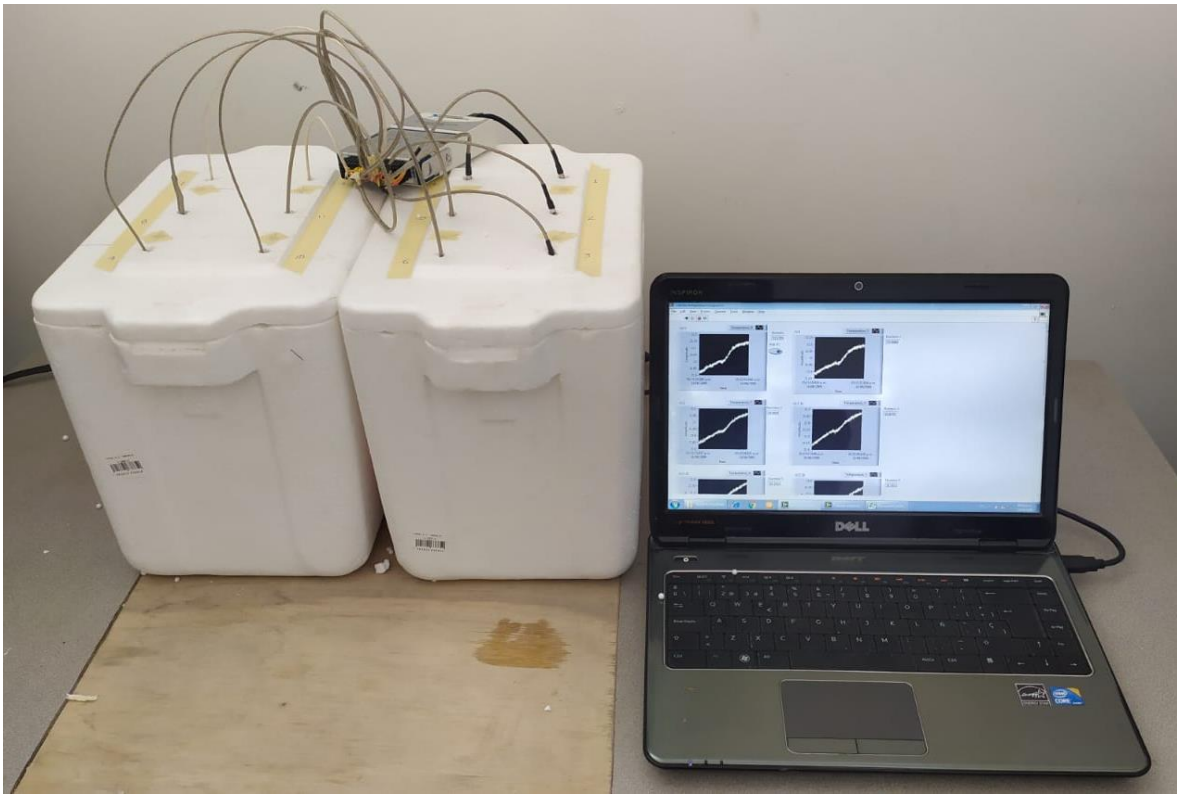

Figure 30. Semi-adiabatic chamber with thermocouple in connection with computer equipment

CHAPTER 5

RESULTS AND DISCUSSION

In this chapter, the results obtained in the experimental phase of this research are presented, among which are:

- The characterization of the raw material:
  - X-ray fluorescence
  - X-ray diffraction
  - Scanning electron microscopy
  - Energy dispersive X-ray Spectroscopy
  - Density
- The characterization of definitive composite cements:
  - Compressive strength
  - X-ray diffraction
  - Scanning electron microscopy
  - Attenuated total reflectance
  - Electrochemical Impedance spectroscopy
  - Hydration temperature

5.1 Characterization of raw material

5.1.1 Ordinary Portland cement

The chemical composition of the OPC studied using X-ray fluorescence can be seen in Table 6, which shows the principal oxides: CaO, SiO_2, Al_2O_3, and Fe_2O_3, obtained from raw materials used in the clinker manufacturing process. The high percentage of CaO is because the main raw material is limestone, with which the fundamental phases of this material are achieved.

Table 6. Chemical composition of Ordinary Portland Cement using XRF

Composition	Unit concentration (%)
CaO	63.17
SiO_2	17.68
Al_2O_3	3.94
Fe_2O_3	3.34
SO_3	3.21
MgO	1.13
K_2O	0.84
Na_2O	0.25
TiO_2	0.22
MnO	0.12
P_2O_5	0.11

X-ray diffraction was performed to qualitatively determine the crystalline phases and amorphous fraction present in the raw material. The reflections obtained by X-ray diffraction (Figure 31) show the mineralogical phases of this cement. The main phases observed were alite (C_3S), belite (C_2S), calcite, and ferrite (C_4AF) phases, of which the first two are mostly rich in calcium and silica. The other two are rich in aluminum and iron. In addition, it was possible to find the presence of gypsum

($CaSO_4$ dihydrate); the content of this material within the cement function as a setting regulator.

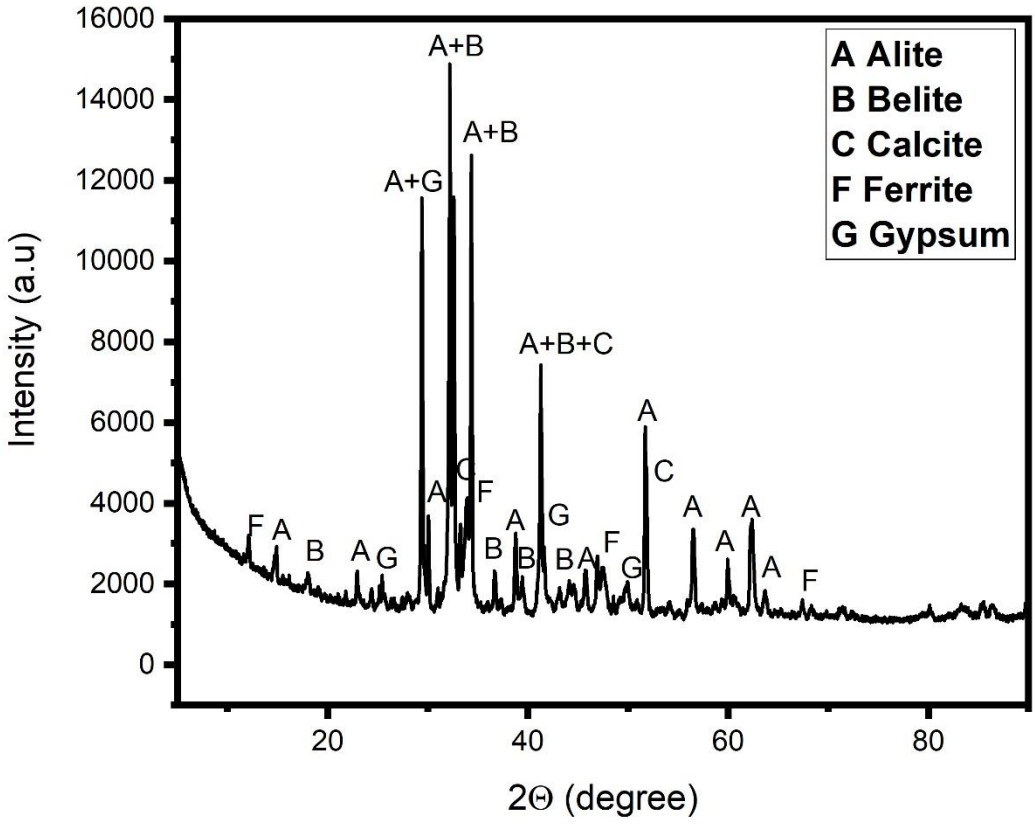

Figure 31. X-ray diffraction of ordinary Portland cement

The morphology of the particles, observed through SEM (Figure 32), shows that the morphology of OPC is irregular and angular; this type of morphology is characteristic of the C_3S (Alite) phase previously reported for Portland cement [139]. In this case, the particle morphology in clinker granules is subjected to continuous grinding, and then they are cooled after leaving the kiln and mixed with the gypsum.

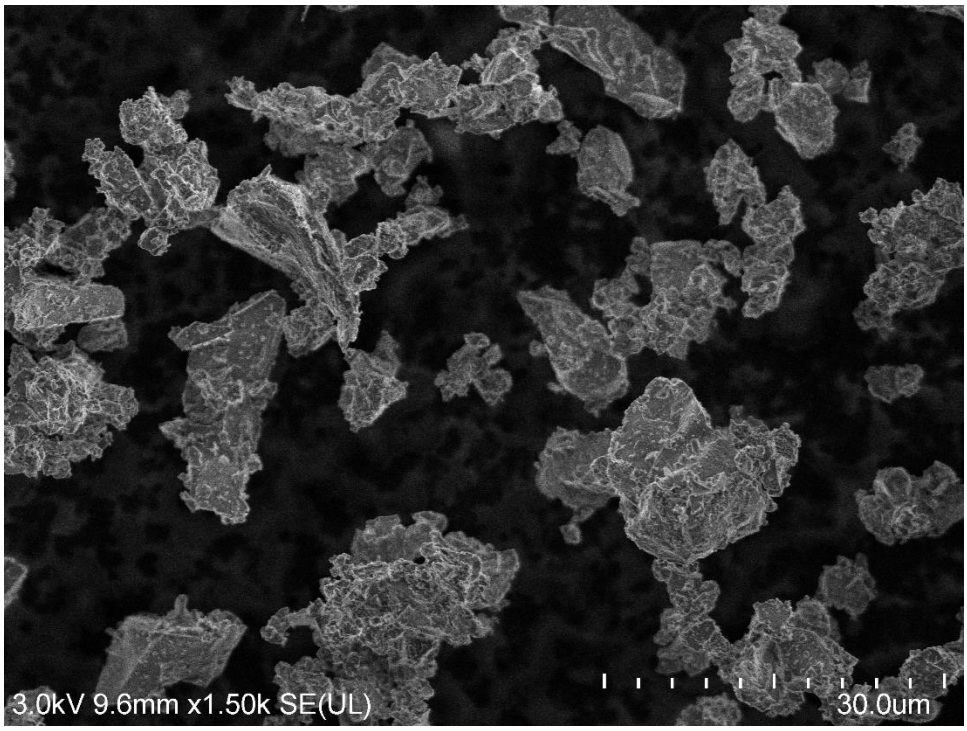

Figure 32. Morphology of ordinary Portland cement obtained through FESEM

The density of ordinary portland cement was obtained as 3.12 g/cm^3.

5.1.2 Calcium sulfoaluminate cement

Table 7 shows the quantitative elemental composition converted to percentages of the main oxides in CSA cement using XRF. When analyzing the presence of these oxides, the CaO content is less than that of OPC due to the lower limestone content as raw material. It can also be seen that both the Al_2O_3 and SO_3 contents increased due to the presence of bauxite and the higher amount of gypsum that was introduced, compared to Portland cement [75]. These three oxides, including silica, are fundamental for forming the phases of this cement and, at the same time, for the subsequent formation of the hydration products.

Table 7. Chemical composition of CSA Cement using XRF

Composition	Unit concentration (%)
CaO	55.1
Al_2O_3	15.05
SO_3	13.88
SiO_2	12.51
Fe_2O_3	0.95
MgO	0.88
K_2O	0.71
TiO_2	0.98
SrO	0.12
CuO	0.04
Cr_2O_3	0.03
ZnO	0.02
ZrO_2	0.02
V_2O_5	0.02

The hkl reflections of the characteristic mineralogical phases of the CSA identified by the diffractometer are shown in Figure 33. It can be seen that the highest intensity is shown for ye'elimite ($Ca_4Al_6(SO_4)O_{12}$, calcium sulfoaluminate), the main phase and the one that gives its name to these cement. This has one of the lowest CaO contents of all the main phases of clinker, reducing the amount of CO_2 released during the calcination of the limestone; this allows for lower clinkerization temperatures in its manufacture. The hydration of ye'elimite regulates the evolution of cement yield at early ages, as it hydrates in the presence of the phase identified as anhydrite ($CaSO_4$, anhydrous calcium sulfate); the reaction products are monosulfate or ettringite and aluminum hydroxide as final products.

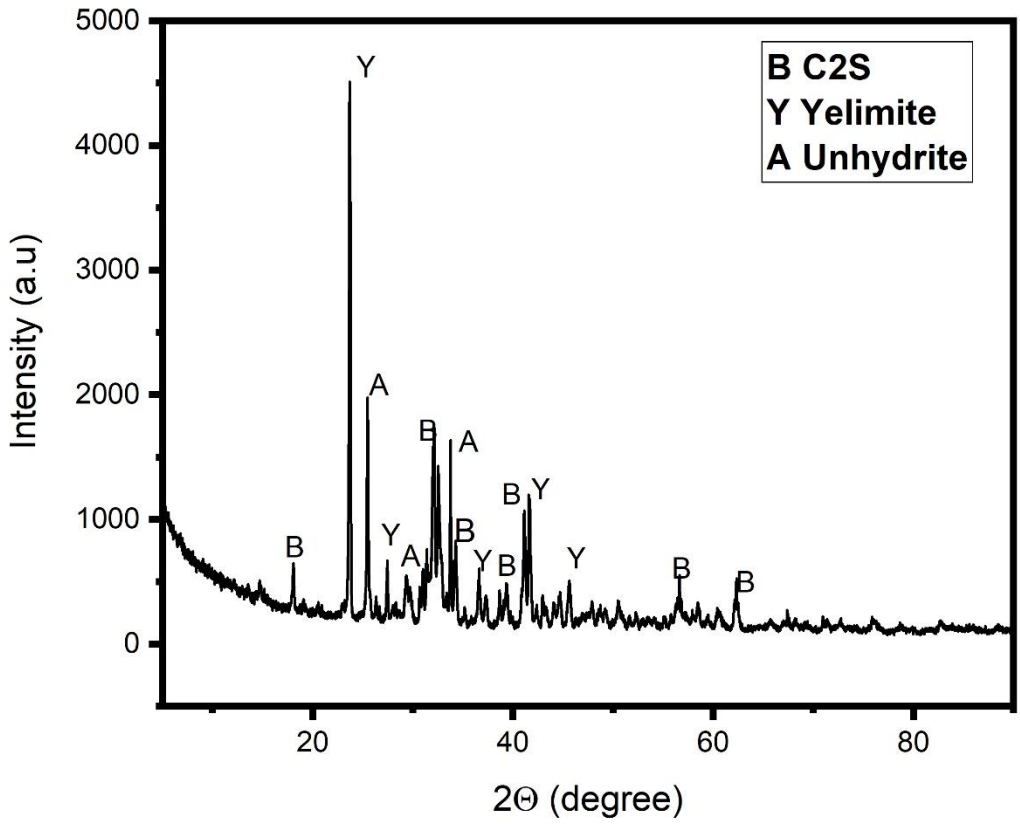

Figure 33. X-ray diffraction of calcium sulfoaluminate cement

The morphology of CSA is irregular, as shown in Figure 34, where it can be said that it is very similar to OPC because its fining process continues to be carried out by grinding and sieving until the desired particle size is reached (less than the 200 mesh of the sieve), which is necessary for all raw materials.

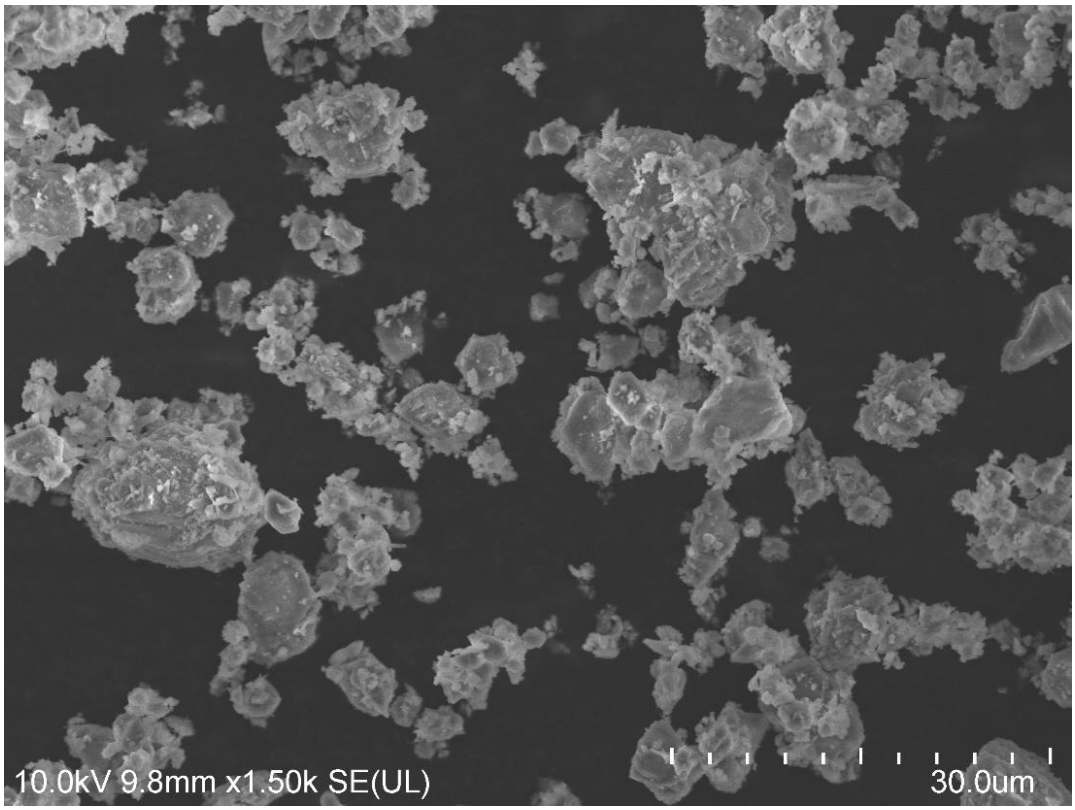

Figure 34. Morphology of CSA observed through FESEM

The density of sulphoaluminate cement was 2.89 g/cm^3.

5.1.3 Fly ash

The chemical composition of FA is shown in Table 8. While observing the main oxides, it can be seen that it is of type F because the sum exceeds the value of 70% (SiO_2+Al_2O_3+Fe_2O_3=90.36%>70%), established in the ASTM C618-14 standard [94]. This indicates that it has a high presence of silica and alumina; for this reason, it is considered a silicoaluminous material.

Table 8. Chemical composition of FA using XRF

Composition	Unit concentration (%)
SiO_2	76.47
Al_2O_3	11.51
Na_2O	0.15
MgO	0.37
Fe_2O_3	2.38
CaO	5.85
K_2O	0.87
TiO_2	0.56
SO_3	1.44
SrO	0.024
V_2O_5	0.013
MnO	0.012
ZnO	0.0056

The mineralogical composition of FA was obtained by XRD analysis and is shown in Figure 35. The diffraction pattern of FA shows the main crystalline phases quartz (SiO_2, CR 01-083-0539), mulite ($3Al_2O_3$-$2S_2O_3$, CR 01-083-0539) ($3Al_2O_3$-$2SiO_2$, CR 00- 002-0415) and calcite ($CaCO_3$ CR 01-088-180)7 in the reflections. An important aspect, the amorphous halo in an approximate range of 17 to 32° of 2θ highlights the amorphous character of the material. It indicates the ability to react rapidly in hydration reactions.

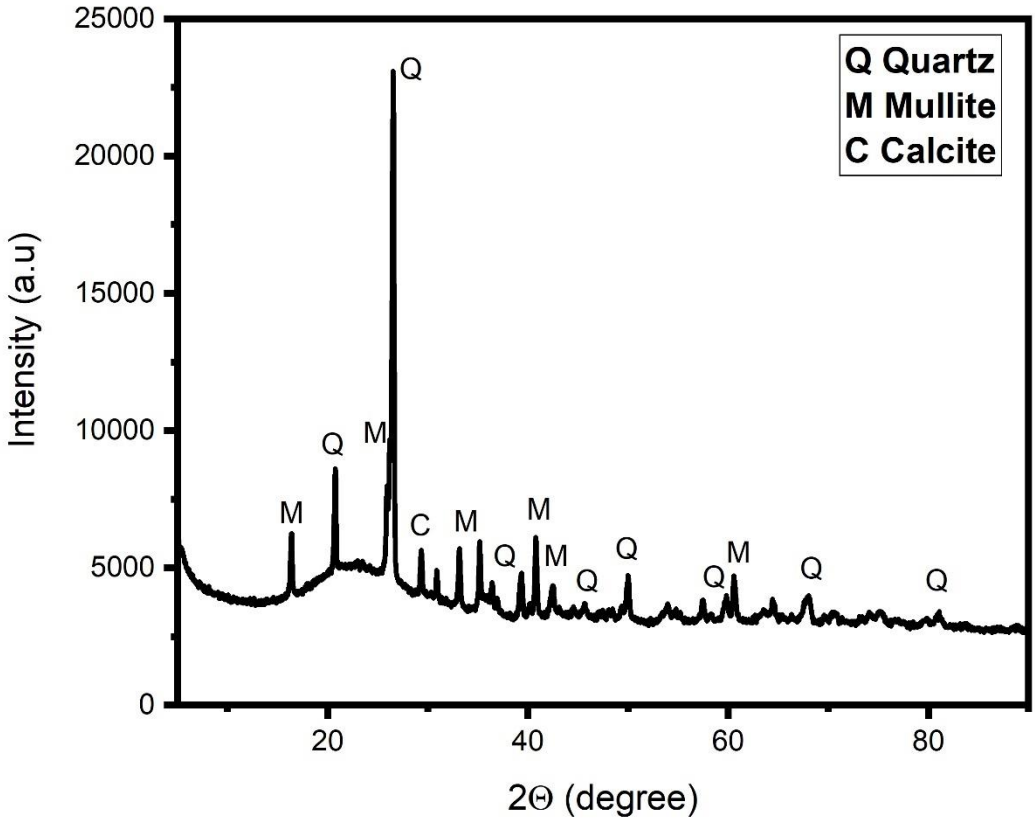

Figure 35. X-ray diffraction of fly ash

Through the scanning electron microscopy characterization technique, particle morphology was observed for FA (see Figure 36), where it could be seen that the particles are spherical. Being seen particles of another morphology in FA, which is associated with contamination during the process or carbon impurities, also observed cenospheres, a characteristic that brings particles that are also spherical in its interior, commonly reported in this material [69].

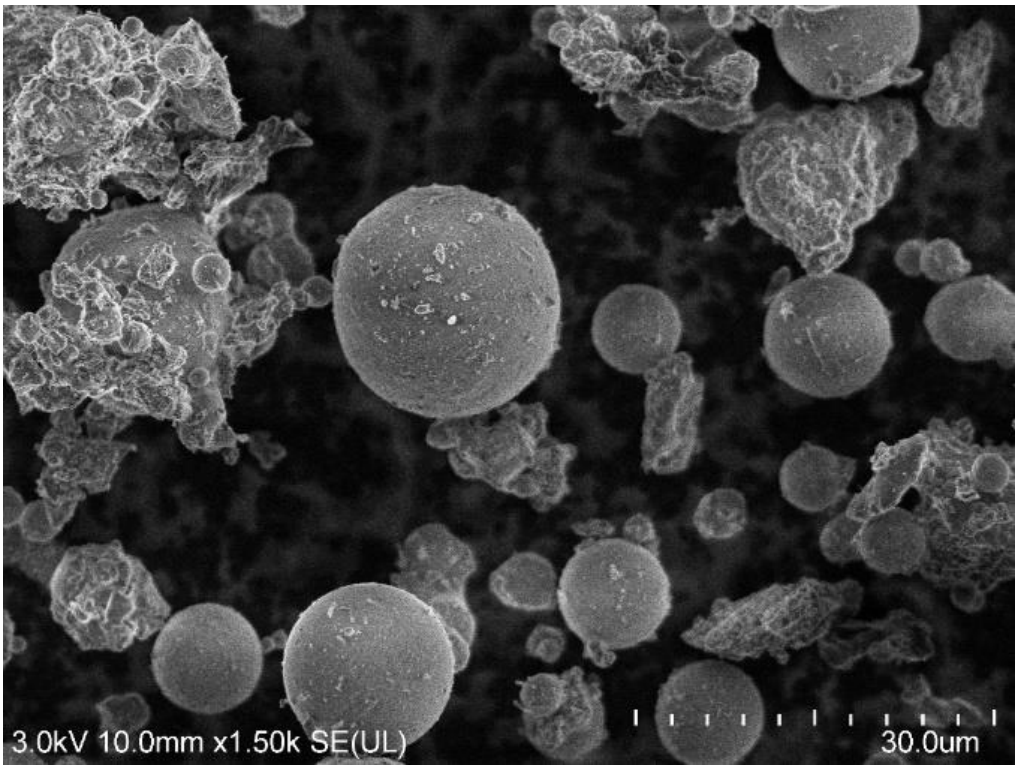

Figure 36. Morphology of FA observed through FESEM

The density of FA was obtained as 2.10 g/cm^3.

5.1.4 Volcanic ash

The chemical composition of VA in Table 9 shows the oxide composition of this material, for which a high amount of oxides of Si and Al can be observed. This also indicates that VA is also considered to be a silicoaluminous material similar to FA.

Table 9. Chemical composition of VA using XRF

Composition	Unit concentration (%)
SiO_2	73.29
Al_2O_3	14.83
K_2O	4.83
Na_2O	3.57
CaO	2.21
Fe_2O_3	0.924
MgO	0.32
TiO_2	270.1 ppm
MnO	0.15

In figure 37, the mineralogical composition of VA is shown. As an essential aspect, the amorphous halo in an approximate range of 17 to 38° of 2θ, highlights the amorphous characteristic of the material and indicates the ability to react rapidly in the hydration reactions. VA shows mains crystalline phases of sanidine, quartz, clinohypersthene, magnetite, albite, and leucite.

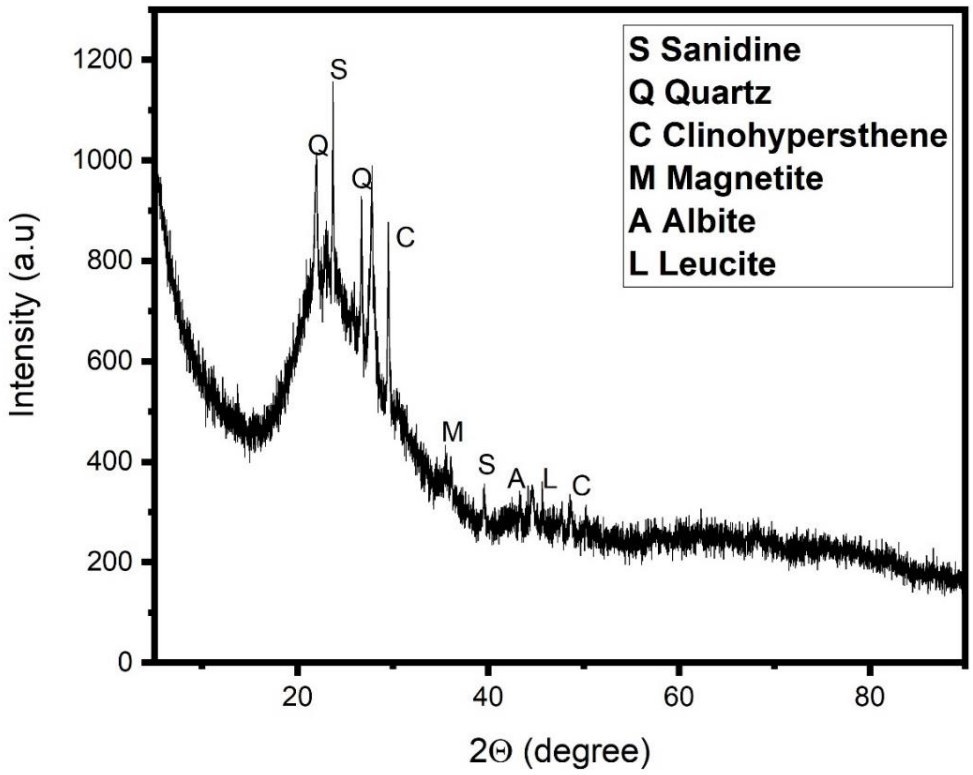

Figure 37. X-ray diffraction of volcanic ash

The morphology of VA is irregular, as shown in Figure 38, where it can be said that it is very similar to OPC and sulphoaluminate cement because its fining process continues to be carried out by grinding and sieving until the desired particle size is reached (less than the 200 mesh of the sieve), which is necessary for all raw materials.

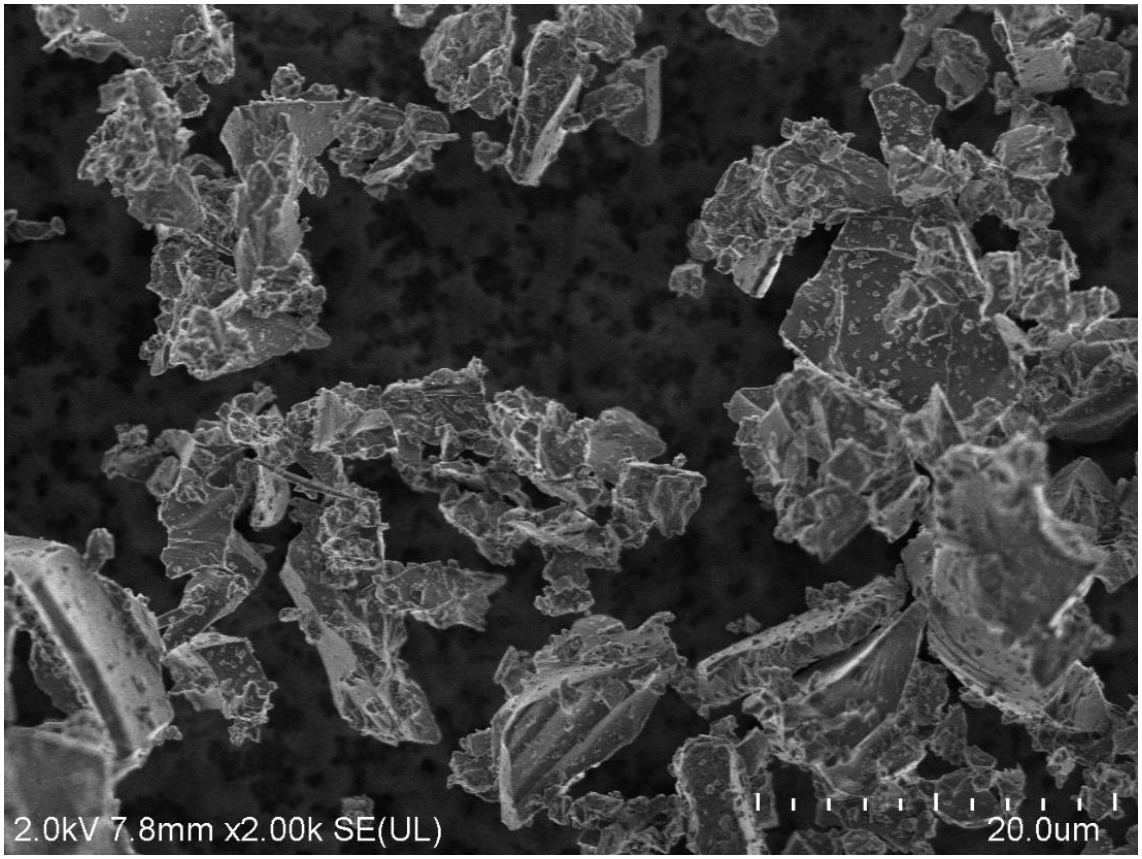

Figure 38. Morphology of VA observed using FESEM

The density of volcanic ash was obtained as 2.37 g/cm^3.

5.1.5 Spent coffee grounds

The chemical composition of SCG obtained using X-ray Fluorescence is shown in table 10. SCG contain a high amount of CaO and K_2O.

Table 10. Chemical composition of spent coffee grounds using XRF

Composition	Unit concentration (%)
CaO	32.89
K_2O	22.57
SO_3	13.71
Fe_2O_3	9.54
MgO	6.78
P_2O_5	4.93
SiO_2	3.08
Al_2O_3	2.66
Cr_2O_3	1.52
CuO	0.97
MnO	0.52
SrO	0.34
ZnO	0.27
Rb_2O	0.18

The characteristic mineralogical phases of the SCG were identified by the X-ray diffraction and is shown in Figure 39. The main characteristic crystalline peaks are for gismondine, $KHCO_3$, and magnesite. The amorphous halo nature is in the approximate range of 17 to 38° of the 2θ, which highlights the amorphous characteristic of the material.

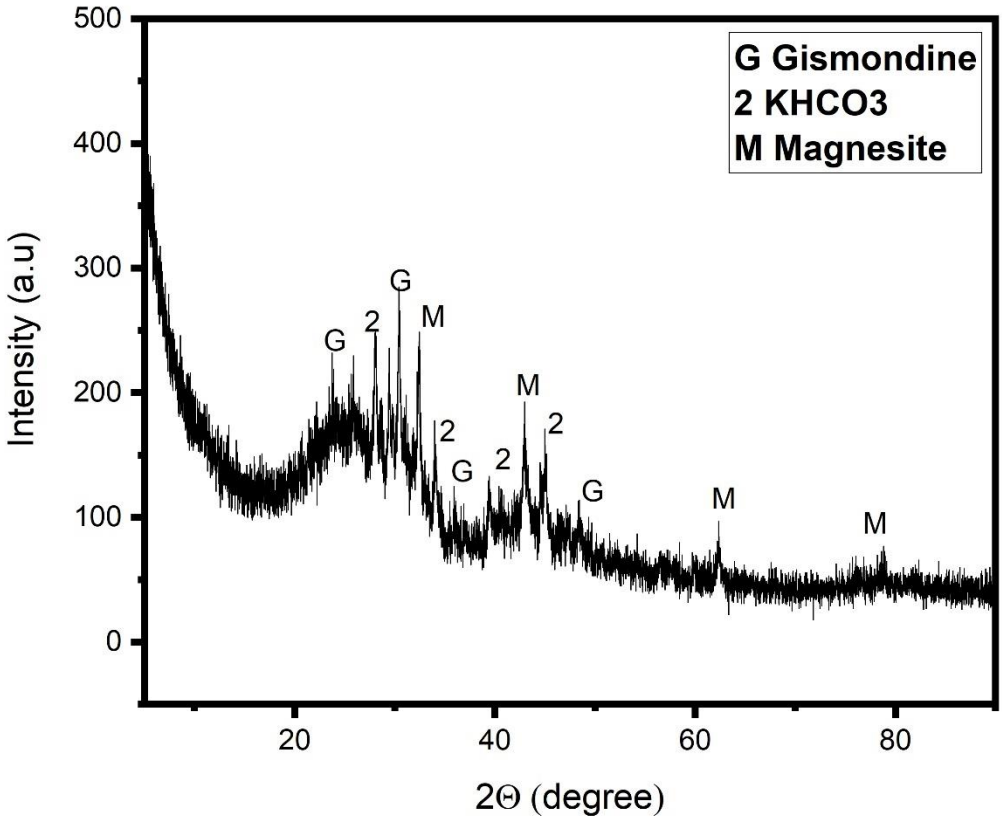

Figure 39. X-ray diffraction of SCG

The morphology of SCG was observed as irregular and is shown in figure 40. Coffee grounds were also passed through a grinding process similar to VA and then sieved through 200 mesh.

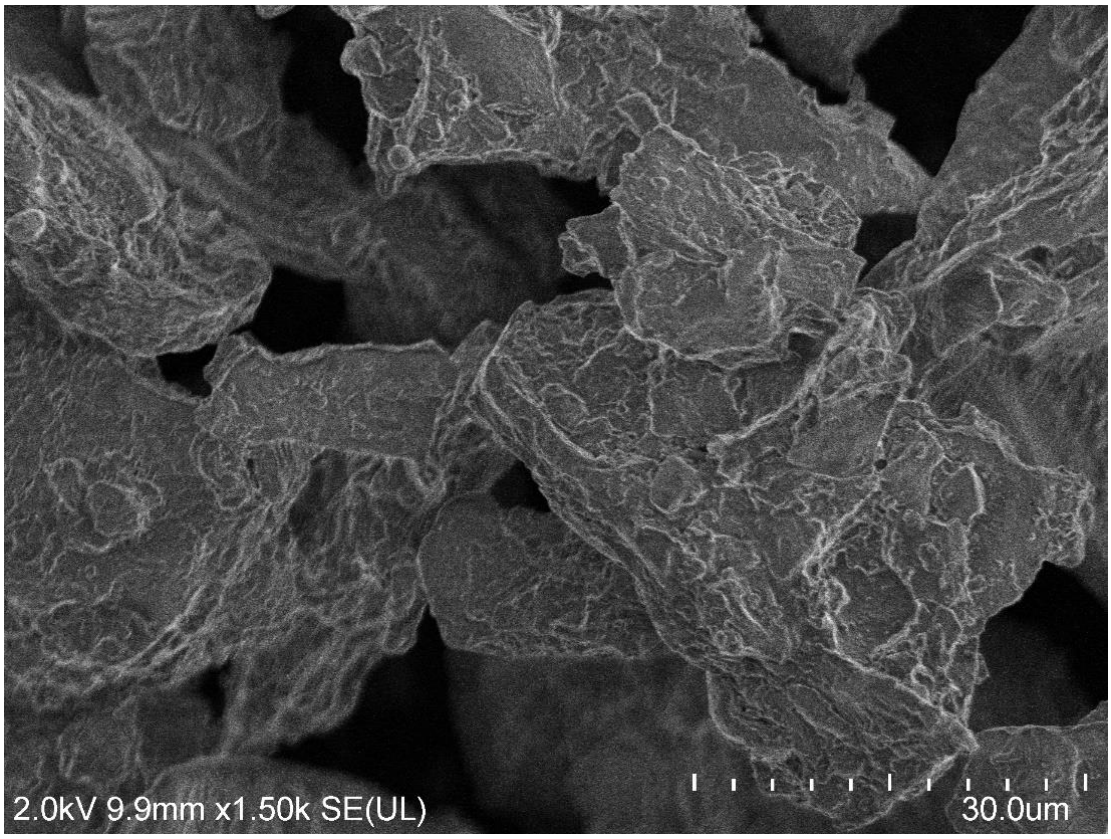

Figure 40. Morphology of spent coffee grounds observed using FESEM

The density of spent coffee grounds was 1.39 g/cm^3.

5.2 Characterization of definitive composite cement pastes

5.2.1 Compressive strength

The compressive strength results were presented for the ages of 3, 7, 28, 90, and 210 days of curing to have the behavior over time of the composite systems created, shown in Tables 4 and 5 of Chapter 3. Tables 11,12 and Figures 41,42 show both numerically and graphically the values obtained for each date tested for each of the systems prepared. To obtain these values, 4 compression tests were performed per date and system with the 25x25mm cubes. These cubes were measured to take the actual reading of their edges and recalculate the areas and the average resistances obtained by the compression machine.

Based on the values obtained, it can be seen how the systems vary in mechanical strength by changing certain variables, such as the percentage of pozzolans used and modification in the curing temperature. Each of these changes brings about a modification in the chemistry of the process and the hydration products obtained. The results were analyzed separately to understand the different effects of each change made.

Table 11. Compressive strength of composite cement of OPC mix at its 3, 7, 28, 90, and 210 days of curing

Sample	Cement replacement (%)	Days	Compressive strength (MPa)				
			3	7	28	90	210
OC0	0		29	34.6	44	49	53.2
OCV10	10% VA		27.9	33.2	38.3	40.4	42.3
OCV20	20% VA		23.8	29.5	37.5	41	43
OCV30	30% VA		21	25.7	35.9	42.9	45
OCF10	10% FA		25.8	32.5	42.7	39	39.9
OCF20	20% FA		24.5	31.2	39	40.1	40.8
OCF30	30% FA		19.8	25.3	32.6	40.4	42.2
OCC1.5	1.5% SCG		14.2	16	20	22	22.4
OCC2.5	2.5% SCG		16.9	19.8	22.8	27.5	26.8
OCC3.5	3.5% SCG		14	16.1	21.7	24.8	24
OCFC	30% FA and 3.5% SCG		14.9	15.8	17.5	18.7	19.6
OCVC	30% VA and 3.5% SCG		13.7	14.3	15.2	18.6	19.9
OCC1.5 (W/T)	1.5% SCG, with the temperature		14.2	16	20	22.2	22.8
OCC2.5 (W/T)	2.5% SCG, with the temperature		18.4	20	22.8	28	29.8
OCC3.5 (W/T)	3.5% SCG, with the temperature		15.4	17.8	21.7	25.2	26.1
OCFC (W/T)	30% FA and 3.5% SCG; with the temperature		12.9	14.8	17.5	19	20.2
OCVC (W/T)	30% VA, and 3.5% SCG; with the temperature		12.8	13.3	15.2	18.8	20.4

Table 12. Compressive strength of the composite cement of CSA mix at its 3, 7, 28, 90, and 210 days of curing

Samples	Cement replacement (%)	Compressive strength (MPa)				
	Days	3	7	28	90	210
SC0	0	19.7	31.5	44.8	52.2	55.4
SCV10	10% VA	17.7	30	40.6	45.1	50.6
SCV20	20% VA	15.6	26.7	41.9	47.3	51.9
SCV30	30% VA	15.9	24.5	38	49	53.6
SCF10	10% FA	19.7	31.8	35	38.4	42.4
SCF20	20% FA	18.7	32.2	37.3	38.4	42.4
SCF30	30% FA	15.6	25.4	34.4	39.6	43
SCC1.5	1.5% SCG	13.8	17	20	23	27.6
SCC2.5	2.5% SCG	17.3	17.8	21.1	25.8	28.7
SCC3.5	3.5% SCG	13.4	19.4	22	25.9	28.9
SCFC	30% FA and 3.5% SCG	10.4	11	15.5	18	21
SCVC	30% VA, and 3.5% SCG	11.6	13.8	14.5	18.1	21.8
SCC1.5 (W/T)	1.5% SCG, with the temperature	12.4	15.6	19	20.9	27.6
SCC2.5 (W/T)	2.5% SCG, with the temperature	15.8	17	20.8	21.2	31.8
SCC3.5 (W/T)	3.5% SCG, with the temperature	13.9	16.4	19.3	21	26.4
SCFC (W/T)	30% FA and 3.5% SCG; with the temperature	10	10.9	15	17.1	20.4
SCVC(W/T)	30% VA and 3.5% SCG; with the temperature	11.	12.9	13.8	16.9	20.3

5.2.1.1 Strength analysis of systems with OPC and pozzolans

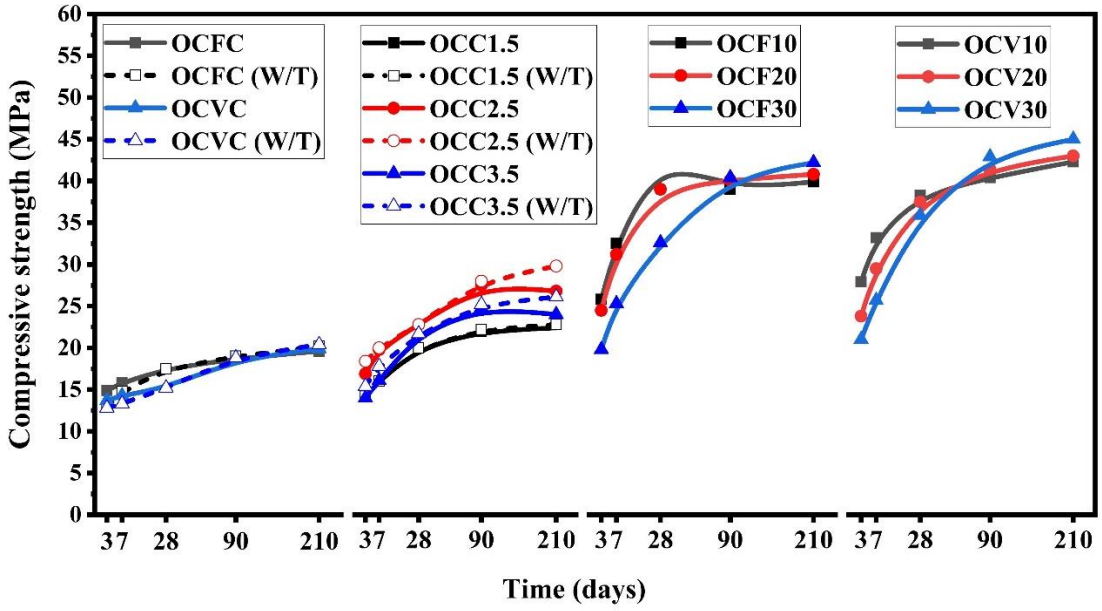

Figure 41. Compressive strength results of the OPC composite cement at 3, 7, 28, 90, and 210 days of curing.

Figure 41 presents the compressive strength results at 3,7, 28, 90, and 210 days of curing of the composite cement with OPC. The graph conclusively demonstrates that their mechanical strength increased as curing days increased for composite cement. It was discovered that none of the composite cement could surpass the compressive strength of the reference sample. Like chemical composition, physical variables, including fineness, mix design, water-to-cement ratio, and curing time, impact the strength of the material.

Temperature assistance was necessary to set and harden the composite cement cubes made with OPC and SCG. The samples of cement were exceedingly difficult to set, and strength decreased without temperature assistance [140]. Jadhav et al. also reported that it is challenging to set cement samples prepared by incorporating SCG without temperature aid and that CS values decreased with the addition of SCG [141]. A higher replacement percentage with SCG resulted in a negative effect in setting the cement. The ultimate percentage obtained was 3.5%

replacement of cement with SCG; it was observed that at 210 days of curing, the compressive strength of composite cement with SCG with temperature and without temperature was respectively 26.1 MPa and 24 MPa. Replacing OPC with SCG requires more water than other supplementary cementitious materials and this affects the workability of the mix. The w/c ratio was fixed at 0.45 to compare the findings. According to the study, it was observed that increasing the water content caused the composite cement to lose strength while lowering it caused shrinkage. This was another justification for setting the ideal replacement rate of OPC with SCG at 3.5%. VA is substituted for 30% of OPC, which results in lower compressive strength at younger ages, 7 and 28 days of curing. After 28 days of curing, the compressive strength increased; higher compressive strength of 45 MPa was obtained after 210 days of curing [15,16,142]. The enhanced compressive strength of VA over FA was partly a result of the fineness of VA [143]. While analyzing the CS results already reported for composite cement with OPC and VA, the CS result obtained in work is the best [16,37,128,143]. Similarly to VA, 30% was the ideal replacement rate for OPC with FA [122,144]. At 210 days of curing, the composite cement made with OPC and FA had a compressive strength of 42.2 MPa [145]. The reaction products formed during the hydration of composite cement containing both FA and VA were better after 90 days of curing. [17,19,37,146].

Here, the SCG functioned as a retarder [141,147]. As per the nucleation theory, the retarder binds to the nuclei of hydration products to reduce their rate of development. By occupying their reactive sides, the retarder primarily prevents the expansion of cement.

Temperature assistance is necessary for setting and hardening OPC and SCG with pozzolans composite cement [140]. Mechanical strength did not differ significantly between composite cement OCFC and OCVC, with or without temperature assistance setting. At 90 days and 210 days, the composite cement OCFC exhibited 19 MPa and 20.2 MPa, respectively. The composite cement

OCVC has a compressive strength of 20.4 MPa after 210 days of curing. When comparing the two composite cements, the one with FA was easier to work with than the one with VA.

5.2.1.2 Strength analysis of systems with CSA and pozzolans

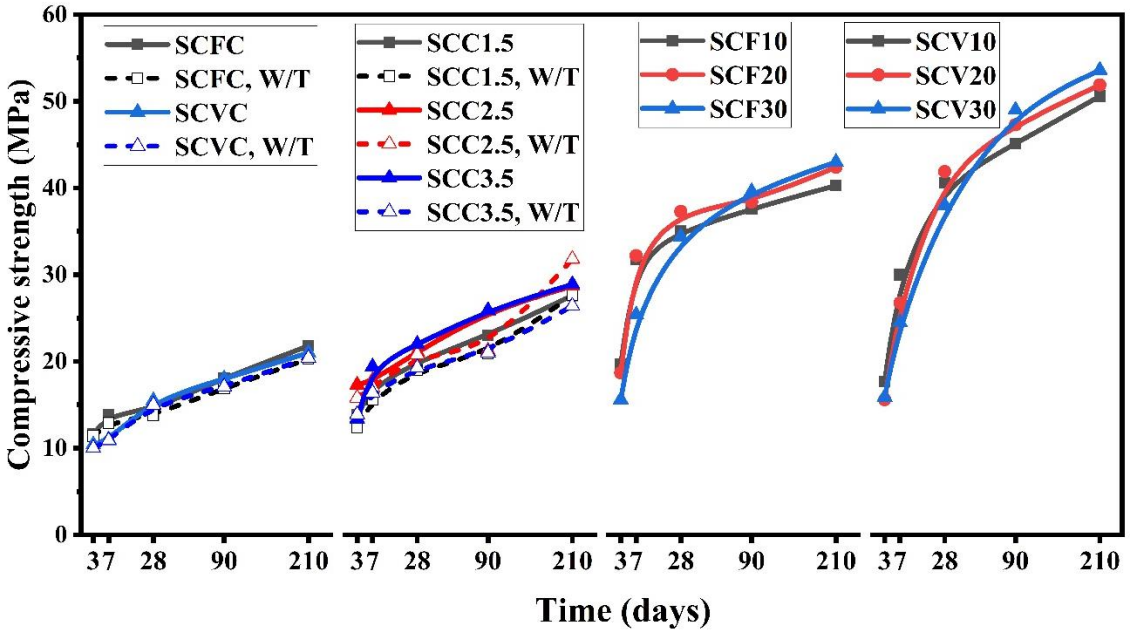

Figure 42. Compressive strength results of the CSA composite cement at 3, 7, 28, 90, and 210 days of curing.

Figure 42 represents the compressive strength results of CSA and its composites at 3,7,28,90, 210 days of curing. By analyzing the CS results of OPC and composites with CSA and composites, it was evident that the CS values of the reference sample of CSA were higher than that of OPC; 55.4 MPa for CSA and 53.2 MPa for OPC at 210 days of curing. Analyzing the compressive strength results of composites prepared using CSA, it can be seen that the compressive strength of composite cement did not reach up to the compressive strength of pure CSA reference sample. But also observed comparable strength obtained for 30 % replacement of CSA with VA. The reference sample had a compressive strength

of 55.4 MPa after 210 days of curing, whereas the composite cement containing VA had a compressive strength of 53.6 MPA. Additionally, it should be noted that 10% and 20% replacement of the CSA initially exhibits superior compressive strength than 30% replacement, indicating that the pozzolanic reaction occurs extremely slowly with both VA and FA. Due to the pozzolanic reaction, the 30% replacement of VA and FA performed better after 28 days than the 20% replacement of cement [148].

Furthermore, the CS results obtained in this study were higher than previous CS results for composite cement prepared with FA and CSA; at 28 days of curing, SCF30 achieved a CS result of 34 MPa. For a similar composite cement composition, Lukas et al. reported a CS result of 29 MPa after 28 days of curing [50]. Garcia found comparable CS results with CSA and FA composites [51].

Since CSA is more exothermic than OPC, the composite cement with CSA did not require temperature assistance for setting the composite cement. It was observed that composite cement without temperature showed a little more compressive strength than with temperature aid composite systems. CSA replaced with VA 30% and FA 30% showed a compressive strength of 53.6 MPa and 43 MPa, respectively, at 210 days of curing. CSA with SCG showed 28.9 MPa at 210 days without temperature aid, and strength decreased to 26.4 MPa with temperature. The SCVC showed 21.8 MPa, and SCFC showed 21 MPa without temperature; the strength decreased to 20.3 MPa and 20.4 MPa, respectively, with temperature aid setting. The 2.5% and 3.5% replacement of CSA showed almost the same compressive strength of 27.8 and 27.9 MPa, respectively, without temperature. CSA is more water-demanding than OPC. The composites with CSA and SCG are also more water-demanding. But the selected water-to-cement ratio was perfect for CSA and its composites.

By comparing figures 41 and 42, VA performed better with CSA than OPC, and the setting time was less than OPC. Also, the composite cements with SCG were better for CSA cement. Pozzolans also work better with CSA cement. 30%

replacement of CSA with VA showed a compressive strength of 53.6 MPa, reaching the compressive strength of reference sample OPC with 53.2 MPa. The composite with FA for cement OPC and CSA produced almost the same compressive strength, 42.2 MPa, and 43 MPa, respectively. As in the case of FA, compressive strength with composite cements prepared with SCG was a little more or almost the same; for composite cement with OPC, it was 26.1 MPa, and for CSA, 28.9 MPa. Composite cement OCFC had 20.2 MPa, while SCFC revealed 21 MPa. Composite cement OCVC and SCVC were respectively 20.4 and 21.8 MPa.

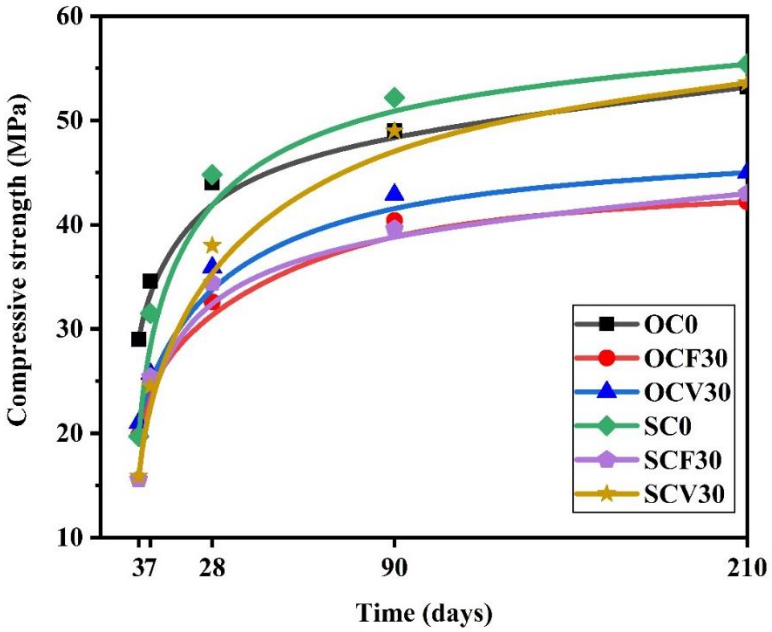

Figure 43. Comparison of compressive strength results of the OPC and CSA and the composite cement at different curing stages.

The CS findings of the reference samples OPC and CSA, together with their composite cement at various curing days, are compared in Figure 43. It became noticeable that by comparing the CS findings of OPC and composites with CSA and composites, SC0 had higher CS values than OC0; after 210 days of curing, SC0 had a value of 55.4 MPa and OC0 had a value of 53.2 MPa. Comparing composite cement developed OCF30 and OCV30 to composite cement prepared

SCF30 and SCV30; the latter demonstrated superior CS. The CS values for SCF30, SCV30, OCF30, and OCV30 were 43, 53.6, 42.2, and 45 MPa, respectively. The results showed that similar CS was obtained for neat CSA cement paste and SCV30, even if the CS results of the composite cement made with CSA did not reach the compressive strength values of the reference sample SC0. The reference sample SC0 had a CS value of 55.4 MPa after 210 days of curing, whereas the composite cement SCV30 resulted in 53.6 MPA. The data also demonstrate that a 30% substitution of CSA with VA has little to no impact on the SC0 CS outcome in the late curing days. In the first three, seven, and 28 days of curing, SCV 30 exhibits low CS values; after 90 and 210 days of curing, the CS result of SCV30 nearly attained that of OC0. According to the CS results, VA-incorporated CSA composite cement may be a preferable replacement for OPC. Compared to composite cement with FA incorporation, VA-incorporated composite cement with CSA demonstrated the best CS.

5.2.2 X-ray Diffraction

5.2.2.1 Diffraction patterns of systems with OPC and pozzolans

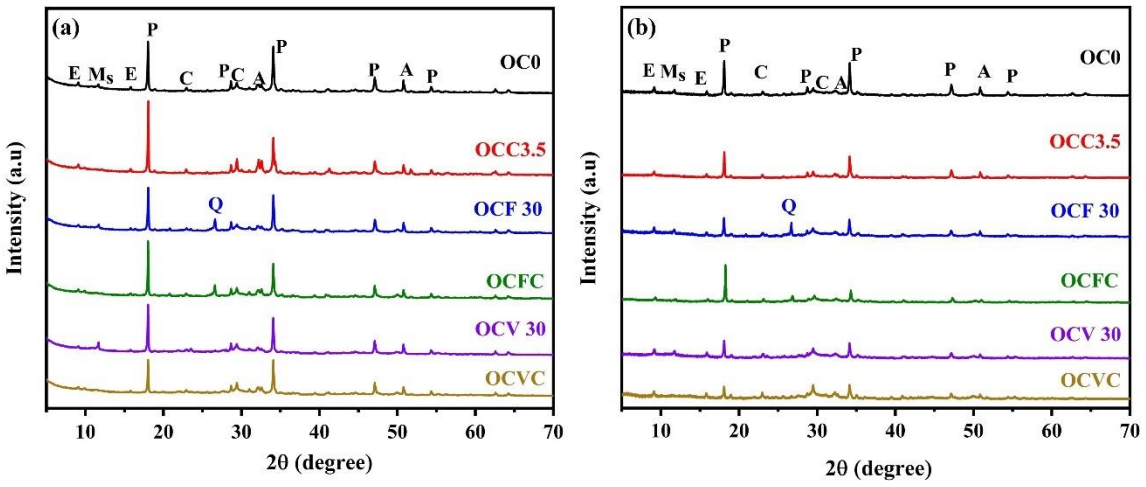

Figure 44. Diffraction pattern of OPC and its composite systems cured at (a) 28 days and (b) 90 days of curing A=Alite, B=Belite, C=Calcite, E=Ettringite, M_S = Monosulfate, P=Portlandite, Q=Quartz

Figure 44 shows the X-Ray Diffraction pattern of the composite cement with OPC at (a) 28 days and (b) 90 days. The AF_t and AF_m phases, calcium hydroxide (CH), and calcium silicate hydrate (C-S-H) are the principal hydration products of regular Portland cement. Hydrated cement contains the AF_t and AF_m phases, mixtures of C_3A, anhydrite, and water. Ettringite and monosulfate are the two most commonly occurring AF_m phases, respectively. The hydrated OPC in this work has a crystalline structure. The diffraction pattern displayed the phases alite, calcite, ettringite, monosulfate, and portlandite, often seen in the hydrated OPC [139,149]. Because of the phase of alite and belite in OPC, were pretty much completely diffused to generate calcium silicate hydrate, which is the primary hydration phase of OPC, developed as an amorphous state [150]; the amorphous nature was observed usually in the range of 24^0 to 36^0 [139,149]. In addition, a reduction in alite content could suggest the C-S-H formation [151]. For the hydrated cement, secondary hydration products formed were portlandite $(CaOH)_2$ and ettringite ($C_3A.3C\hat{S}.32H$) which was expected due to their crystallinity and as reported in the literature [152]. The VA, FA, and SCG did not show any other phase other than the hydrated phases formed in OPC. This indicates that the strength formation in the composite cement is mainly supported by OPC. The quartz phase was observed in the composite cement with FA, and composite cement with OPC FA and SCG [51]. From the XRD analysis, it can determine the crystal phases qualitatively; the quantitative analysis of cement hydrates was not measured here.

The portlandite phase was detected at 2θ equal to 18.04^o and 34.3^o degrees for all the composite systems. Due to the consumption of portlandite, 90 days of curing results in a drop in portlandite phase intensity, suggesting an increase in hydration reaction and pozzolanic reaction [153–155]. The portlandite phase diminishes in composite cements, including OPC and FA, OPC and VA, and more pozzolanic reactions may be seen as the material ages, according to the CS data. The decrease in portlandite phase leads to formation of secondary C-S-H. In comparison to the reference system made just with OPC and other composite

cement systems, the alite phase at 32º was more noticeable in composite cement developed with SCG. This means that the inclusion of used coffee grounds delays the formation of hydration reaction products, which reduces mechanical strength; CS data corroborate this conclusion. The only systems that could see the monosulfate peak at 11.7º were the reference system, the composite cement with FA, and the composite cement with VA. The absence of the peak of monosulfate in composite cements that contained SCG suggests that their presence had an impact on monosulfate formation. We may infer that SCG had an impact on the generation of hydrates during the early stages of hydration. One of the causes might be that SCG dissolve fast in the water, increasing the viscosity of the liquid. Due to the adsorption of SCG on cement particles, the migration rate of ions like Ca^{2+}, SO_4^{2-}, and OH^- slows down, which delays the nucleation, growth, and precipitation of hydrates [156].

No additional phases developed even after 90 or 210 days suggests that OPC had a major role in the growth of strength for composite cement. It can be shown that ettringite development in composite cement was delayed but that ettringite intensity increased over time. Because of this, the compressive strength decreases when more pozzolans are used in place of cement, and it improves after 90 days.

5.2.2.2 Diffraction patterns of systems with CSA, pozzolans

The diffraction pattern of CSA and the composite systems cured at 28 and 90 days of curing are shown in figure 45. The reaction of crystalline phases, the appearance of amorphous phases, the decrease of free water, and the incorporation of this water into the crystalline and amorphous fractions all these phenomenons occur during the hydration process of cement [157]. The larnite phase is hydraulically inactive at early ages, so its percentage should remain constant during the first hours of hydration; however, the reaction values of the larnite phase increase with time up to 8.5 hours of hydration [157]. In the case of calcite, this is simply due to its insolubility in water. With the content of anhydrite in the CSA, the ettringite becomes the main hydration product of the ye'elimite

phase [158]. The configuration of the crystal structure of ettringite favors the substitution of atomic species in the crystallographic positions occupied by cations and anions. Also, it allows the mobility of water molecules and ions [158].

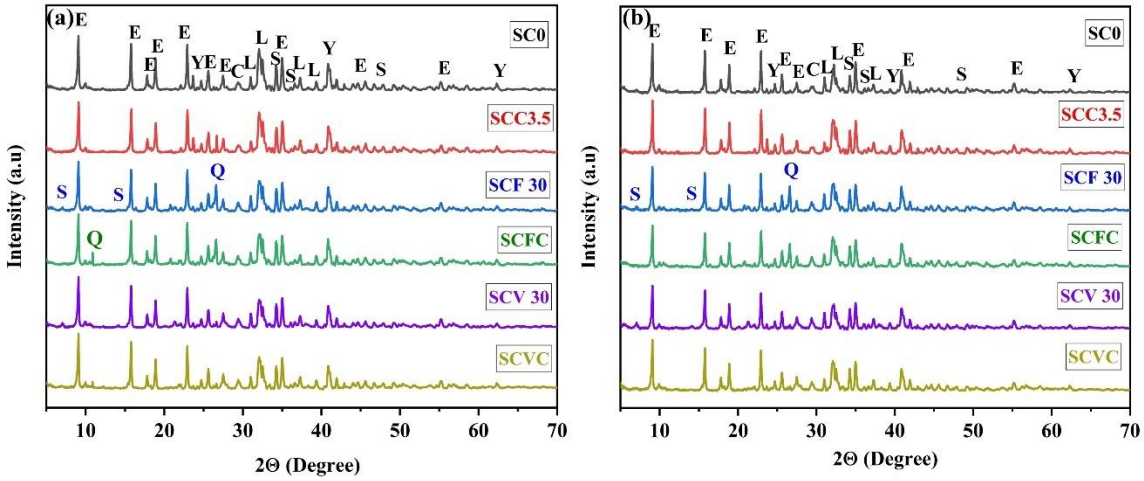

Figure 45. Diffraction pattern of CSA and its composite systems cured at (a) 28 days (b) 90 days of curing, C=Calcite, E=Ettringite, L=Larnite, Y=Ye'elimite, Q=Quartz

The phases of the composite cement made with CSA are the same as those of hydrated CSA, much like OPC composites. Larnite, calcite, ettringite, and ye'elimite were the minerals that showed up as diffraction patterns. Some of the phases (ye'elimite, calcite, and larnite) present in the CSA as raw material are still in the hydrated CSA. Ettringite, formed at 2θ equal to 9°, 15.7° 22.89° degrees, is the main product produced during the hydration of CSA7 [51,159]. The hydration product $Al(OH)_3$ was not observed in the neat and composite cement, indicating that the formation of $Al(OH)_3$ is amorphous [82]. The decrease in intensity of the ye'elimite phase showed an increase in the ettringite phase in long-term curing conditions [160].

The quartz phase of FA at 2θ equal to 10.89° was presented for 7 and 28 days of curing, and it was not visible in the later ages. After 90 days of curing, the peak of

quartz at 26.65° continues to exist [51]. This demonstrates that during the first 28 days, the strength of the composite cement was mainly derived from CSA cement. Afterward, some quartz from FA also participated in the hydration process and increased the strength of composite cement. The ye'elimite phase was seen at 23.65°, 40.9°, and 62°. Compared to other pozzolans with CSA, the composite cement made with VA exhibits reduced intensity for ye'elimite at 40.9° and nearly vanishes at 62° degrees, indicating the further production of ettringite. Compared to SC0, composite cement made with VA and FA (SV30 SCVC, SF30, SCFC) exhibit a rise in the ye'elimite phase at 25.65°, which is also noticeable. The presence of SCG affected the hydration reaction by restricting the rapid formation of hydration products. The intensity of the calcite phase rose for composite cement, and the calcite phase experienced the same impact.

Strätlingite (S) was observed after 28 and 90 days of curing. It was formed through the reaction of larnite, aluminum hydroxide, and water [51,77,82,161,162], and its presence aided in the formation of denser microstructures in the later stages of hydration, resulting in a reduction in porosity for the cement samples. For all cement samples, including the reference sample, the phase was observed at 2θ equal to 34.2°, 36.5°, and 47°. Because the extra silica was supplied from reacted FA and VA, forming additional strätlingite and ettringite [22].

When comparing the two graphs, it was found that the intensity of the Ettringite phase grew from 28 to 90 days of curing but was less intense for the composite cement at that age.

5.2.3 Scanning electron microscopy and Energy dispersive electron spectroscopy

The SEM images of 90-day hydrated pastes of the reference sample OPC and its composites are shown in figure 46. The SEM images showed the development of

the hydration products C-S-H, ettringite, and portlandite, which supported the XRD results of the composite cement. The SEM scans showed the cementitious gel C-S-H, which was not visible in the XRD data. Portlandite has a laminar structure, whereas Ettringite has a needle-like structure [163–166]. According to the SEM image of the OC0, portlandite is more intense and significant than the composite cement, showing that the OC0 has a high CS. The XRD graph also reveals a high-intensity peak for the OC0. The XRD graphs showed a similar decrease in portlandite intensity for the composites in SEM pictures. The picture of OCFC composite cement revealed unreacted FA particles.

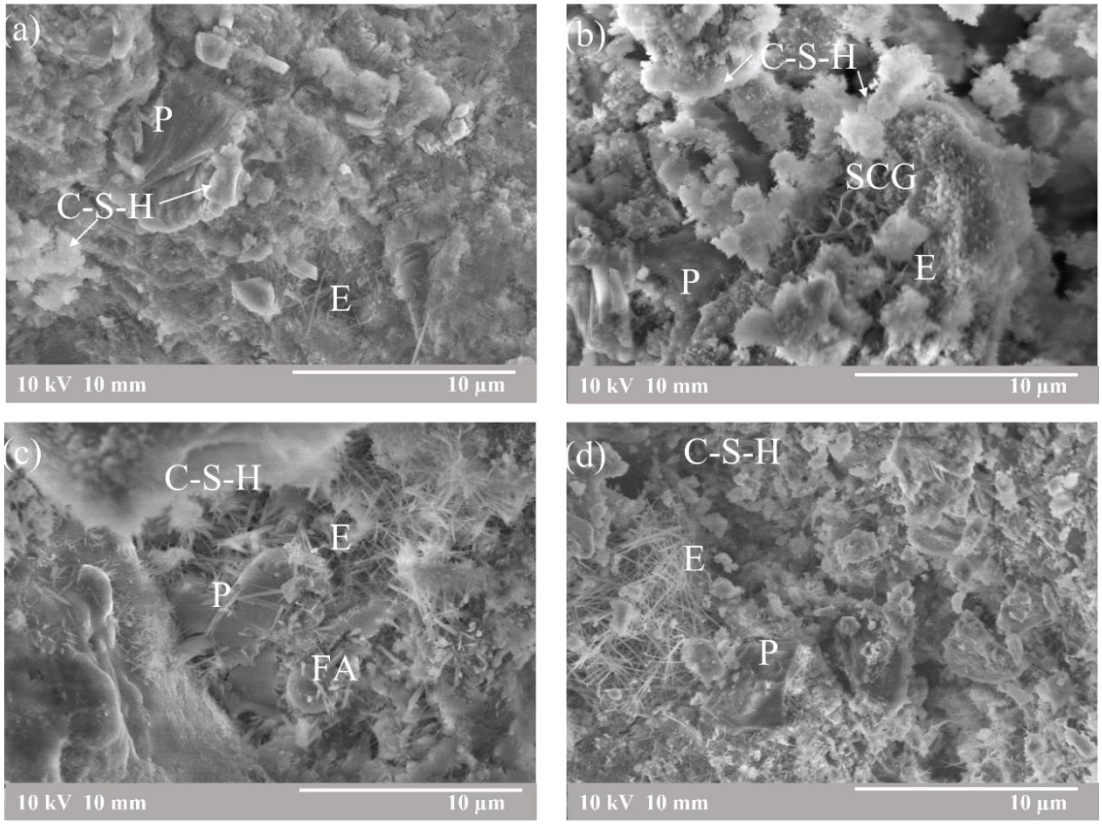

Figure 46. SEM images of the reference cement and the composite (a) OPC (b) OCC 3.5 (c) OCFC (d) OCVC, P=portlandite, E = ettringite, C-S-H= calcium silicate hydrate

Considering that each region of the cementitious matrix near the different grains showed specific characteristics of the hydration gels formed and reported in the literature, an example of this, where partially hydrated cement particles were observed, an amorphous precipitate region rich in Ca was found in a C-S-H type gel [167] (grey color due to its water content), as well as porous regions we observed in all the systems, there are unreacted particles of each of the raw materials used (semi-white color) [167]. High mechanical strength was another indicator of a homogeneous matrix with little porosity. Individual analysis of each cementitious matrix is carried out since these regions of the cement matrix typically become poorer or richer in the different oxides. In this way, it is possible to define which was the predominant gel for each composite cement.

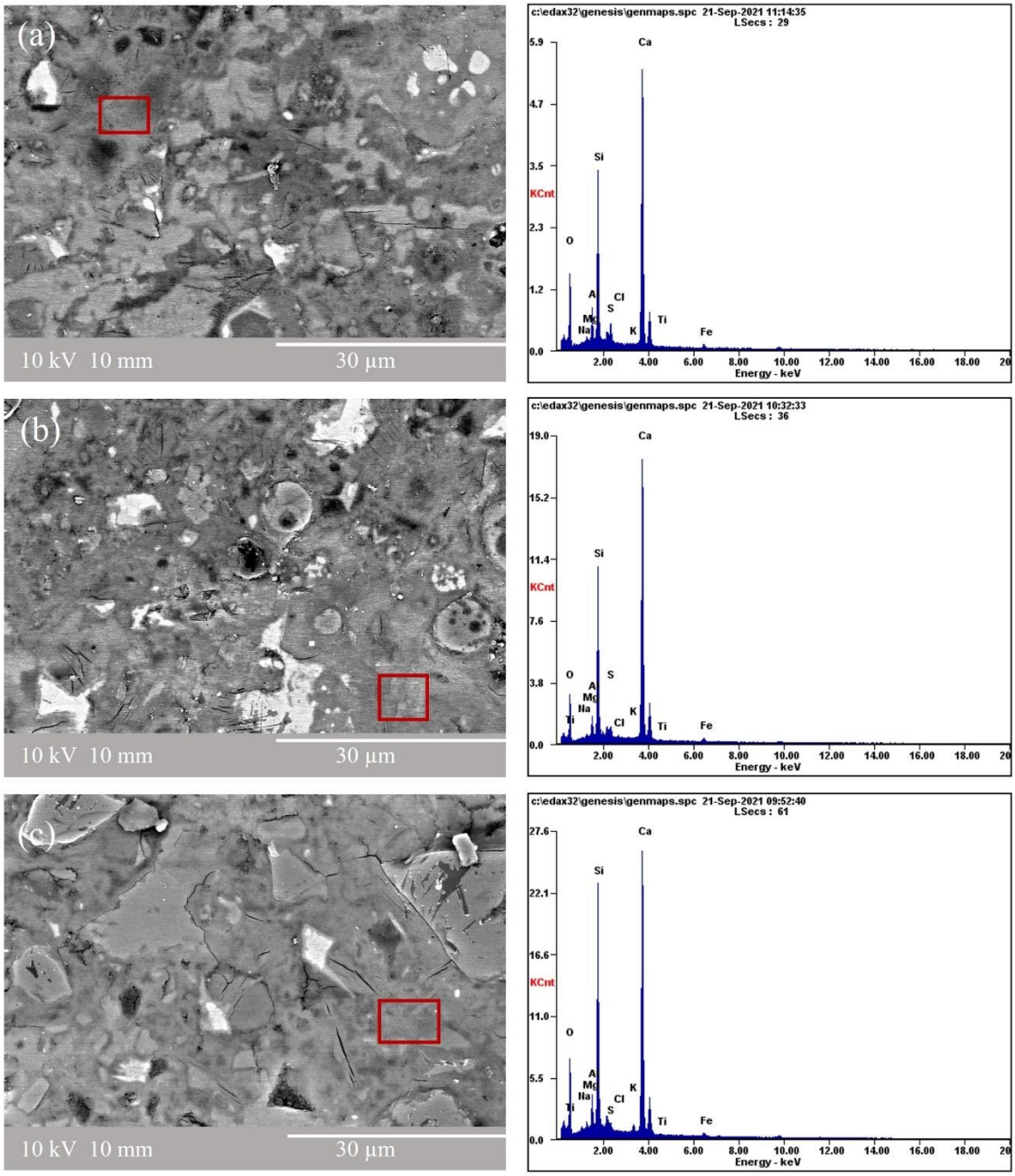

Figure 47. SEM-EDS of the composite cement prepared using OPC at 90 days of curing (a) OCC 3.5 (b) OCVC (c) OCFC.

Table 13. Oxides in the OPC, SCG, and composite cement OCC 3.5

	(%)	CaO	SiO_2	Al_2O_3	Na_2O
OPC		69.48	22.62	7.13	0.77
Spent coffee grounds		42.22	11.28	15.68	30.81
OCC3.5		54.83	37.2	6.95	1.02

Composite cements containing OPC and SCG are shown in figure 47(a), and following hydration, a dense cementitious matrix was found. C-S-H served as the primary hydration product of composite cement. The quantity of CaO in SCG and OPC is greater, with atomic percentages of 42.22 and 69.48, respectively. Both samples had larger concentrations of SiO_2 than Al_2O_3, Na_2O, Fe_2O_3, and other elements; it was discovered while studying the EDS data. Even while SCG contain more Na_2O—30.81 percent, the percentage of Na_2O replaced by cement is so small, i.e., 3.5%, that is why N was not present in the gel generated. Therefore, the primary hydration product, C-S-H, is produced when used coffee grounds are combined with regular Portland cement. For the composite cement OCC3.5, which was made using 3.5% SCG and the remaining OPC, the oxide composition ratio was CaO/SiO_2 1.47, Al_2O_3/SiO_2 0.19, and Na_2O/ SiO_2 0.15, falling between the range of $0.72 \leq CaO / SiO_2 \leq 1.9$ y $0 \leq Al_2O_3 / SiO_2 \leq 0.07$ as described by [167] and [168].

Table 14. Oxides in the OPC, FA, SCG and composite cement OCFC

	(%)	CaO	SiO_2	Al_2O_3	Na_2O
OPC		69.48	22.62	7.13	0.77
Fly ash		1.83	63.36	33.88	0.93
Spent coffee grounds		42.22	11.28	15.68	30.81
OCFC		47.42	41.09	10.76	0.73

Figure 47(b) depicts a composite cement of 30% FA, 3.5% SCG, and the rest OPC with temperature aids. The image makes it evident that unreacted raw materials are present, including FA, used coffee grounds, and OPC. When combined with OPC, FA functions as a pozzolan, and when it reacts with portlandite, more C-S-H is produced in the composite cement matrix [22]. A dense and compact cement matrix is produced in the prepared composite cement. FA has more Al_2O_3 and SiO_2 than other types of ash. The gel created for the composite cement was C-S-H, as determined by the oxide ratios in table 14, as evidenced by the results of the EDS analysis. The obtained oxide ratios were CaO/SiO_2 1.15, Al_2O_3/SiO_2 0.26, and Na_2O/SiO_2 0.07; values of oxides in the range of $0.72 \leq CaO / SiO_2 \leq 1.9$ y $0 \leq Al_2O_3 / SiO_2 \leq 0.07$ indicate the development of C-S-H gel in the composite cement [167]. Studies carried out by Barbara Lothenbach and I. García-Lodeiro also reported C-S-H gel formed in the composite cement prepared with FA and OPC [8,152].

Table 15. Oxides in the OPC, VA, SCG, and composite cement OCVC

(%)	CaO	SiO_2	Al_2O_3	Na_2O
OPC	69.48	22.62	7.13	0.77
Volcanic ash	0.91	77.59	16.48	5.03
Spent coffee grounds	42.22	11.28	15.68	30.81
OCVC	47.97	42.48	8.27	1.28

Figure 47(c) displays a composite of SCG and VA with OPC and a temperature assist setting. A dense and compact cement matrix was also visible in the composite cement with VA. In the studies with VA, K. Kupwade-Patil and R. Siddique reported that the hydration process of composite cement transforms C-S-H into C-A-S-H due to the high amount of Al in its composition [16,104]. VA also has higher amounts of SiO_2, similar to FA from table 15. The values of oxides lie in the range $0.72 \leq CaO / SiO_2 \leq 1.9$ and $0 \leq Al_2O_3 / SiO_2 \leq 0.07$; they have the oxide ratio as CaO/SiO_2 1.13, Al_2O_3/SiO_2 0.19 and Na_2O/SiO_2 0.16, and implies the formation of

C-S-H gel in the composite cement [167]. Studies carried out by Barbara Lothenbach and I. García-Lodeiro also reported C-S-H gel formed in the composite cement prepared with FA and OPC [8,152]; since VA shows a similar composition of FA, it could be concluded that the cementitious gel here formed with VA is also C-S-H.

Figures 47(a), 47(b), and 47(c) show that each composite system contains porous regions in its matrix, which indicates low-strength composites. These findings were also reflected in the compressive strength data. Additionally, the composite cement systems 47(b) OCFC and 47(c) OCVC, which both assisted in filling the micropores of the cement matrix and produced more reaction products, showed more compact hydration products. The filler effect reduced pore size in the composites OCFC and OCVC. The SCG adsorbs the nuclei of the hydration products, limiting their development, following the nucleation theory [147]. The SCG greatly hinders the production of highly reactive micronuclei of cement hydrates by occupying their reactive sides; this is the main cause of the reduced compressive strength values with SCG [141]. According to the EDS data in tables 13,14 and 15, the matrix for OPC composite cement systems is made up gel that is high in calcium and silica, known as C-S-H.

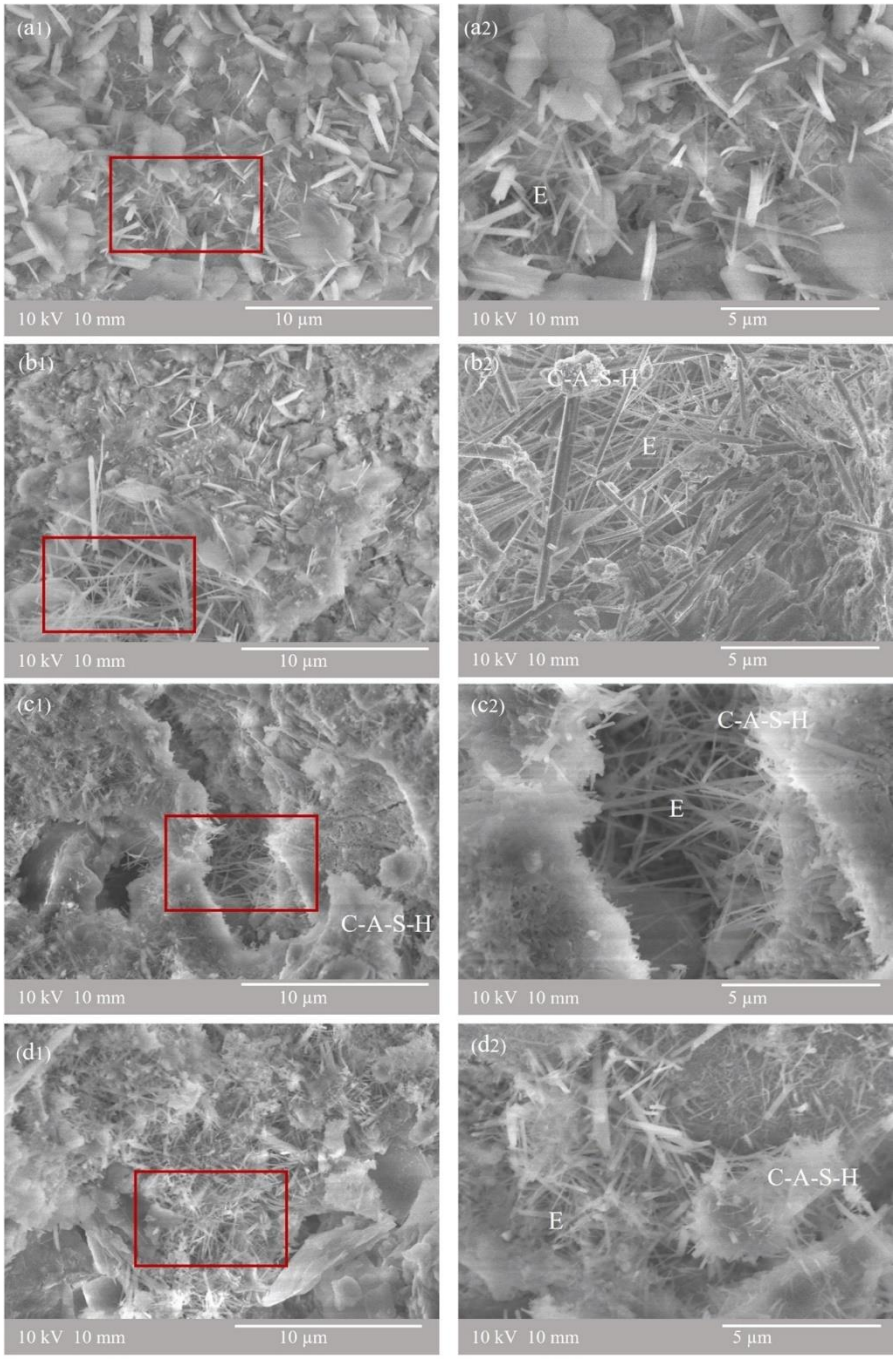

Figure 48. SEM images of the reference cement and its composite (a1) CSA at 10 µm (a2) CSA at 5 µm (b1) SCC 3.5 at 10 µm (b2) SCC 3.5 at 5 µm (c1) SCFC at 10 µm (c2) SCFC at 5 µm (d1) SCVC at 10 µm (d2) SCVC at 5 µm, E = ettringite, C-A-S-H= calcium alumino silicate hydrate

Figure 48 displays SEM images of the CSA and the composites after 90 days of curing [140,169]. Ettringite is the main hydration product of CSA, and its production is seen in the image along with trace quantities of C-S-H [170,171]. The EDS data show that C-S-H is formed, with lower quantities of aluminum forming C-A-S-H [172], and the XRD data support the ettringite formation. All cement systems showed ettringite, which has a needle-like structure and a propensity to develop in the pores of the cementitious matrix. It is seen from SCFC that ettringite is forming in fractures. The XRD data showed that ettringite needles were more intense for SCC 3.5.

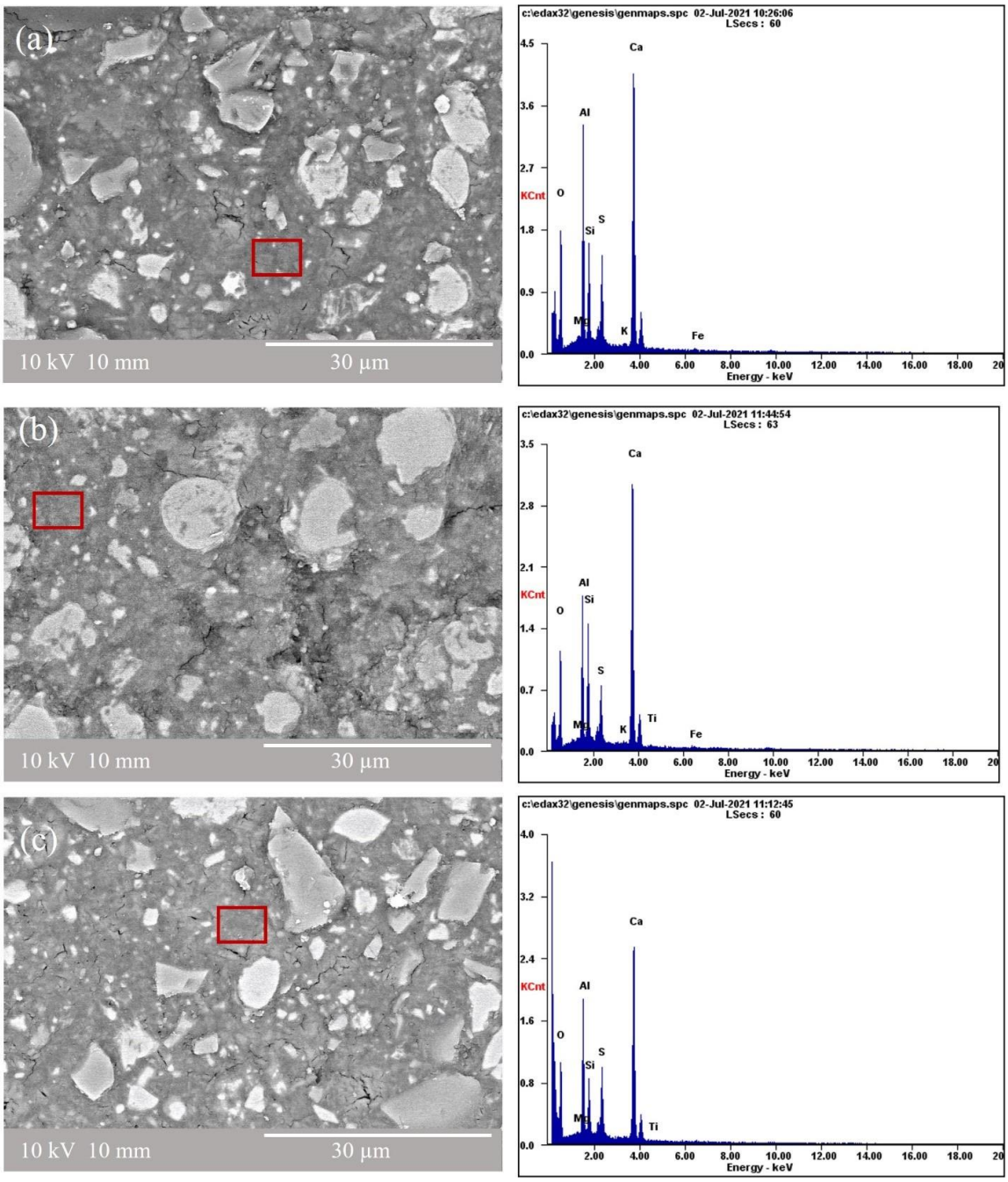

Figure 49. SEM-EDS of the composite cement prepared using CSA at 90 days of curing [(a) SCC 3.5 (b) SCFC (c) SCVC

Figure 49 (a) showed the dense C-A-S-H matrix in the composite cement with CSA and SCG. The oxides in CSA SCG and its composite are listed in Table 16. The resultant composite cement SCC3.5 comprises a high percentage of CaO and Al_2O_3, as CaO and Al_2O_3 are more abundant in SCG and CSA than SiO_2. The oxide ratios were 3.22 for CaO, 2.77 for Al_2O_3, and 0.01 for Na_2O, and the values were within the range of Garcia Lodeiro. It is indicated that C-A-S-H gel will develop in the composite cement by $0.72 \leq CaO / SiO_2 \leq 1.9$ and $0 \leq Al_2O_3 / SiO_2 \leq 0.07$ values [167] .

Table 16. Oxides in the CSA, SCG, and composite cement SCC3.5

(%)	CaO	SiO_2	Al_2O_3	Na_2O
CSA	80.01	10.59	9.26	0.14
Spent coffee grounds	42.22	11.28	15.68	30.81
SCC3.5	46	14.27	39.53	0.21

Table 17. Oxides in the CSA, FA, SCG, and composite cement SCFC

(%)	CaO	SiO_2	Al_2O_3	Na_2O
CSA	80.01	10.59	9.26	0.14
Fly ash	1.83	63.36	33.88	0.93
Spent coffee grounds	42.22	11.28	15.68	30.81
SCFC	46.8	15.2	38.67	0.2

The SEM-EDS of a composite cement, including SCG, CSA FA, and other materials, is shown in Figure 49(b). The oxide percentages of composite and raw material are shown in Table 17. High SiO_2 and Al_2O_3 content may be found in FA, and more Al_2O_3 was found in the developed composite cement. The production of the gel was seen as C-A-S-H for this reason. The hydration gels generated and reported in each region of the cementitious matrix surrounding the distinct grains

display specific characteristics. C-A-S-H gel was formed near the areas of cenospheres of FA; here, FA showed a high amount of CaO and Al_2O_3 [173–175]. Analyzing the EDS data, we found CaO/ SiO_2 3.07, Al_2O_3/ SiO_2 2.54, and Na_2O/ SiO_2 0.01, and these oxide values lie in the range of $0.72 \leq CaO / SiO_2 \leq 1.9$ and $0 \leq Al_2O_3 / SiO_2 \leq 0.07$, which suggests the production of C-A-S-H gel in the composite cement [22].

Table 18. Oxides in the CSA, VA, SCG, and composite cement SCVC

	(%)	CaO	SiO_2	Al_2O_3	Na_2O
CSA		80.01	10.59	9.26	0.14
Volcanic ash		0.91	77.59	16.48	5.03
Spent coffee grounds		42.22	11.28	15.68	30.81
SCVC		46.71	14.56	38.53	0.2

Figure 49(c) depicts VA with CSA and SCG. The figure demonstrates the creation of a thick matrix. VA also contains a high SiO_2 content, similar to FA. The value of the oxide ratio for Al_2O_3/SiO_2 did not fall within the following range as indicated by [167] based on the findings of the oxide percentage provided in table 18. The oxide ratios that were found were CaO/SiO_2 3.21, Al_2O_3/SiO_2 2.65, and Na_2O/SiO_2 0.01, similar to FA, indicates C-A-S-H gel is formed.

Figure 49(a) with CSA and SCG has more porous areas than the other two composite systems, as can be seen when comparing Figures 49(a), 49(b), and 49(c); The image also shows more unreacted coffee particles, which suggests that the low pozzolanic reaction of the coffee and SCC3.5 is a weaker cement system, as shown by the compressive strength data. Additionally, the 49(b) SCFC and 49(c) SCVC composite cement systems produced more dense cementitious hydration products, which tried to fill the micro pores of the cement matrix and generated more reaction products. Pores in the composites SCFC and SCVC were decreased by the filler effect. More mechanical strength and fewer pores than in

previous composites were made possible by the filler effect of VA. The EDS data of the CSA composite cement matrix showed that it was mostly made up of Ca, Si, and Al, suggesting that the matrix is built of two different types of gels: (a) one that is rich in calcium and silica and is known as C-S-H, and (b) one that is also rich in calcium, silica, and aluminum and is known as C-A-S-H. This gel is comparable to the one that was found following the hydration of CSA, but it also contains Al [104].

The CSA composite cement has denser matrices than the composite cement prepared with OPC, as seen in Figures 47 and 49. CSA composites performed better than OPC composite cement systems in compressive strength. The development of dense reaction products and reduced pores throughout the CSA composite cement systems has caused a rise in mechanical strength.

5.2.4 Attenuated Total Reflectance Infrared Spectroscopy

The ATR infrared spectra of hydrated OPC and cured composite cement at 90 days are shown in Figure 50. The technique was used to confirm the presence of the gels formed by interpreting the bonds obtained in spectra. The H-O-H bond deformation vibration and molecular water present in the structure, or the water that remains after the chemical reaction, are represented by the 1650 cm^{-1} band. The SCG need more water, and they use up most of the available water during mixing, leading to less workability. SCG affected the setting and hardening of the composite cement mix even though the amount of SCG used in the mix was minimal. The band saw at 1415 cm^{-1} related to the presence of carbonates due to the presence of calcite, as observed in XRD results [176].

The asymmetric stretching vibration of the Si-O bond accounted for the 1112 cm^{-1} band, while the O-Si-O bending vibrations were noticed at 450 cm^{-1} [177]. The crystallinity of the materials employed is the cause of the intensity fluctuation. Si-O linkages may be observed at 850 cm^{-1}, 900 cm^{-1}, 950 cm^{-1}, 1100 cm^{-1}, and 1200 cm^{-1}, respectively, and are related to Q^n units, where n=0,1,2,3,4. All data in the 873 cm^{-1} and 960 cm^{-1} range bands showed the typical silicate group

polymerization for the C-S-H gel, with robust production of Q^1 and Q^2 tetrahedra and stretching of Si-O-Si or Al-O-Si [178] and is observed in all systems. The existence of the gels in the composite cement is linked to its mechanical strength [179]. The bandwidth of the composite cement sample increased compared to the OPC cement sample, and the broadening of the band was caused by a decrease in silicate polymerization, which is connected to the CaO/SiO ratio [176]. The replacement of OPC with SCG and pozzolans decreased the mechanical strength of the cement pastes due to a decrease in the formation of hydration products. The increased compressive strength implies the formation of higher amounts of hydration product C-S-H.

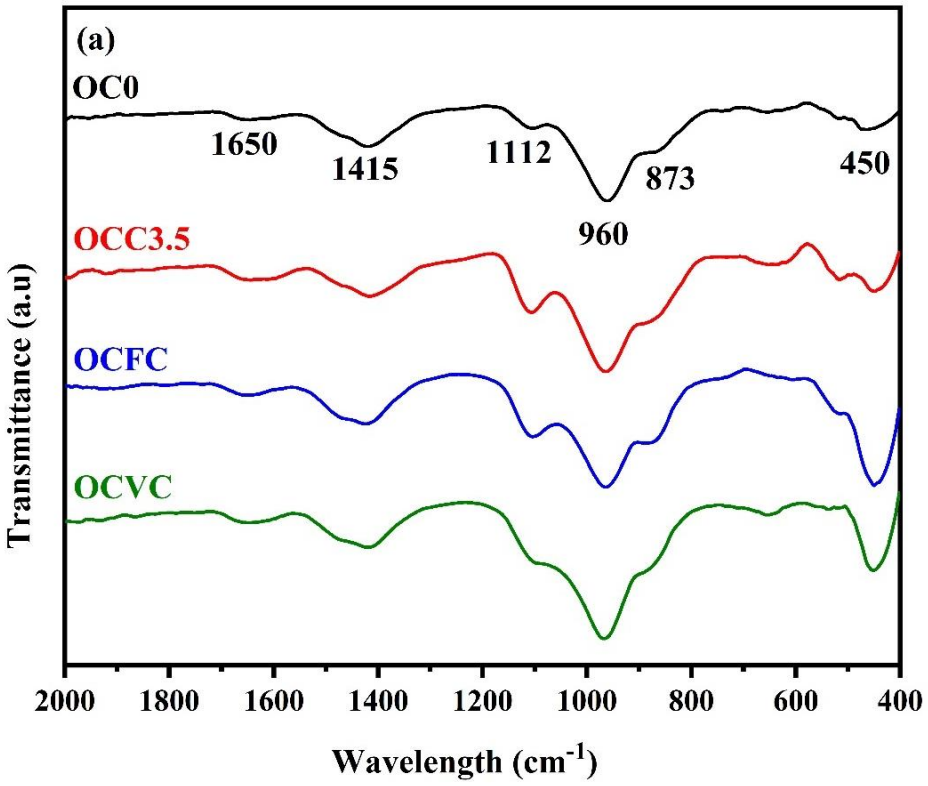

Figure 50. ATR infrared spectra of OPC and its composites cured at 90 days

Figure 51 represents the ATR infrared spectra of CSA cement and its composite cement cured at 90 days. The band located at 1660 cm^{-1} corresponds to the bending mode of the H-O-H bond, the molecular water [177,180] present in the structure. The intensity increased for the composite cement prepared with SCG and pozzolans than the cement sample prepared only with CSA. Because SCG takes up most of the water in composite, free water is present, which is the source of this. The carbonate phase was observed to have a band at 1425-1590 cm^{-1} and 872 cm^{-1}, which may be due to the carbonation during preparation and storage before the characterization experiments [176,178,181]. Compared with CSA, the composite cement with SCG and pozzolans show a more intensified peak of the Si-O-Si bond and is represented by the 522 cm^{-1} bands, which might be C-A-S-H. The results for compressive strength suggest a drop in silicate polymerization and a corresponding reduction in composite cement intensity. Between 1100 cm^{-1} and 1170 cm^{-1} are the stretching vibrations of SO_4^{2-} (v3). Since ettringite is the primary hydration product of CSA cement, its presence may be related to it [178], which is the principle hydration product of sulfoaluminate cement. All of the systems were found to have the C-A-S-H gel, defined by the asymmetric stretching of Si-O-Si or Al-O-Si, at a thickness of around 1110 cm^{-1} [178,180] and is observed in all systems. This implies the presence of the gel C-A-S-H credits to the compressive strength of the composite cement [177]. Peak width increased for composite cement prepared with coffee grounds pozzolans and CSA; the alkalinity of SCG could be the possible reason for this.

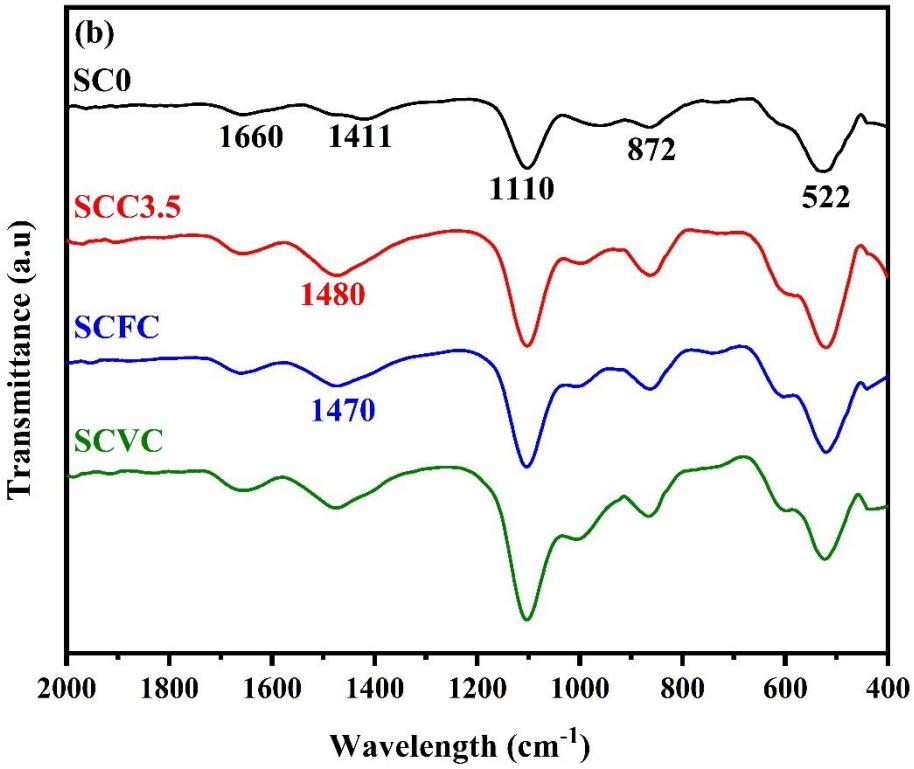

Figure 51. ATR spectra of CSA and its composites cured at 90 days

5.2.5 Hydration temperature of composite cement

The hydration temperature of the composite cement samples with OPC and CSA is shown in Figures 52(a) and (b). An exothermic reaction takes place when cement is mixed with water. The heat released during the hydration process of cement is the heat of hydration [182]. Binding gels are created during this physical chemical reaction, causing the cement to set and harden [183]. The type of cement used, the water-to-cement ratio, the fineness of the cement, the curing temperature, the use of supplements or additives, etc., all affect how much heat is released during the hydration process [184]. The heat emission will be more significant in the early stages or within 24 h. Both the initial setting and the final setting are made at or just before the temperature peak, which is the area where the C-S-H and CH reaction products formed [136,185]. A similar experimental

setup was used by Xiaotian Zou for the analysis of the hydration temperature of concrete [186].

The dissolution of several ionic species in the fresh mixture caused intense chemical activity during the first 4 h. However, according to recent studies, the first four hours could be linked to period one, the end of the induction period [187–189]. And the main hydration peak is from 4 to 24 h in period 2. The initial setting begins during the induction period (from where the temperature rises). The final set is shortly before the peak temperature; here is where C-S-H, CH reaction products form [136,185]. OC0 and OCF30 reached maximum temperatures of 43 ℃ and 42 ℃, respectively, during the hydration process at 11.15 and 11.50 h. At 12.15 h, the peak of hydration for OCV30 was 37 ℃; a similar decline in hydration temperature was also noted in tests done by S.Al. Fadala. [34]. The graph shows that adding SCG would lower the hydration temperature for both OPC and CSA cement [141]. Additionally, coffee grounds reduced the hydration temperature of composite cements containing FA and VA.

The temperatures at 12 h during the hydration process were shown in figure 52(a) as OC0 and OCF30 at 43 ℃ and 42 ℃, respectively. The temperature of OCV30 at 12 h of hydration was 37 ℃ [190,191]. This shows that the acceleration-deceleration duration and hydration temperature of composite cement are both influenced by the degree of substitution [184]. The acceleration period is delayed, and the peak of the hydration curve is extended, both of which slow down the response. According to the absorption principle, hydration causes a considerable quantity of Ca^{2+} ions to be released. Because these ions move through the system more quickly than the SiO_4^{-2} ion group, this will encourage the formation of crystal CH [16,192]. The hydration temperature is lowered for OCC 3.5 when the cement is replaced with SCG, which was 27 ℃. The hydration temperature was initially reduced to 25 ℃ after OPC replacement with SCG and pozzolans, and it was then kept within a stable range. The amount of heat flow is reduced by roughly 41% when using coffee grounds in place of cement. Therefore, temperature assistance

is necessary for the setting and hardening of composite cements made using OPC [193].

The hydration temperature for CSA, which is more exothermic than OPC, is shown in Figure 52 (b). It exhibits an exothermic peak with a wide shape, indicating that the final set of the reference sample SC0 was at 10:45 h and a greater reactivity reaching up to 64 ℃. As previously stated, the hydration reaction products are generated during the induction period of 4 to 24 h. Ettringite and monosulfate production is thought to be what caused this particular peak in the CSA instance [194,195]. Strätlingite and/or C-S-H are produced due to the reaction of belite in CSA cement. Similar reactions take place when more magnesium and sulfate ions are present. More magnesium causes hydrotalcite ($CH_{24}Al_2Mg_6O_{23}$) to form, while more sulfate causes ettringite and/or monosulfate to develop [196]. The partial substitution of CSA with FA resulted in a temperature of 54 ℃ and a delay of the final set to 11:15 h, whereas VA delayed the final set by 12 h and decreased the temperature to 45 ℃. In the case of SCG, the hydration process was delayed by another 3 hours, and the final setting time for the composite cement SCC3.5 was 13:45 h [197]. In the case of FA, the nucleation and hydrate formation are sped up by the presence of extra surfaces. The temperature rose within the first few hours for SCVC and SCFC when SCG were mixed with cement pozzolan composite. For CSA composite made using SCG, there was a reduction in hydration temperature of around 37%. Even though SCG reduce the hydration temperature of composite cement, the heat decline had no impact on the setting and hardening of the cement paste.

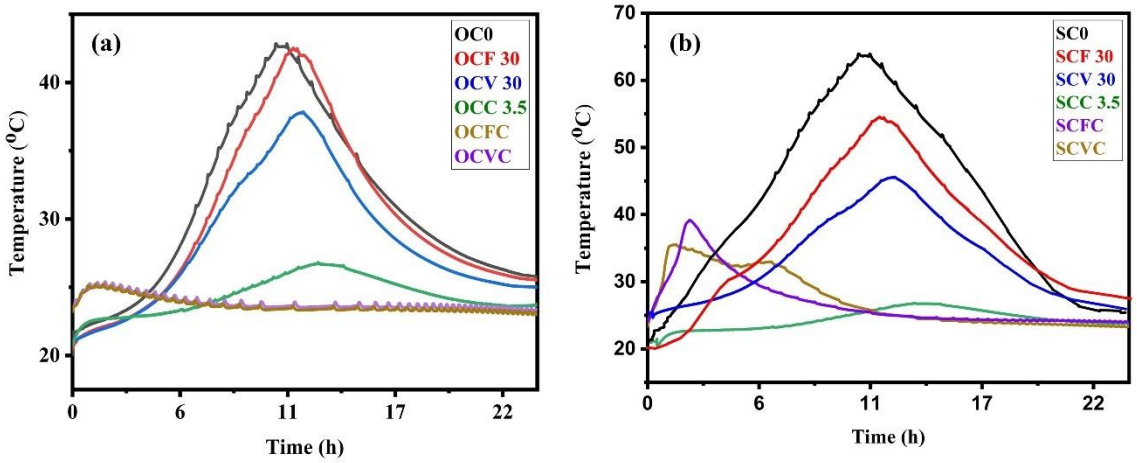

Figure 52. (a)The hydration temperature of the OPC composite cement pastes, (b) The hydration temperature of the CSA composite cement pastes

5.2.6 Electrochemical Impedance Spectroscopy

Figure 53 shows the electrochemical impedance spectroscopy of OPC and its composites at 7 and 90 days of curing. The characterization technique helps better understand the microstructure of the composite cement paste during hydration [198] and the movement of ionic species. Cement-based materials are porous materials, and the pore solution electric charge depends on the ionic composition and pH [153,199]. Concrete pores are randomly dispersed, vary in size, and are unevenly linked to one another. Permeability, absorption, and numerous diffusion processes control the transport of water and different ions in these curved channels [200]. Electrical experiments indicate a decreased conductivity in the system, implying that the binder phase is more resistant to ionic transport. The key criteria determining the qualities of hardened concrete, such as mechanical and durability properties, are porosity and pore structure [153].

The correlations between the frequency-related characteristics and paste structure have been developed and validated through the development of electrochemical

impedance spectroscopy (EIS) technology. The semicircle arc obtained in the high-frequency area generally represents the bulk-cement effect in the standard Nyquist curve [201]. The graph clearly explains that as the curing period increases, the electrical impedance also increases and the durability of the composite cement systems also increases. The increase in the electrical impedance is very much related to the compressive strength of the cement systems, indicating a linear correlation between mechanical strength and electrical impedance [201]. The compressive strength increases due to the dense formation of cementitious gel, and thus the impedance also increases. The increased electrical impedance is also because of the generation of hydration products within the composite cement systems [202]. The creation of a dense microstructural network, including essentially a calcium hydroxide and C-S-H gel, is well recognized when C_3S and C_2S are hydrated [203]. At 7 days of curing, OPC, OCV30, OFC30, and OCFC composite only show an impedance range of 250 Ω, and 400 Ω for OCC3.5 composite. The better electrical impedance was shown by composite with OCVC; it was 750 Ω at 7 days of curing. While comparing the curing days, 90 days curing samples showed improved electrical impedance. All the composite cements improved the electrical impedance. OPC improved to 500 Ω from 250 Ω, OCC3.5 composite from 400 Ω to 625 Ω, OCF30 composite showed an electrical impedance of 1000 Ω, OCFC showed around 850 Ω. For OCV30 composite and OCVC composite the electrical impedance increased to 1400 Ω and 1300 Ω respectively. The introduction of VA improved the impedance due to its fine granulates, with the potential to partly restrict voids and pores after hydration. As the pore structure was refined, this resulted in a decreased effective diffusivity for chloride or other species, indicates durable composite [16,128]. The addition of supplementary cementitious materials helps in the refined pore structure of the composite cement, which leads to improved electrical impedance [153]. The electrical impedance of the composite cement is directly connected with the pore structure and porosity of the system. The passage of ions via the pore spaces is

the primary source of electrical current in hydrating cement mortar. As a result, electrical resistivity is a proxy for porosity and diffusivity [16,200,202].

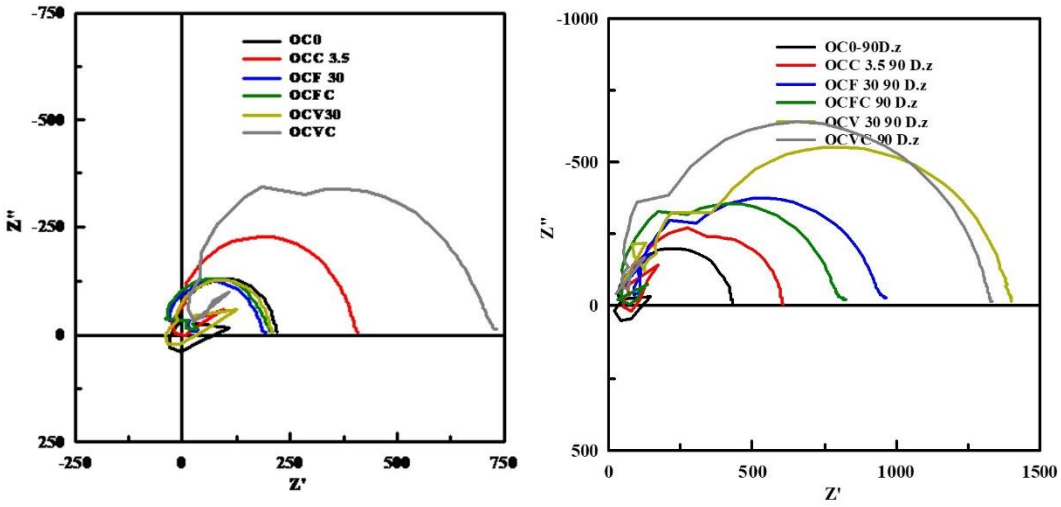

Figure 53. Electrical Impedance Spectroscopy of OPC composite cement at 7 and 90 days.

Figure 54 shows the electrochemical impedance spectroscopy of CSA and its composites at 7 and 90 days of curing. The electrical impedance spectrum of the cement paste with imaginary versus real component of impedance values is plotted (Nyquist plot) in figure 54; as the hydration process progress, the diameter of the semi-circle increases. The electrical impedance for the composite with VA showed an improved performance that other composite cement pastes from 7 to 90 days curing period. As already explained for the OPC composite with VA, the electrical impedance was better due to its fine-grind ability. For the composite CSA VA, the refinement of pore structure during the gradual increase of curing leads to better impedance for the composite cement paste [16,128]. The impedance value increased from 900 Ω to 2000 Ω for the composite with CSA and VA (SCV30). The composite cement with CSA and FA also improved; the impedance value was 800 Ω at 7 days of curing and increased to 1100 Ω at 90 days. The result supports the fact that the early age hydration of CSA cement and also its composite cement. The composite cement with CSA and SCG did not vary much, it kept the same

impedance value from 7 to 90 days of curing, 1100 Ω this indicates that the early formation of the hydration products in the system. The total resistance water solution in blocked pores decreases, indicating that hydration products are continually producing pores [202]. Because of the appearance of hydration products and water consumption during the cement-hydration process, the structures of cementitious materials have been discovered to be continually reconstructive in terms of factors such as pore solution chemistry, porosity, and pore size distribution. Electrical impedance was utilized to offer the most precise and comprehensive perspective of the transport properties of cement-based materials, as well as to represent hydration processes and microstructural features [201].

Between the hydration reaction gel and the cement-based components, air-filled voids, micro-cracks, and internal surface pores exist. Pores come in a variety of shapes and sizes. Air voids are unavoidable during the mixing and compaction of cement pastes, mortars, and concretes. Capillary pores are formed between mixing-water-filled channels that link to each other and the concrete surface. The gel pores are too tiny to get saturated during hydration; their existence is determined by the ambient humidity, concrete porosity, and moisture content. The physical qualities of cement-based materials during hydration, and their ultimate physical properties, such as strength, permeability, shrinkage, and creep, are governed by the constantly growing network of pores. The amount of evaporable water in the paste and the concentration of mobile ions in the pore fluid affect the impedance of the composite cement pastes [204,205].

The main reaction product, ettringite, was responsible for the higher impedance values for the composite cement prepared using CSA. While comparing the impedance values, the composite cement paste system with CSA and VA showed a better impedance value than that of the composite cement system prepared with OPC and VA, and the values are 2000 Ω and 1400 Ω, respectively.

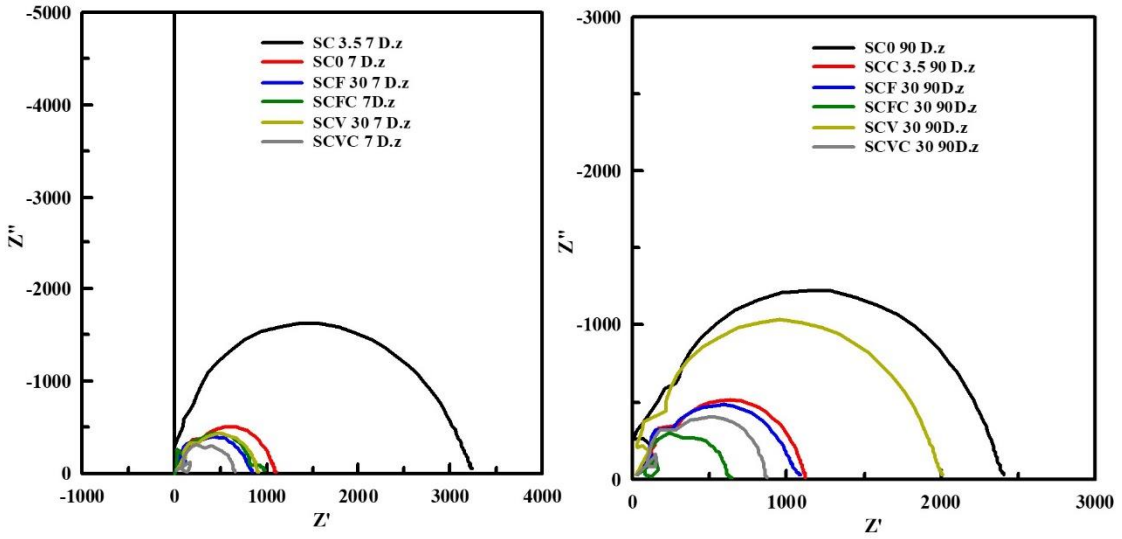

Figure 54. Electrical Impedance Spectroscopy of CSA composite cement at 7 and 90 days.

CHAPTER 6

CONCLUSIONS

6.1 General

It was possible to synthesize composite cement with OPC and CSA with good mechanical properties for nonstructural applications.

The proposed synthesis processes allow the design of versatile materials using industrial wastes as raw materials for developing materials with good cementitious properties.

Technologically, this composite cement with CSA is comparable to most of the portland cement that is sold today, with the advantage of environmental improvements, its manufacture is significantly more sustainable than traditional portland cement, and with a good plan for growth and industrialization, they can become much more economical.

6.2 Characterization of raw materials

The preparation of the raw material was necessary to obtain the best results since drying, milling, and sieving, left the materials in optimal conditions to be used in the design of mixtures.

The characterization of each material used as raw material (OPC, CSA, FA, VA, and SCG) was fundamental since, in this way, it was possible to know: the

chemical composition in the form of oxides, mineralogical phases, infrared spectra, and morphology of each one of them that allowed us to form a more accurate design of experiments possible.

The FA used in the research project belonged to the Type F group according to ASTM 618-2014, which was confirmed by the XRF technique. The phases present in the FA were: quartz, mullite, and calcite; for the VA, were sanidine, quartz, clinohypersthyne, magnetite, albite and leucite, calcite, and gehlenite; for SCG: gismondine, $KHCO_3$, and magnesite. For the CSA, ye-elimite, grossite, larnite, anhydrite, or calcium sulfate, and in the OPC, the characteristic phases observed were: alite, belite, aluminate, ferite, and calcium sulfate.

6.3 Compressive strength

Replacing the cement OPC and CSA with SCG modified the compressive strength of the cement pastes. The optimum replacement for cement OPC and CSA with FA and VA was found to be 30%, and SCG with 3.5 %. Above these percentages, the compressive strength decreased for FA and VA. The compressive strength decreased for SCG above 3.5%. Also, while increasing the percentage of SCG, the workability of the cement paste decreased. Pozzolans attained maximum strength at their later ages. Without alkali activation on the composite cements, the compressive strength decreased**.**

6.4 X-ray Diffraction

The diffraction pattern for OPC and CSA composite cement was the same as that of the cement itself. This shows the cement helped in the reaction mechanism for the composite cement. The main hydration product for OPC is C-S-H, and it was assumed to be formed as amorphous. Ettringite, the main hydration product of CSA, was visible from the diffraction pattern.

6.5 Scanning electron microscopy with energy dispersive electron spectroscopy

SEM images did not show much difference in the formation of hydrated cement matrix for CSA with and without temperature setting. Still, the dense matrix was observed for composite cement prepared using OPC with temperature aid setting. EDS results showed the formation of reaction product C-S-H for OPC and its composites; for CSA cement, the reaction product formed was C-A-S-H.

6.6 Attenuated total reflection

ATR infrared spectroscopy supported the analysis obtained from XRD and SEM-EDS, which showed the formation of new hydration gels or hybrid gels because the characteristic bands of the spectra in all the composite cement systems showed the formation of different peaks: for the peak band at 960 cm^{-1} for OPC and its composite cement, is a common value for the silicate group to polymerize, resulting in the production of C-S-H and for the CSA and its composites the peak band at 1110 cm^{-1}, is a common value for the silicate group to polymerize, resulting in the production of C-A-S-H.

6.7 Hydration temperature

The hydration temperature of OPC was 42 ℃, while it was 64 ℃ for CSA. SCG decrease the hydration temperature of the cement and extended the time. Composite cement with OPC and SCG shows a hydration temperature of 25 ℃. In the case of CSA with SCG and pozzolans did not decrease the hydration temperature. Hence, OPC with SCG and other pozzolans require a temperature of 80 ℃ for the setting and hardening of the cement cubes. The composite cements with OPC, SCG and pozzolans, the temperature-cured cement samples showed better compressive strength results than those without temperature-cured cement samples. In the case of CSA, the compressive strength decreased/ slight change

was observed when the samples cured at temperature because the CSA releases more heat than OPC during the hydration process.

6.8 Electrochemical impedance spectroscopy

The characterization technique helps better understand the microstructure of the composite cement paste during hydration. Electrical experiments indicate a decreased conductivity in the system, implying that the binder phase is more resistant to ionic transport. The key criteria determining the qualities of hardened concrete, such as mechanical and durability properties, are porosity and pore structure. The compressive strength increases due to the dense formation of hydration products; thus, the impedance also increases. The introduction of VA improved the impedance due to fine granulates, with the potential to restrict voids and pores after hydration. As the pore structure was refined, this decreased effective diffusivity for chloride or other species, indicating a durable composite. For the composite CSA-VA, the refinement of pore structure during the gradual increase of curing leads to better impedance for the composite cement paste. The main reaction product, ettringite, was responsible for the higher impedance values for the composite cement prepared using CSA. While comparing the impedance values, it can be observed that the composite cement paste system with CSA and VA showed a better impedance value than that of the composite cement system prepared with OPC and VA, and the values are 2000 Ω and 1400 Ω respectively.

Cement pastes with SCG can be used in the construction sites of countries with sweltering climatic conditions because the setting time of the cement paste is delayed when replacing cement with SCG. The mechanical strength decreased by replacing cement paste with SCG and a mix of cement with pozzolans and SCG. So, composite cement cannot be used for structural works. But possibly, it can be used for nonstructural elements, subgrade filling material in pavement construction, drainage construction, etc., requiring minimal mechanical strength.

Hence, we can reduce the amount of cement by replacing it with natural pozzolans and SCG.

While comparing the compressive strength results, it can be concluded that it is worth replacing the OPC with CSA since it gives comparable mechanical strength. Also, the partial replacement of CSA with FA VA SCG can be used for nonstructural applications,

7. FUTURE WORK

Globally, we are going through an environmental contingency; warming the surface of the earth is causing enormous environmental damage. This will provoke that in the year 2050, 150 million climate refugees will be forced to migrate from their homes due to climate problems in their region of origin.

It has been demonstrated that conventional building materials are insufficient and do not contribute to climate change; on the contrary, they promote more environmental problems by resorting to the overexploitation of raw materials.

It is urgent to search for and provide new options for the construction of homes and buildings so that they can be energy efficient. For that following future work will aid in solving the issues:

- Strength and microstructure study of hybrid cement with SCG, VA, FA, and blast furnace slag.
- Strength and microstructure of calcinated SCG and oven-dried SCG.
- Strength and microstructure study of hybrid cement with calcinated SCG, VA, FA, and blast furnace slag.

REFERENCES

[1] S.A. Miller, V.M. John, S.A. Pacca, A. Horvath, Cement and Concrete Research Carbon dioxide reduction potential in the global cement industry by 2050, Cem. Concr. Res. (2017) 0–1. https://doi.org/10.1016/j.cemconres.2017.08.026.

[2] U.N. Environment, K.L. Scrivener, V.M. John, E.M. Gartner, Cement and Concrete Research Eco-e fficient cements : Potential economically viable solutions for a low-CO_2 cement-based materials industry, (2018). https://doi.org/10.1016/j.cemconres.2018.03.015.

[3] R. Robayo-Salazar, J. Mejía-Arcila, R. Mejía, D. Gutiérrez, E. Martínez, Life cycle assessment (LCA) of an alkali-activated binary concrete based on natural volcanic pozzolan: A comparative analysis to OPC concrete, Constr. Build. Mater. 176 (2018) 103–111. https://doi.org/10.1016/j.conbuildmat.2018.05.017.

[4] H.M. Ludwig, W. Zhang, Research review of cement clinker chemistry, Cem. Concr. Res. 78 (2015) 24–37. https://doi.org/10.1016/j.cemconres.2015.05.018.

[5] R. Snellings, G. Mertens, J. Elsen, Supplementary Cementitious Materials, 74 (2012) 211–278. https://doi.org/10.2138/rmg.2012.74.6.

[6] E.M. Gartner, D.E. MacPhee, A physico-chemical basis for novel cementitious binders, Cem. Concr. Res. 41 (2011) 736–749. https://doi.org/10.1016/j.cemconres.2011.03.006.

[7] P.C. Aïtcin, Supplementary cementitious materials and blended cements, in: Sci. Technol. Concr. Admixtures, Elsevier, 2016: pp. 53–73. https://doi.org/10.1016/B978-0-08-100693-1.00004-7.

[8] B. Lothenbach, K. Scrivener, R.D. Hooton, Supplementary cementitious materials, Cem. Concr. Res. 41 (2011) 1244–1256. https://doi.org/10.1016/j.cemconres.2010.12.001.

[9] E. Gartner, Industrially interesting approaches to “low-CO_2” cements, Cem. Concr.

Res. 34 (2004) 1489–1498. https://doi.org/10.1016/j.cemconres.2004.01.021.

[10] M. A. G. Aranda, A. G. de La Torre, Sulfoaluminate cement, in: Eco-Efficient Concr., 2013: pp. 488–522. https://doi.org/https://doi.org/10.1533/9780857098993.4.488.

[11] T. Hanein, J.L. Galvez-Martos, M.N. Bannerman, Carbon footprint of calcium sulfoaluminate clinker production, J. Clean. Prod. 172 (2018) 2278–2287. https://doi.org/10.1016/j.jclepro.2017.11.183.

[12] M.C.G. Juenger, F. Winnefeld, J.L. Provis, J.H. Ideker, Advances in alternative cementitious binders, Cem. Concr. Res. 41 (2011) 1232–1243. https://doi.org/10.1016/j.cemconres.2010.11.012.

[13] K. Kupwade-Patil, C. De Wolf, S. Chin, J. Ochsendorf, A.E. Hajiah, A. Al-Mumin, O. Büyüköztürk, Impact of Embodied Energy on materials/buildings with partial replacement of ordinary Portland Cement (OPC) by natural Pozzolanic Volcanic Ash, J. Clean. Prod. 177 (2018) 547–554. https://doi.org/10.1016/j.jclepro.2017.12.234.

[14] K. Kupwade-Patil, M. Tyagi, C.M. Brown, O. Büyüköztürk, Water dynamics in cement paste at early age prepared with pozzolanic volcanic ash and Ordinary Portland Cement using quasielastic neutron scattering, Cem. Concr. Res. 86 (2016) 55–62. https://doi.org/10.1016/j.cemconres.2016.04.011.

[15] K. Celik, M.D. Jackson, M. Mancio, C. Meral, A. Emwas, P.K. Mehta, P.J.M. Monteiro, Cement & Concrete Composites High-volume natural volcanic pozzolan and limestone powder as partial replacements for portland cement in self-compacting and sustainable concrete, Cem. Concr. Compos. 45 (2014) 136–147. https://doi.org/10.1016/j.cemconcomp.2013.09.003.

[16] R. Siddique, Effect of volcanic ash on the properties of cement paste and mortar, Resour. Conserv. Recycl. 56 (2011) 66–70. https://doi.org/10.1016/j.resconrec.2011.09.005.

[17] K. Khan, M.N. Amin, Influence of fineness of volcanic ash and its blends with quarry dust and slag on compressive strength of mortar under different curing temperatures, Constr. Build. Mater. 154 (2017) 514–528.

https://doi.org/10.1016/j.conbuildmat.2017.07.214.

[18] K.J. Owens, Y. Bai, D. Cleland, P.A.M. Basheer, J. Kwasny, M. Sonebi, S. Taylor, A. Gupta, Activation of high volume fly ash pastes using chemical activators, 2nd Int. Conf. Sustain. Constr. Mater. Technol. (2010) 1759–1770.

[19] P.S. Peng, Sustainability in Construction : Using Fly Ash as a Cement Replacement, (2020) 1–7. http://www.ecosmartconcrete.com/docs/csrliulevelton.pdf.

[20] L. Black, Low clinker cement as a sustainable construction material, in: Sustain. Constr. Mater., Elsevier, 2016: pp. 415–457. https://doi.org/10.1016/B978-0-08-100370-1.00017-2.

[21] J. Chakraborty, S. Banerjee, Replacement of cement by fly ash in concrete, Int. J. Civ. Eng. 3 (2016) 58–60. https://doi.org/10.14445/23488352/IJCE-V3I8P110.

[22] L.H.J. Martin, F. Winnefeld, E. Tschopp, C.J. Müller, B. Lothenbach, Cement and Concrete Research Influence of fly ash on the hydration of calcium sulfoaluminate cement, 95 (2017) 152–163. https://doi.org/10.1016/j.cemconres.2017.02.030.

[23] International coffee Organization, Historical data on the global coffee trade, (2020). http://www.ico.org/new_historical.asp?section=Statistics.

[24] L.F. Ballesteros, J.A. Teixeira, S.I. Mussatto, Chemical, functional, and structural properties of spent coffee grounds and coffee silverskin, Food Bioprocess Technol. 7 (2014) 3493–3503. https://doi.org/10.1007/s11947-014-1349-z.

[25] T.A. Kua, A. Arulrajah, S. Horpibulsuk, Y.J. Du, S.L. Shen, Strength assessment of spent coffee grounds-geopolymer cement utilizing slag and fly ash precursors, Constr. Build. Mater. 115 (2016) 565–575. https://doi.org/10.1016/j.conbuildmat.2016.04.021.

[26] F. Andreola, A. Borghi, S. Pedrazzi, G. Allesina, P. Tartarini, I. Lancellotti, L. Barbieri, Spent coffee grounds in the production of lightweight clay ceramic aggregates in view of urban and agricultural sustainable development, Materials (Basel). 12 (2019). https://doi.org/10.3390/ma12213581.

[27] L.L.P. Chung, Y.C. Wong, A. Arulrajah, The application of spent coffee grounds and tea wastes as additives in alkali-activated bricks, Waste and Biomass Valorization. (2021). https://doi.org/10.1007/s12649-021-01453-7.

[28] T.A. Kua, A. Arulrajah, A. Mohammadinia, S. Horpibulsuk, M. Mirzababaei, Stiffness and deformation properties of spent coffee grounds based geopolymers, Constr. Build. Mater. 138 (2017) 79–87. https://doi.org/10.1016/j.conbuildmat.2017.01.082.

[29] J.. Escalante-Garcia, The effect of temperature on the hydration of portland cement and composite cement pastes, 1996.

[30] J.I. Escalante-García, J.H. Sharp, Effect of temperature on the hydration of the main clinker, Cem. Concr. Res. 28 (1998) 1245–1257. https://doi.org/https://doi.org/10.1016/S0008-8846(98)00107-0.

[31] J.I. Escalante-Garcia, J.H. Sharp, Effect of temperature on the early hydration of Portland cement and blended cements, Adv. Cem. Res. 12 (2000) 121–130. https://doi.org/10.1680/adcr.2000.12.3.121.

[32] J.I. Escalante-Garcia, Nonevaporable water from neat OPC and replacement materials in composite cements hydrated at different temperatures, Cem. Concr. Res. 33 (2003) 1883–1888. https://doi.org/10.1016/S0008-8846(03)00208-4.

[33] J.I. Escalante-Garcia, J.H. Sharp, The chemical composition and microstructure of hydration products in blended cements, Cem. Concr. Compos. 26 (2004) 967–976. https://doi.org/10.1016/j.cemconcomp.2004.02.036.

[34] S. Al-Fadala, J. Chakkamalayath, S. Al-Bahar, A. Al-Aibani, S. Ahmed, Significance of performance based specifications in the qualification and characterization of blended cement using volcanic ash, Constr. Build. Mater. 144 (2017) 532–540. https://doi.org/10.1016/j.conbuildmat.2017.03.180.

[35] C. Suksiripattanapong, T.A. Kua, A. Arulrajah, F. Maghool, S. Horpibulsuk, Strength and microstructure properties of spent coffee grounds stabilized with rice husk ash and slag geopolymers, Constr. Build. Mater. 146 (2017) 312–320. https://doi.org/10.1016/j.conbuildmat.2017.04.103.

[36] A. Arulrajah, T.-A. Kua, C. Phetchuay, S. Horpibulsuk, F. Mahghoolpilehrood, M.M. Disfani, Spent coffee grounds–fly ash geopolymer used as an embankment structural fill material, J. Mater. Civ. Eng. 28 (2016) 04015197. https://doi.org/10.1061/(asce)mt.1943-5533.0001496.

[37] Agboola Shamsudeen Abdulazeez, Mamman Adamu Idi, Tapgun Justin, Bappah Hamza, Strength performance of concrete produced with volcanic ash as partial replacement of cement, Int. J. Eng. Res. V9 (2020) 372–378. https://doi.org/10.17577/ijertv9is030396.

[38] R. Siddique, M. Iqbal Khan, Fly ash, in: 2011: pp. 1–66. https://doi.org/10.1007/978-3-642-17866-5_1.

[39] D. Tupayachy-Quispe, J. Almirón, F. Apaza, R. Churata, E. Paredes, M. Torres-Carrasco, A. Bautista, Peruvian volcanic ashes as new alternative material in geopolymer preparation: Influence of dissolution concentration and wear resistance, Proc. LACCEI Int. Multi-Conference Eng. Educ. Technol. (2020) 27–31. https://doi.org/10.18687/LACCEI2020.1.1.5.

[40] F. Zou, C. Hu, F. Wang, Y. Ruan, S. Hu, Enhancement of early-age strength of the high content fly ash blended cement paste by sodium sulfate and C–S–H seeds towards a greener binder, J. Clean. Prod. 244 (2020) 118566. https://doi.org/10.1016/j.jclepro.2019.118566.

[41] Š. Slanička, The influence of fly ash fineness on the strength of concrete, Cem. Concr. Res. 21 (1991) 285–296. https://doi.org/10.1016/0008-8846(91)90010-F.

[42] S.H. Lee, H.J. Kim, E. Sakai, M. Daimon, Effect of particle size distribution of fly ash-cement system on the fluidity of cement pastes, Cem. Concr. Res. 33 (2003) 763–768. https://doi.org/10.1016/S0008-8846(02)01054-2.

[43] P. Chindaprasirt, C. Jaturapitakkul, T. Sinsiri, Effect of fly ash fineness on compressive strength and pore size of blended cement paste, Cem. Concr. Compos. 27 (2005) 425–428. https://doi.org/10.1016/j.cemconcomp.2004.07.003.

[44] E. Sakai, S. Miyahara, S. Ohsawa, S.H. Lee, M. Daimon, Hydration of fly ash cement, Cem. Concr. Res. 35 (2005) 1135–1140.

https://doi.org/10.1016/j.cemconres.2004.09.008.

[45] M. Reiner, K. Rens, High-Volume Fly Ash Concrete: Analysis and Application, Pract. Period. Struct. Des. Constr. 11 (2006) 58–64. https://doi.org/10.1061/(ASCE)1084-0680(2006)11:1(58).

[46] M. Narmluk, T. Nawa, Effect of fly ash on the kinetics of Portland cement hydration at different curing temperatures, Cem. Concr. Res. 41 (2011) 579–589. https://doi.org/10.1016/j.cemconres.2011.02.005.

[47] T. Hemalatha, M. Mapa, N. George, S. Sasmal, Physico-chemical and mechanical characterization of high volume fly ash incorporated and engineered cement system towards developing greener cement, J. Clean. Prod. 125 (2016) 268–281. https://doi.org/10.1016/j.jclepro.2016.03.118.

[48] T. Hemalatha, A. Ramaswamy, A review on fly ash characteristics – Towards promoting high volume utilization in developing sustainable concrete, J. Clean. Prod. 147 (2017) 546–559. https://doi.org/10.1016/j.jclepro.2017.01.114.

[49] E. Aprianti S, A huge number of artificial waste material can be supplementary cementitious material (SCM) for concrete production – a review part II, Elsevier Ltd, 2017. https://doi.org/10.1016/j.jclepro.2015.12.115.

[50] L.H.J. Martin, F. Winnefeld, E. Tschopp, C.J. Müller, B. Lothenbach, Influence of fly ash on the hydration of calcium sulfoaluminate cement, Cem. Concr. Res. 95 (2017) 152–163. https://doi.org/10.1016/j.cemconres.2017.02.030.

[51] M. García-Maté, A.G. De La Torre, L. León-Reina, M.A.G. Aranda, I. Santacruz, Hydration studies of calcium sulfoaluminate cements blended with fly ash, Cem. Concr. Res. 54 (2013) 12–20. https://doi.org/10.1016/j.cemconres.2013.07.010.

[52] A. Telesca, A. Mobili, F. Tittarelli, M. Marroccoli, Calcium sulfoaluminate cement and fly ash-based geopolymer as sustainable binders for mortars, Chem. Eng. Trans. 74 (2019) 1249–1254. https://doi.org/10.3303/CET1974209.

[53] C. Ruiz-Santaquiteria, A. Fernández-Jiménez, J. Skibsted, A. Palomo, Clay reactivity: Production of alkali activated cements, Appl. Clay Sci. 73 (2013) 11–16. https://doi.org/10.1016/j.clay.2012.10.012.

[54] E.M.G. Karen L. Scrivener, Vanderley M. John, Eco- efficient cements: Potential, economically viable solutions for a low- CO2, cement-based materials industry, World Bus. Counc. Sustain. Dev. (2016) 64. https://wedocs.unep.org/bitstream/handle/20.500.11822/25281/eco_efficient_cements.pdf.

[55] T. Constructors, Manufacture of cement materials and manufacturing process of portland cement, (n.d.). https://theconstructor.org/building/manufacture-of-cement/13709/.

[56] H. Substances, O.S. Response, Standard terminology relating to hydraulic cement, Current. 93 (1998) 1–3. https://doi.org/10.1520/C0219-07A.2.

[57] H.F.W. Taylor, Cement chemistry, Cem. Chem. (1997). https://doi.org/10.1680/cc.25929.

[58] K.L. Scrivener, A. Capmas, Lea's Chemistry of cement and concrete : Chapter 13, 2004. http://www.dbpia.co.kr/view/ar_view.asp?arid=1536305.

[59] S.A. Rodger, G.W. Groves, Electron microscopy study of ordinary Portland cement and ordinary Portland cement–pulverized fuel ash blended pastes, J. Am. Ceram. Soc. 72 (1989) 1037–1039. https://doi.org/10.1111/j.1151-2916.1989.tb06265.x.

[60] D.L. Rayment, A.J. Majumdar, The composition of the C-S-H phases in Portland cement pastes, Cem. Concr. Res. 12 (1982) 753–764. https://doi.org/10.1016/0008-8846(82)90039-4.

[61] E.E.L. D L Rayment, The analysis of OPC pastes: A comparison between analytical electron microscopy and electron probe microanalysis, Cem. Concr. Res. 14 (1984) 43–48.

[62] H.F.W. Taylor, D.E. Newbury, An electron microprobe study of a mature cement paste, Cem. Concr. Res. 14 (1984) 565–573. https://doi.org/10.1016/0008-8846(84)90134-0.

[63] K.L. Scrivener, Backscattered electron imaging of cementitious microstructures: Understanding and quantification, Cem. Concr. Compos. 26 (2004) 935–945. https://doi.org/10.1016/j.cemconcomp.2004.02.029.

[64] G. Renaudin, Y. Filinchuk, J. Neubauer, F. Goetz-Neunhoeffer, A comparative structural study of wet and dried ettringite, Cem. Concr. Res. 40 (2010) 370–375. https://doi.org/10.1016/j.cemconres.2009.11.002.

[65] H.J.H. Brouwers, 5. Reacciones de las fases del aluminato y del sulfato (PARTE II), 12 (2007) 6–42.

[66] C. Ferraris, P. Stutzman, M. Peltz, J. Winpigler, Developing a more rapid test to assess sulfate resistance of hydraulic cements, J. Res. Natl. Inst. Stand. Technol. 110 (2005) 529–540. https://doi.org/10.6028/jres.110.080.

[67] Z. Zhang, G.W. Scherer, A. Bauer, Morphology of cementitious material during early hydration, Cem. Concr. Res. 107 (2018) 85–100. https://doi.org/10.1016/j.cemconres.2018.02.004.

[68] M. García-Maté, A.G. De La Torre, L. León-Reina, E.R. Losilla, M.A.G. Aranda, I. Santacruz, Effect of calcium sulfate source on the hydration of calcium sulfoaluminate eco-cement, Cem. Concr. Compos. 55 (2015) 53–61. https://doi.org/10.1016/j.cemconcomp.2014.08.003.

[69] C. Shi, A.F. Jiménez, A. Palomo, New cements for the 21st century: The pursuit of an alternative to Portland cement, Cem. Concr. Res. 41 (2011) 750–763. https://doi.org/10.1016/j.cemconres.2011.03.016.

[70] M. Gallardo H., J.M. Almanza R., D.A. Cortés H., J.C. Escobedo B., Comportamiento mecánico y químico de cementos de sulfoaluminato de calcio obtenido a partir de desechos industriales, Rev. ALCONPAT. 6 (2016) 15–27. https://doi.org/10.21041/ra.v6i1.112.

[71] S. Ioannou, L. Reig, K. Paine, K. Quillin, Properties of a ternary calcium sulfoaluminate-calcium sulfate-fly ash cement, Cem. Concr. Res. 56 (2014) 75–83. https://doi.org/10.1016/j.cemconres.2013.09.015.

[72] I. Mehdipour, K.H. Khayat, Enhancing the performance of calcium sulfoaluminate blended cements with shrinkage reducing admixture or lightweight sand, Cem. Concr. Compos. 87 (2018) 29–43. https://doi.org/10.1016/j.cemconcomp.2017.12.001.

[73] I. Bolaños-Vásquez, R. Trauchessec, J.I. Tobón, A. Lecomte, Influence of the ye'elimite/anhydrite ratio on PC-CSA hybrid cements, Mater. Today Commun. 22 (2020). https://doi.org/10.1016/j.mtcomm.2019.100778.

[74] C.N. B.V, The advantages of CSA cement, (2015) 4.

[75] P. Chaunsali, P. Mondal, Physico-chemical interaction between mineral admixtures and OPC-calcium sulfoaluminate (CSA) cements and its influence on early-age expansion, Cem. Concr. Res. 80 (2016) 10–20. https://doi.org/10.1016/j.cemconres.2015.11.003.

[76] P. Chaunsali, P. Mondal, Influence of mineral admixtures on early-age behavior of calcium sulfoaluminate cement, ACI Mater. J. 112 (2015) 59–68. https://doi.org/10.14359/51687240.

[77] A. Rungchet, P. Chindaprasirt, S. Wansom, K. Pimraksa, Hydrothermal synthesis of calcium sulfoaluminate-belite cement from industrial waste materials, J. Clean. Prod. 115 (2016) 273–283. https://doi.org/10.1016/j.jclepro.2015.12.068.

[78] F.P. Glasser, L. Zhang, High-performance cement matrices based on calcium sulfoaluminate-belite compositions, Cem. Concr. Res. 31 (2001) 1881–1886. https://doi.org/10.1016/S0008-8846(01)00649-4.

[79] T. Desbois, R. Le Roy, A. Pavoine, G. Platret, A. Feraille, A. Alaoui, Effect of gypsum content on sulfoaluminate mortars stability, Eur. J. Environ. Civ. Eng. 14 (2010) 579–597. https://doi.org/10.1080/19648189.2010.9693248.

[80] I.A. Chen, C.W. Hargis, M.C.G. Juenger, Understanding expansion in calcium sulfoaluminate-belite cements, Cem. Concr. Res. 42 (2012) 51–60. https://doi.org/10.1016/j.cemconres.2011.07.010.

[81] J. Bizzozero, Hydration and dimensional stability of calcium aluminate cement based systems, 6336 (2014).

[82] F. Winnefeld, B. Lothenbach, Hydration of calcium sulfoaluminate cements - Experimental findings and thermodynamic modelling, Cem. Concr. Res. 40 (2010) 1239–1247. https://doi.org/10.1016/j.cemconres.2009.08.014.

[83] M. García-Maté, I. Santacruz, Á.G. De La Torre, L. León-Reina, M.A.G. Aranda, Rheological and hydration characterization of calcium sulfoaluminate cement pastes, Cem. Concr. Compos. 34 (2012) 684–691. https://doi.org/10.1016/j.cemconcomp.2012.01.008.

[84] P. Chaunsali, P. Mondai, Early-age volume change and hydration of expansive cements, Proc. 10th Fib Int. PhD Symp. Civ. Eng. C (2014) 117–122.

[85] M.J. Sánchez-Herrero, A. Fernández-Jiménez, A. Palomo, C4A3Š hydration in different alkaline media, Cem. Concr. Res. 46 (2013) 41–49. https://doi.org/10.1016/j.cemconres.2013.01.008.

[86] F. Winnefeld, S. Barlag, Calorimetric and thermogravimetric study on the influence of calcium sulfate on the hydration of ye'elimite, J. Therm. Anal. Calorim. 101 (2010) 949–957. https://doi.org/10.1007/s10973-009-0582-6.

[87] M. Dovál, M. Palou, V. Kovár, Heat evolution and mechanism of hydration in CaO-Al 2O 3-SO 3 system, Ceram. - Silikaty. 49 (2005) 104–108.

[88] M. Ossa M., H. Jorquera S., Cementos con cenizas volantes, Mater. Construcción. 34 (1984) 3–17. https://doi.org/10.3989/mc.1984.v34.i193.956.

[89] M. Ahmaruzzaman, A review on the utilization of fly ash, Prog. Energy Combust. Sci. 36 (2010) 327–363. https://doi.org/10.1016/j.pecs.2009.11.003.

[90] P.V. A. Durán-Herrera1, C. A. Juárez, Evaluation of Sustainable High-Volume Fly Ash Concretes, 2009.

[91] G.C. Isaia, A.L.G. Gastaldini, R. Moraes, Physical and pozzolanic action of mineral additions on the mechanical strength of high-performance concrete, Cem. Concr. Compos. 25 (2003) 69–76. https://doi.org/10.1016/S0958-9465(01)00057-9.

[92] O.I.M. Bas, A.M. Terrades, La influencia del cemento Portland en las propiedades mecánicas , permeabilidad y estructura porosa de los hormigones con cenizas volantes 1 influence of Portland cement in the mechanical properties , permeability and pore structure of concretes mixed wit, 9 (2009) 1–10.

[93] S.H. Hwang, R. Shahsavari, High calcium cementless fly ash binder with low

environmental footprint: Optimum Taguchi design, J. Am. Ceram. Soc. 102 (2018) jace.15873. https://doi.org/10.1111/jace.15873.

[94] Astm, Standard Specification for Coal Fly Ash and Raw or Calcined Natural Pozzolan for Use, Annu. B. ASTM Stand. (2010) 3–6. https://doi.org/10.1520/C0618.

[95] K.-Y. Show, J.-H. Tay, D.-J. Lee, Cement replacement materials, 2018. https://doi.org/10.1142/9789813238268_0005.

[96] U. Costa, Factors affecting the reaction with lime of italian pozzolanas ., (2020).

[97] P.K. Mehta, Studies on blended Portland cements containing Santorin earth, Cem. Concr. Res. 11 (1981) 507–518. https://doi.org/10.1016/0008-8846(81)90080-6.

[98] A. Tironi, M.A. Trezza, A.N. Scian, E.F. Irassar, Assessment of pozzolanic activity of different calcined clays, Cem. Concr. Compos. 37 (2013) 319–327. https://doi.org/10.1016/j.cemconcomp.2013.01.002.

[99] J.P. J.Ambroise, M.Murat, Hydration reaction and hardening of calcined clays and related minerals. V. Extension of the research and general conclusions., Cem. Concr. Res. 15 (1985) 261–268.

[100] H. Muntaha, B.M. Program, C. Program, Micro and pore structure analysis of volcanic ash blended cement paste, (2018) 35–44.

[101] K. Kupwade-Patil, S.D. Palkovic, A. Bumajdad, C. Soriano, O. Büyüköztürk, Use of silica fume and natural volcanic ash as a replacement to Portland cement: Micro and pore structural investigation using NMR, XRD, FTIR and X-ray microtomography, Constr. Build. Mater. 158 (2018) 574–590. https://doi.org/10.1016/j.conbuildmat.2017.09.165.

[102] Ash from Icelandic volcano falls in Aberdeen, (n.d.). https://www.hutton.ac.uk/news/ash-icelandic-volcano-falls-aberdeen.

[103] R. Walker, S. Pavía, Physical properties and reactivity of pozzolans, and their influence on the properties of lime-pozzolan pastes, Mater. Struct. Constr. 44 (2011) 1139–1150. https://doi.org/10.1617/s11527-010-9689-2.

[104] K. Kupwade-Patil, A.F. Al-Aibani, M.F. Abdulsalam, C. Mao, A. Bumajdad, S.D. Palkovic, O. Büyüköztürk, Microstructure of cement paste with natural pozzolanic volcanic ash and Portland cement at different stages of curing, Constr. Build. Mater. 113 (2016) 423–441. https://doi.org/10.1016/j.conbuildmat.2016.03.084.

[105] S.I. Mussatto, E.M.S. Machado, S. Martins, J.A. Teixeira, Production, composition, and application of coffee and its industrial residues, Food Bioprocess Technol. 4 (2011) 661–672. https://doi.org/10.1007/s11947-011-0565-z.

[106] S.C. Grisel Corro, Umapada Pal, Enhanced biogas production from coffee pulp through delingninocellulosic photocatalytic pretreatment, Online Libr. Open Access. 2 (2014) 177–187. https://onlinelibrary.wiley.com/doi/full/10.1002/ese3.44.

[107] B. Janissen, T. Huynh, Chemical composition and value-adding applications of coffee industry by-products: A review, Resour. Conserv. Recycl. 128 (2018) 110–117. https://doi.org/10.1016/j.resconrec.2017.10.001.

[108] M.S. Kim, H.G. Min, N. Koo, J. Park, S.H. Lee, G.I. Bak, J.G. Kim, The effectiveness of spent coffee grounds and its biochar on the amelioration of heavy metals-contaminated water and soil using chemical and biological assessments, J. Environ. Manage. 146 (2014) 124–130. https://doi.org/10.1016/j.jenvman.2014.07.001.

[109] J. Kim, H. Kim, G. Baek, C. Lee, Anaerobic co-digestion of spent coffee grounds with different waste feedstocks for biogas production, Waste Manag. 60 (2017) 322–328. https://doi.org/10.1016/j.wasman.2016.10.015.

[110] M.J. Kim, S.W. Choi, H. Kim, S. Mun, K.B. Lee, Simple synthesis of spent coffee ground-based microporous carbons using K2CO3 as an activation agent and their application to CO2 capture, Chem. Eng. J. 397 (2020) 125404. https://doi.org/10.1016/j.cej.2020.125404.

[111] L. Massaro Sousa, M.C. Ferreira, Spent coffee grounds as a renewable source of energy: An analysis of bulk powder flowability, Particuology. 43 (2019) 92–100. https://doi.org/10.1016/j.partic.2018.06.002.

[112] M. Ramos-Andrés, C. Andrés-Iglesias, J. García-Serna, Production of molecular

weight fractionated hemicelluloses hydrolyzates from spent coffee grounds combining hydrothermal extraction and a multistep ultrafiltration/diafiltration, Bioresour. Technol. 292 (2019) 121940. https://doi.org/10.1016/j.biortech.2019.121940.

[113] T.A. Kua, Application of spent coffee ground as a road subgrade construction material, Pdfs.Semanticscholar.Org. (2017). https://pdfs.semanticscholar.org/d72a/a133d275420f8110c1551915db308be13cdf.pdf.

[114] A. Arulrajah, T.A. Kua, C. Suksiripattanapong, S. Horpibulsuk, J.S. Shen, Compressive strength and microstructural properties of spent coffee grounds-bagasse ash based geopolymers with slag supplements, J. Clean. Prod. 162 (2017) 1491–1501. https://doi.org/10.1016/j.jclepro.2017.06.171.

[115] B. Sena Da Fonseca, A. Vilão, C. Galhano, J.A.R. Simão, Reusing coffee waste in manufacture of ceramics for construction, Adv. Appl. Ceram. 113 (2014) 159–166. https://doi.org/10.1179/1743676113Y.0000000131.

[116] R. Padmapriya, J.A. Tharian, T. Thirunalasundari, Coffee waste management-An overview, Int J Curr Sci. 9 (2013) 83–91. http://www.currentsciencejournal.info/issuespdf/Coffee waste12.pdf.

[117] P.F. Hsieh, T.Y. Wen, Evaluation of ozone removal by spent coffee grounds, Sci. Rep. 10 (2020) 1–8. https://doi.org/10.1038/s41598-019-56668-5.

[118] I. Safarik, K. Horska, B. Svobodova, M. Safarikova, Magnetically modified spent coffee grounds for dyes removal, Eur. Food Res. Technol. 234 (2012) 345–350. https://doi.org/10.1007/s00217-011-1641-3.

[119] S.C.C. Bate, Guide for structural lightweight aggregate concrete: report of ACI committee 213, Int. J. Cem. Compos. Light. Concr. 1 (1979) 5–6. https://doi.org/10.1016/0262-5075(79)90004-6.

[120] A. Arulrajah, F. Maghoolpilehrood, M.M. Disfani, S. Horpibulsuk, Spent coffee grounds as a non-structural embankment fill material: Engineering and environmental considerations, J. Clean. Prod. 72 (2014) 181–186.

https://doi.org/10.1016/j.jclepro.2014.03.010.

[121] M. Kaya, Evaluating organic waste sources (spent coffee ground) as metal-free catalyst for hydrogen generation by the methanolysis of sodium borohydride, Int. J. Hydrogen Energy. 45 (2020) 12743–12754. https://doi.org/10.1016/j.ijhydene.2019.10.180.

[122] S. Mukarjee, Study on the physical and mechanical property of ordinary portland cement and fly ash paste, Int. J. Civ. Struct. Eng. 2 (2012). https://doi.org/10.6088/ijcser.00202030003.

[123] S. Donatello, A. Fernández-Jimenez, A. Palomo, Very high volume fly ash cements. Early age hydration study using Na 2SO4 as an activator, J. Am. Ceram. Soc. 96 (2013) 900–906. https://doi.org/10.1111/jace.12178.

[124] K.M.A. Hossain, Blended cement using volcanic ash and pumice, Cem. Concr. Res. 33 (2003) 1601–1605. https://doi.org/10.1016/S0008-8846(03)00127-3.

[125] Y. Senhadji, G. Escadeillas, H. Khelafi, M. Mouli, A.S. Benosman, Evaluation of natural pozzolan for use as supplementary cementitious material, Eur. J. Environ. Civ. Eng. 16 (2012) 77–96. https://doi.org/10.1080/19648189.2012.667692.

[126] K. Kupwade-Patil, S. Chin, J. Ilavsky, R.N. Andrews, A. Bumajdad, O. Büyüköztürk, Hydration kinetics and morphology of cement pastes with pozzolanic volcanic ash studied via synchrotron-based techniques, J. Mater. Sci. 53 (2018) 1743–1757. https://doi.org/10.1007/s10853-017-1659-4.

[127] K. Kupwade-Patil, S.H. Chin, M.L. Johnston, J. Maragh, A. Masic, O. Büyüköztürk, Particle size effect of volcanic ash towards developing engineered Portland cements, J. Mater. Civ. Eng. 30 (2018) 04018190. https://doi.org/10.1061/(asce)mt.1943-5533.0002348.

[128] K.M.A. Hossain, M. Lachemi, Corrosion resistance and chloride diffusivity of volcanic ash blended cement mortar, Cem. Concr. Res. 34 (2004) 695–702. https://doi.org/10.1016/j.cemconres.2003.10.021.

[129] A. Husain, K. Kupwade-Patil, A.F. Al-Aibani, M.F. Abdulsalam, In situ electrochemical impedance characterization of cement paste with volcanic ash to

examine early stage of hydration, Constr. Build. Mater. 133 (2017) 107–117. https://doi.org/10.1016/j.conbuildmat.2016.12.054.

[130] T. Chappex, K. Scrivener, Alkali fixation of C-S-H in blended cement pastes and its relation to alkali silica reaction, Cem. Concr. Res. 42 (2012) 1049–1054. https://doi.org/10.1016/j.cemconres.2012.03.010.

[131] T.K. Arul, A. Suksun, Engineering and environmental evaluation of spent coffee grounds stabilized with industrial by-products as a road subgrade material, Clean Technol. Environ. Policy. (2016). https://doi.org/10.1007/s10098-016-1188-x.

[132] A. Arulrajah, T. Kua, C. Phetchuay, S. Horpibulsuk, Spent Coffee Grounds – Fly Ash Geopolymer Used as an Embankment Structural Fill Material, (2011) 1–8. https://doi.org/10.1061/(ASCE)MT.1943-5533.0001496.

[133] T. Modulus, C. Modulus, H. Rates, S. Rates, Standard Practice for Mechanical mixing of hydraulic Cement Pastes and Mortars of Plastic Consistency, 92 (2005) 6–8. https://doi.org/10.1520/C0305-06.2.

[134] A. Content, C. Concrete, M. Units, M. Rooms, P. Concrete, Standard practice for making and curing concrete test specimens in the field 1, 04 (2001) 1–5. https://doi.org/10.1520/C0031.

[135] A. C109/109M-16a, Standard test method for compressive strength of hydraulic cement mortars (Using 2-in. or cube specimens), Annu. B. ASTM Stand. (2016) 1–10. https://doi.org/10.1520/C0109.

[136] ASTM C186- 05, Standard test method for heat of hydration of hydraulic cement, Chem. Anal. 95 (2005) 1–2. https://doi.org/10.1520/C0186-05.2.

[137] ASTM C188, Standard test method for density of hydraulic cement, ASTM Int. 95 (2009) 1–3. https://doi.org/10.1520/C0188-09.2.

[138] W. Lerch, R.H. Bogue, Heat of hydration of portland cement pastes, Bur. Stand. J. Res. 12 (1934) 645. https://doi.org/10.6028/jres.012.057.

[139] K. Scrivener, R. Snellings, B. Lothenbach, A practical guide to microstructural analysis of cementitious materials, 2018. https://doi.org/10.1201/b19074.

[140] S. Ioannou, L. Reig, K. Paine, K. Quillin, Properties of a ternary calcium sulfoaluminate–calcium sulfate–fly ash cement, Cem. Concr. Res. 56 (2014) 75–83. https://doi.org/10.1016/j.cemconres.2013.09.015.

[141] R. Jadhav, T.K. Sen, S. Deshprabhu, Coffee as a cement retarder, SPE Middle East Oil Gas Show Conf. MEOS, Proc. 2017-March (2017) 308–317. https://doi.org/10.2118/183693-ms.

[142] M.A. Kebede, Investigation of calcite and volcanic ash for their utilizations as cement filling and additive Materials, 2010.

[143] R.D. Susanti, R. Tambunan, A. Waruwu, M. Syamsuddin, Studies on concrete by partial replacement of cement with volcanic ash, J. Appl. Eng. Sci. 16 (2018) 161–165. https://doi.org/10.5937/jaes16-16494.

[144] N.P.S. Anamika Singh, Sukirti Gupta, Janhavi Singh, Hydration mechanism and strength of OPC and blended OPC with fly ash in the presence of metakaolin, Int. J. Res. Eng. Technol. 04 (2015) 60–68. https://doi.org/10.15623/ijret.2015.0405012.

[145] G. K. Al-Chaar, M. Alkadi, P.G. Asteris, Natural Pozzolan as a Partial Substitute for Cement in Concrete, Open Constr. Build. Technol. J. 7 (2013) 33–42. https://doi.org/10.2174/1874836801307010033.

[146] J. Chakraborty, S. Banerjee, Replacement of cement by fly Ash in concrete, Int. J. Civ. Eng. 3 (2016) 58–60. https://doi.org/10.14445/23488352/ijce-v3i8p110.

[147] N.L. Thomas, J.D. Birchall, The retarding action of sugars on cement hydration, Cem. Concr. Res. 13 (1983) 830–842. https://doi.org/10.1016/0008-8846(83)90084-4.

[148] N. Leklou, V.H. Nguyen, P. Mounanga, The effect of the partial cement substitution with fly ash on delayed ettringite formation in heat-cured mortars, KSCE J. Civ. Eng. 21 (2017) 1359–1366. https://doi.org/10.1007/s12205-016-0778-9.

[149] M.A.G. Aranda, Á.G. De La Torre, L. León-Reina, Rietveld quantitative phase analysis of OPC clinkers, cements and hydration products, Rev. Mineral. Geochemistry. 74 (2012) 169–209. https://doi.org/10.2138/rmg.2012.74.5.

[150] T.F. Yen, Cement Chemistry, Chem. Eng. (2008) 387–433. https://doi.org/10.1142/9781860949982_0010.

[151] J. Zhang, G. Ke, Y. Liu, Early hydration heat of calcium sulfoaluminate cement with influences of supplementary cementitious materials and water to binder ratio, Materials (Basel). 14 (2021) 642. https://doi.org/10.3390/ma14030642.

[152] I. García-Lodeiro, A. Fernández-Jiménez, A. Palomo, Variation in hybrid cements over time. Alkaline activation of fly ash-portland cement blends, Cem. Concr. Res. 52 (2013) 112–122. https://doi.org/10.1016/j.cemconres.2013.03.022.

[153] Y. Dhandapani, M. Santhanam, Assessment of pore structure evolution in the limestone calcined clay cementitious system and its implications for performance, Cem. Concr. Compos. 84 (2017) 36–47. https://doi.org/10.1016/j.cemconcomp.2017.08.012.

[154] G. Rodríguez de Sensale, I. Rodríguez Viacava, A study on blended Portland cements containing residual rice husk ash and limestone filler, Constr. Build. Mater. 166 (2018) 873–888. https://doi.org/10.1016/j.conbuildmat.2018.01.113.

[155] R. Campos-Silva, J.L. Acevedo Dávila, L.Y. Gomez-Zamorano, Effect of the addition of superabsorbent polymer in concretes mixes with supplementary cementitious materials, Eur. J. Environ. Civ. Eng. 0 (2021) 1–19. https://doi.org/10.1080/19648189.2021.1871964.

[156] G. Zhang, J. Zhao, P. Wang, L. Xu, Effect of HEMC on the early hydration of Portland cement highlighted by isothermal calorimetry, J. Therm. Anal. Calorim. 119 (2015) 1833–1843. https://doi.org/10.1007/s10973-014-4346-6.

[157] Á.G. De Torre, M.C. Martín-sedeño, L. León-reina, A.J.M. Cuberos, G. Álvarez-pinazo, M.A.G. Aranda, Hidratación de cementos de sulfoaluminato de calcio, (2011) 10–22. https://www.bing.com/search?q=Hidratación+de+cementos+de+sulfoaluminato+de+calcio+Article+·+January+2011+CITATIONS&qs=n&form=QBRE&sp=-1&pq=&sc=8-0&sk=&cvid=8BBDDDB46F8A478AACBE7FAA153FB198.

[158] A. Jiménez, M. Prieto, Incorporación de Se (VI) en Etringita, Rev. La Soc.

Española Mineral. 6 (2010) 127–128.

[159] N. Chitvoranund, F. Winnefeld, S. Sinthupinyo, B. Lothenbach, Phase assemblage study of alite-calcium sulfoaluminate cement blended with supplementary cementitious materials, 14th Int. Congr. Chem. Cem. (2015). http://www.iccc2015beijing.org/dct/page/1.

[160] F. Winnefeld, L.H.J. Martin, C.J. Müller, B. Lothenbach, Using gypsum to control hydration kinetics of CSA cements, Constr. Build. Mater. 155 (2017) 154–163. https://doi.org/10.1016/j.conbuildmat.2017.07.217.

[161] X. Ke, S.A. Bernal, J.L. Provis, Uptake of chloride and carbonate by Mg-Al and Ca-Al layered double hydroxides in simulated pore solutions of alkali-activated slag cement, Cem. Concr. Res. 100 (2017) 1–13. https://doi.org/10.1016/j.cemconres.2017.05.015.

[162] Y. Jeong, C.W. Hargis, S.C. Chun, J. Moon, The effect of water and gypsum content on strätlingite formation in calcium sulfoaluminate-belite cement pastes, Constr. Build. Mater. 166 (2018) 712–722. https://doi.org/10.1016/j.conbuildmat.2018.01.153.

[163] D.V. Ribeiro, S.Y. Yuan, M.R. Morelli, Effect of chemically treated leather shaving addition on characteristics and microstructure of OPC mortars, Mater. Res. 15 (2012) 136–143. https://doi.org/10.1590/S1516-14392012005000006.

[164] A.R. Alizadeh, Nanostructure and engineering properties of basic and modified calcium- nanostructure and engineering properties of basic and modified calcium-silicate-hydrate systems by Department of Civil Engineering University of Ottawa, (2015). https://doi.org/10.13140/RG.2.1.3892.8089.

[165] M. Frías, O. Rodriguez, R. Vigil De La Villa, R. García, S. Martínez-Ramiréz, L.J. Fernández-Carrasco, I. Vegas, The influence of activated coal mining wastes on the mineralogy of blended cement pastes, J. Am. Ceram. Soc. 99 (2016) 300–307. https://doi.org/10.1111/jace.13840.

[166] F. Matalkah, P. Soroushian, Synthesis and characterization of alkali aluminosilicate hydraulic cement that meets standard requirements for general use, Constr. Build.

Mater. 158 (2018) 42–49. https://doi.org/10.1016/j.conbuildmat.2017.10.002.

[167] I. Garcia-Lodeiro, A. Palomo, A. Fernández-Jiménez, D.E. MacPhee, Compatibility studies between N-A-S-H and C-A-S-H gels. Study in the ternary diagram Na2O-CaO-Al2O3-SiO 2-H2O, Cem. Concr. Res. 41 (2011) 923–931. https://doi.org/10.1016/j.cemconres.2011.05.006.

[168] E. L'Hôpital, B. Lothenbach, D.A. Kulik, K. Scrivener, Influence of calcium to silica ratio on aluminium uptake in calcium silicate hydrate, Cem. Concr. Res. 85 (2016) 111–121. https://doi.org/10.1016/j.cemconres.2016.01.014.

[169] J. Dong, Y. Tang, A. Nzihou, Y. Chi, E. Weiss-hortala, M. Ni, Z. Zhou, Hydrothermal synthesis of calciumsulfoaluminate -belite cement from industrial waste materials, (2018) 1–23. https://doi.org/10.1016/j.jclepro.2015.12.068.This.

[170] P. Li, Z. Ma, Z. Zhang, X. Li, X. Lu, P. Hou, P. Du, Effect of gypsum on hydration and hardening properties of alite modified calcium sulfoaluminate cement, Materials (Basel). 12 (2019). https://doi.org/10.3390/ma12193131.

[171] M. Borštnar, N. Daneu, S. Dolenec, Phase development and hydration kinetics of belite-calcium sulfoaluminate cements at different curing temperatures, Ceram. Int. 46 (2020) 29421–29428. https://doi.org/10.1016/j.ceramint.2020.05.029.

[172] J. Seo, S. Kim, S. Park, H.N. Yoon, H.K. Lee, Carbonation of calcium sulfoaluminate cement blended with blast furnace slag, Cem. Concr. Compos. 118 (2021) 103918. https://doi.org/10.1016/j.cemconcomp.2020.103918.

[173] M.J. Sánchez-Herrero, A. Fernández-Jiménez, A. Palomo, Studies about the hydration of hybrid "alkaline-belite" cement, Front. Mater. 6 (2019) 1–9. https://doi.org/10.3389/fmats.2019.00066.

[174] S. Donatello, A. Fernández-Jimenez, A. Palomo, Very high volume fly ash cements. early age hydration study using Na_2SO_4 as an activator, J. Am. Ceram. Soc. 96 (2013) 900–906. https://doi.org/10.1111/jace.12178.

[175] I. García-Lodeiro, A. Fernández-Jiménez, A. Palomo, Variation in hybrid cements over time. Alkaline activation of fly ash–portland cement blends, Cem. Concr. Res. 52 (2013) 112–122. https://doi.org/10.1016/j.cemconres.2013.03.022.

[176] X.C. Ping Yu,, R. James Kirkpatrick,, Brent Poe, Paul F. McMillan, Structure of calcium silicate hydrate (C-S-H): Near-, mid-, and far-Infrared spectroscopy, J. Am. Ceram. Soc. 82 (1999) 742–748. https://doi.org/https://doi.org/10.1111/j.1151-2916.1999.tb01826.x.

[177] J.L. García Calvo, M.S. Moreno, M.C.A. Alonso, A.H. López, J.G. Olmo, Study of the microstructure evolution of low-pH cements based on Ordinary portland cement (OPC) by mid- and near-infrared spectroscopy, and their influence on corrosion of steel reinforcement, Materials (Basel). 6 (2013) 2508–2521. https://doi.org/10.3390/ma6062508.

[178] F. Kontoleontos, P. Tsakiridis, A. Marinos, N. Katsiotis, V. Kaloidas, M. Katsioti, Dry-grinded ultrafine cements hydration. Physicochemical and microstructural characterization, Mater. Res. 16 (2013) 404–416. https://doi.org/10.1590/S1516-14392013005000014.

[179] D. Barbir, P. Dabić, P. Krolo, Hydration study of ordinary Portland cement in the presence of lead(II) oxide, Chem. Biochem. Eng. Q. 27 (2013) 95–99. https://doi.org/DOI: 10.1590/S1516-14392007000400002.

[180] I. García Lodeiro, D.E. Macphee, A. Palomo, A. Fernández-Jiménez, Effect of alkalis on fresh C-S-H gels. FTIR analysis, Cem. Concr. Res. 39 (2009) 147–153. https://doi.org/10.1016/j.cemconres.2009.01.003.

[181] R. Ylmén, U. Jäglid, Carbonation of Portland cement studied by diffuse reflection Fourier Transform Infrared Spectroscopy, Int. J. Concr. Struct. Mater. 7 (2013) 119–125. https://doi.org/10.1007/s40069-013-0039-y.

[182] Portland Cement Association, P.C. Assocation, Portland Cement, Concrete, and Heat of Hydration, 1997. http://cement.org/tech/pdfs/pl972.pdf.

[183] O.. Silva, Hydration process of cement, Hydration Process Cem. (2018). https://www.360enconcreto.com/blog/detalle/proceso-hidratacion-del-cemento.

[184] B. Pacewska, I. Wilińska, Hydration of cement composites containing large amount of waste materials, Procedia Eng. 57 (2013) 53–62. https://doi.org/10.1016/j.proeng.2013.04.009.

[185] H. Herrmann, H. Bucksch, Cement and Concrete Chemistry, 2014. https://doi.org/10.1007/978-3-642-41714-6_33900.

[186] X. Zou, A. Chao, Y. Tian, N. Wu, H. Zhang, T.Y. Yu, X. Wang, An experimental study on the concrete hydration process using Fabry-Perot fiber optic temperature sensors, Meas. J. Int. Meas. Confed. 45 (2012) 1077–1082. https://doi.org/10.1016/j.measurement.2012.01.034.

[187] K. Scrivener, A. Ouzia, P. Juilland, A. Kunhi Mohamed, Advances in understanding cement hydration mechanisms, Cem. Concr. Res. 124 (2019) 105823. https://doi.org/10.1016/j.cemconres.2019.105823.

[188] K.L. Scrivener, P. Juilland, P.J.M. Monteiro, Advances in understanding hydration of Portland cement, Cem. Concr. Res. 78 (2015) 38–56. https://doi.org/10.1016/j.cemconres.2015.05.025.

[189] S. Bishnoi, K.L. Scrivener, Studying nucleation and growth kinetics of alite hydration using μic, Cem. Concr. Res. 39 (2009) 849–860. https://doi.org/10.1016/j.cemconres.2009.07.004.

[190] S. Zeynalova, F. Bayramov, N. Cement, Application of high content of volcanic ash in high strength concretes, in: 2017. https://isites.info/PastConferences/ISITES2017/ISITES2017/papers/A9-ISITES2017ID149.pdf.

[191] F. Han, R. Liu, D. Wang, P. Yan, Characteristics of the hydration heat evolution of composite binder at different hydrating temperature, Thermochim. Acta. 586 (2014) 52–57. https://doi.org/10.1016/j.tca.2014.04.010.

[192] N. Garg, K. Wang, Comparing the performance of different commercial clays in fly ash-modified mortars, J. Sustain. Cem. Mater. 1 (2012) 111–125. https://doi.org/10.1080/21650373.2012.745217.

[193] R. Rajamma, R.J. Ball, L.A.C. Tarelho, G.C. Allen, J.A. Labrincha, V.M. Ferreira, Characterisation and use of biomass fly ash in cement-based materials, J. Hazard. Mater. 172 (2009) 1049–1060. https://doi.org/10.1016/j.jhazmat.2009.07.109.

[194] G. Ke, J. Zhang, Y. Liu, S. Xie, Early hydration heat of calcium sulfoaluminate

cement with influences of supplementary cementitious materials and water to binder ratio, Materials (Basel). 387 (2021) 146–155. https://doi.org/10.1016/j.powtec.2021.04.027.

[195] M. Isabel, B. Vásquez, Análisis de la mineralogía y del desempeño en cementos híbridos de sulfoaluminato de calcio y Pórtland, (2018).

[196] M. Dhoury, C. Cau Dit Coumes, J.-B. Champeones, C. Mercier, D. Damidot, Controlling the rate of hydration of calcium sulfoaluminate cements : the case of lithium and borate ions, 14th Int. Congr. Chem. Cem. (ICCC 2015). (2015).

[197] A.F. Sanabria, Estudio de cementos sulfoaluminosos parcialmente remplazados en presencia de materiales de cambio de fase, Universidad Autonoma de Nuevo leon, 2019.

[198] F. He, Evaluation of sample-electrode contact impedance in two-point measured AC Impedance Spectroscopy of cement-based materials, Int. J. Mater. Sci. Appl. 7 (2018) 106. https://doi.org/10.11648/j.ijmsa.20180703.15.

[199] Q.H. Nguyen, S. Lorente, A. Duhard-Barone, Effect of the pore size of cement based materials on ionic transport, Constr. Build. Mater. 147 (2017) 160–167. https://doi.org/10.1016/j.conbuildmat.2017.04.157.

[200] V. Vass, The electrical resistivity of concrete, Budapest University of Technology and Economics, 2012. https://www.researchgate.net/publication/273310444.

[201] L. Chi, Z. Wang, S. Lu, D. Zhao, Y. Yao, Development of mathematical models for predicting the compressive strength and hydration process using the EIS impedance of cementitious materials, Constr. Build. Mater. 208 (2019) 659–668. https://doi.org/10.1016/j.conbuildmat.2019.03.056.

[202] H.C. Kim, S.Y. Kim, S.S. Yoon, Electrical properties of cement paste obtained from impedance spectroscopy, J. Mater. Sci. 30 (1995) 3768–3772. https://doi.org/10.1007/BF01153933.

[203] P. Gu, Y. Fu, P. Xie, J.J. Beaudoin, Electrochemical behaviour of Portland-cement/high-alumina-cement systems at early hydration times, J. Mater. Sci. Lett. 12 (1993) 1771–1773. https://doi.org/10.1007/BF00517606.

[204] B.J. Christensen, T. Coverdale, R.A. Olson, S.J. Ford, E.J. Garboczi, H.M. Jennings, T.O. Mason, Impedance Spectroscopy of hydrating cement-based materials: Measurement, Interpretation, and Application, J. Am. Ceram. Soc. 77 (1994) 2789–2804. https://doi.org/10.1111/j.1151-2916.1994.tb04507.x.

[205] L. Chi, Z. Wang, S. Lu, H. Wang, K. Liu, W. Liu, Early assessment of hydration and microstructure evolution of belite-calcium sulfoaluminate cement pastes by electrical impedance spectroscopy, Electrochim. Acta. 389 (2021) 138699. https://doi.org/10.1016/j.electacta.2021.138699.